Fadia Ahmed

Fadia Thesis Final.docx

Delhi Technological University

Document Details

Submission ID
trn:oid:::27535:128588863

Submission Date
Feb 18, 2026, 10:27 PM GMT+3

Download Date
Feb 18, 2026, 10:37 PM GMT+3

File Name
Fadia Thesis Final.docx

File Size
56.7 MB

185 Pages

36,671 Words

217,523 Characters

9% Overall Similarity

The combined total of all matches, including overlapping sources, for each database.

Filtered from the Report

- Bibliography
- Quoted Text
- Cited Text
- Small Matches (less than 8 words)
- Submitted works
- Internet sources

Exclusions

- 5 Excluded Sources

Match Groups

281 Not Cited or Quoted 9%
Matches with neither in-text citation nor quotation marks

0 Missing Quotations 0%
Matches that are still very similar to source material

0 Missing Citation 0%
Matches that have quotation marks, but no in-text citation

0 Cited and Quoted 0%
Matches with in-text citation present, but no quotation marks

Top Sources

0% Internet sources
9% Publications
0% Submitted works (Student Papers)

Integrity Flags

1 Integrity Flag for Review

Replaced Characters
13 suspect characters on 5 pages
Letters are swapped with similar characters from another alphabet.

Our system's algorithms look deeply at a document for any inconsistencies that would set it apart from a normal submission. If we notice something strange, we flag it for you to review.

A Flag is not necessarily an indicator of a problem. However, we'd recommend you focus your attention there for further review.

Match Groups

281 Not Cited or Quoted 9%
Matches with neither in-text citation nor quotation marks

0 Missing Quotations 0%
Matches that are still very similar to source material

0 Missing Citation 0%
Matches that have quotation marks, but no in-text citation

0 Cited and Quoted 0%
Matches with in-text citation present, but no quotation marks

Top Sources

0% Internet sources
9% Publications
0% Submitted works (Student Papers)

Top Sources

The sources with the highest number of matches within the submission. Overlapping sources will not be displayed.

1 Publication
Narjes Ibrahem Khaled, Deenan Santhiya. "Multifunctional poly(allylamine hydro... <1%

2 Publication
Atul Singh Rajput, Manas Das, Sajan Kapil. "Investigations on a hybrid chemo-ma... <1%

3 Publication
Andrzej Zieliński, Tomasz Moskalewicz, Aldo R. Boccaccini. "Surface Modifications ... <1%

4 Publication
"Advances in Unconventional Machining and Composites", Springer Science and ... <1%

5 Publication
Ruixia Zhang, Steven Mankoci, Nicholas Walters, Hongyu Gao et al. "Effects of las... <1%

6 Publication
Liu, X.. "Surface nano-functionalization of biomaterials", Materials Science & Engi... <1%

7 Publication
Advanced Tribology, 2010. <1%

8 Publication
Vijay Kumar Jain. "Nanofinishing Science and Technology - Basic and Advanced Fi... <1%

9 Publication
Yogendra Kumar, Harpreet Singh. "Experimental investigations on chemo-mecha... <1%

10 Publication
"Processing and Fabrication of Advanced Materials, Volume 3", Springer Science a... <1%

11 Publication
Modi, Richa. "An Investigation on Ro Based Membrane Process Development for ... <1%

12 Publication
Xiao Han, Jianxiong Ma, Aixian Tian, Yan Wang, Yan Li, Benchao Dong, Xue Tong, ... <1%

13 Publication
"TMS 2025 154th Annual Meeting & Exhibition Supplemental Proceedings", Spring... <1%

14 Publication
Eko Budiyanto, Kusmono, Rini Dharmastiti, Maria Goreti Widiastuti. "Experiment... <1%

15 Publication
Patel, Sunil Ramlal. "Removal of Heavy Metal Ions From Waste Water Using Electr... <1%

16 Publication
Raganya, Mampai Lereto. "Design of Ti-Mo-Nb-Zr Alloys with Low Elastic Modulus ... <1%

17 Publication
Abhinay Thakur, Ashish Kumar. "Recent advancements in the surface treatments ... <1%

18 Publication
Maheshkumar, Patel Dharmin. "Parametric Investigation on Forming of Magnesi... <1%

19 Publication
Ratilal, Raiyani Hitesh. "Experimental Investigation on Fracture Characteristic of ... <1%

20 Publication
Wei Wang, Shijun Ji, Ji Zhao. "Review of magnetorheological finishing on compon... <1%

21 Publication
A. Biswas. "Chemical oxidation of Ti–6Al–4V for improved wear and corrosion resi... <1%

22 Publication
"Additive Manufacturing of Emerging Materials", Springer Science and Business ... <1%

23 Publication
Chander Prakash, Sunpreet Singh, Alokesh Pramanik, Animesk Basak et al. "Expe... <1%

24 Publication
Jibin T. Philip, Jerin Jose, Soney C. George. "Natural Fiber Composites for a Sustain... <1%

25 Publication
Zafar Alam, Sunil Jha. "Reprint of “Modeling of surface roughness in ball end mag... <1%

26 Publication
Dung Hoang Tien, Trinh Nguyen Duy. "Novel magnetic field array optimization m... <1%

27 Publication
Mayank Srivastava, Kheelraj Pandey, Pulak M. Pandey, Ashwani Sharma. "Experi... <1%

28 Publication
"Advances in Abrasive Based Machining and Finishing Processes", Springer Scienc... <1%

29 Publication
"Biomaterial-based Additive Manufacturing in Tissue Engineering and Regenerati... <1%

30 Publication
Chaudhari, Ashokkumar Ramjibhai. "Experimentation and Simulation of Electroc... <1%

31 Publication
Nitin Dixit, Varun Sharma, Pradeep Kumar. "Research trends in abrasive flow mac... <1%

32 Publication
Sunpreet Singh, Chander Prakash, Alokesh Pramanik, Animesh Basak et al. "Mag... <1%

33 Publication
"Recent Advances in Mechanical Engineering", Springer Science and Business Me... <1%

34 Publication
Dung Hoang Tien, Pham Thi Thieu Thoa, Nguyen Duy Trinh. "Investigation of the ... <1%

35 Publication
Hirpara, Keyur Parsottambhai. "Experimental Investigations on Multi-Layered Pla... <1%

36 Publication
Larissa Mayra Silva Ribeiro, Luziane Aparecida Costa da Rosa Simões, Melina Espa... <1%

37 Publication
Manjesh Kumar, Hari Narayan Singh Yadav, Abhinav Kumar, Manas Das. "An over... <1%

38 Publication
Pratik Kumar Shaw, Suryank Dwivedi, Amit Rai Dixit, Alokesh Pramanik. "Enginee... <1%

39 Publication

Atul Singh Rajput, Manas Das, Sajan Kapil. "A comprehensive review of magnetor... <1%

40 Publication

Andrej Jeromen, Anish Nair, Peter Rodič, Denis Sačer et al. "DED-LB manufactured... <1%

41 Publication

Mustafa M. Nasr, Saqib Anwar, Ali M. Al-Samhan, Mageed Ghaleb, Abdulmajeed D... <1%

42 Publication

Sidpara, Ajay. "Magnetorheological and Allied Finishing Processes", Micromanufa... <1%

43 Publication

Zeliang Ding, Yi Wang, Quan Zhou, Ziyu Ding, Yiyong Wu, Yuefang Zhu, Wensong ... <1%

44 Publication

Adriel Magalhães Souza, Eraldo Jannone da Silva, Jason Ratay, Hitomi Yamaguchi.... <1%

45 Publication

Shuai Zhang, Dong Wang, Feng Zhao, Zhenyu Zhang, Hongxiu Zhou, Leilei Chen, L... <1%

46 Publication

Vipin Goyal, Girish Verma, Nisheeth Kr. Prasad. "Bio-corrosion Behavior of Direct ... <1%

47 Publication

Z. Ozdemir, A. Ozdemir, G.B. Basim. "Application of chemical mechanical polishin... <1%

48 Publication

Zenghua Fan, Xiang Zhang, Jiyong Li, Zihao Yang, Jun Gao, Yebing Tian. "Rheologi... <1%

49 Publication

"Advances in Manufacturing and Materials", Springer Science and Business Medi... <1%

50 Publication

Masoud Sarraf, Erfan Rezvani Ghomi, Saeid Alipour, Seeram Ramakrishna, Nazatu... <1%

51 Publication

Sathish Kumar Adapa Jagadish, Divya Zindani. "Statistical Modelling and Analysis ... <1%

52 Publication

Sundar, Shalini. "Exploring the Transport of Poly(Styrene) Sulfonate-Based Polyel... <1%

53 Publication

Xin Chen, Shucong Xu, Juan Ignacio Ahuir-Torres, Zixuan Wang, Xun Chen, Tianbi... <1%

54 Publication

Yebing Tian, Chen Shi, Zenghua Fan, Qiang Zhou. "Experimental investigations on... <1%

55 Publication

"Biomanufacturing", Springer Science and Business Media LLC, 2019 <1%

56 Publication

"Handbook of Vibroacoustics, Noise and Harshness", Springer Science and Busine... <1%

57 Publication

R. Venkata Rao. "Advanced Modeling and Optimization of Manufacturing Process... <1%

58 Publication

Shengqiang Yang, Wenhui Li. "Surface Finishing Theory and New Technology", Sp... <1%

59 Publication

V K Jain, A Sidpara, M R Sankar, M Das. "Nano-finishing techniques: a review", Pro... <1%

60 Publication

Xifeng Ma, Yebing Tian, Cheng Qian, Zhen Ma, Shadab Ahmad, Ling Li, Zenghua F... <1%

61 Publication

"Biomaterials in Clinical Practice", Springer Science and Business Media LLC, 2018 <1%

62 Publication

Govindbhai, Patel Miteshkumar. "Optimization of WEDM Process Parameters for ... <1%

63 Publication

Joshi, Ayanesh Yogeshkumar. "Experimental Investigation and Microstructure Ch... <1%

64 Publication

Melika Babaei, Simone Murchio, Lorena Emanuelli, Raffaele De Biasi et al. "Metal ... <1%

65 Publication

Seals, Cheryl Denise. "A framework for learning and reuse in visual programming... <1%

66 Publication

Somabhai, Patel Sandipkumar. "Experimental Investigation With Parametric Opti... <1%

67 Publication
Yoshiki Oshida, Toshihiko Tominaga. "Nickel-Titanium Materials", Walter de Gruy... <1%

68 Publication
Nawal, Tahiat. "Effect of Thermal Treatments on Electrochemical Behavior of Bin... <1%

69 Publication
Beni, Faeze Akbari. "Reaction Kinetics Analysis of Furfural Production From Xylos... <1%

70 Publication
Manjesh Kumar, Anupam Alok, Vikash Kumar, Manas Das. "Advanced abrasive-ba... <1%

71 Publication
Yogendra Kumar, Harpreet Singh. "Chemomechanical magnetorheological finishi... <1%

72 Publication
Ning Hou, Minghai Wang, Ben Wang, Yaohui Zheng, Siyu Zhou, Ce Song. "Fundam... <1%

73 Publication
Ranjan, Prabhat, R. Balasubramaniam, and V.K. Suri. "Modelling and simulation o... <1%

74 Publication
Tang'an, Diret Bitrus. "Remediation of Petroleum Hydrocarbon Contaminated Soi... <1%

75 Publication
Anand Sharma, Mahendra Singh Niranjan. "Chemical assisted ball end magnetor... <1%

76 Publication
Bruno Ribeiro, Ruben Offoiach, Ehsan Rahimi, Elisa Salatin, Maria Lekka, Lorenzo ... <1%

77 Publication
Chaudhary, Nanjibhai Nilabhai. "Experimental Investigations on Free-Form Magn... <1%

78 Publication
Guolong Wu, Zhenzhen Yang, Yelei Xu, Ye Wang, Haojie Zhang, Yi Tian, Jianhua Ya... <1%

79 Publication
Yixiang Yuan, ZunYun Ke, Lei Zhang, YeHua Jiang, Zhengyuan He. "Mechanical, co... <1%

80 Publication
"Advanced Engineering Optimization Through Intelligent Techniques", Springer S... <1%

81 Publication

"Advances in Industrial and Production Engineering", Springer Science and Busin... <1%

82 Publication

"Orthopedic Biomaterials", Springer Science and Business Media LLC, 2017 <1%

83 Publication

Arvind Dagur, Karan Singh, Pawan Singh Mehra, Dhirendra Kumar Shukla. "Artific... <1%

84 Publication

Biing-Hwa Yan, Geeng-Wei Chang, Jung-Hsien Chang, Rong-Tzong Hsu. "Improvin... <1%

85 Publication

Dharamjit Debbarma. "The study of wear behaviour of the Inconel 800 material i... <1%

86 Publication

Krzysztof Aniołek, Marian Kupka, Adrian Barylski. "Characteristics of the tribologi... <1%

87 Publication

Prasanta Sahoo, Suman Kalyan Das, J. Paulo Davim. "Tribology of materials for bi... <1%

88 Publication

Shengdong Zhang, Zhilin Long, Xiuying Yang. "Lubrication performance of magn... <1%

89 Publication

Zhaokun Yan, Shengqiang Yang, Yonggang Li, Xiuhong Li, Wenhui Li, Xingai Yao. ... <1%

90 Publication

"Cold-Spray Coatings", Springer Science and Business Media LLC, 2018 <1%

91 Publication

Anwesa Barman, Manas Das, Vimal Kumar Pathak. "Optimization of magnetic fiel... <1%

92 Publication

Burak Dikici, Kubilay Aslantas, Xiaoli Zhao, Mitsuo Niinomi. "Comprehensive anal... <1%

93 Publication

Cheng Qian, Zenghua Fan, Yebing Tian, Yanhou Liu, Jinguo Han, Jinhui Wang. "A r... <1%

94 Publication

Daniyar Syrlybayev, Aidana Seisekulova, Didier Talamona, Asma Perveen. "The Po... <1%

95 Publication

Dhrubajit Sarma, Rupshree Ozah, Jyotisman Borah, Muthumari Chandrasekaran, ... <1%

96 Publication

Eva Bittrich, Stefania Cometa, Elvira De Giglio, Rosa Di Mundo et al. "Polymer Surf... <1%

97 Publication

Guijiang Wei, Meiying Tan, Shokouh Attarilar, Jie Li, Vasilievich Vladimir Uglov, Bi... <1%

98 Publication

Ludovico Andrea Alberta, Jithin Vishnu, Yohan Douest, Kevin Perrin et al. "Triboco... <1%

99 Publication

Luis Gustavo Cordiolli Russi, Lucíola Lucena de Sousa, Alfeu Saraiva Ramos, Piter ... <1%

100 Publication

Pralhad Pesode, Shivprakash Barve. "Comparison and performance of α, α+β and ... <1%

101 Publication

Teng Li, Ying Meng, Yanan Pan, Xiuli Fu, Yuhan Sun, Hao Liang. "Functionalized S... <1%

102 Publication

Zhen Ma, Yebing Tian, Cheng Qian, Shadab Ahmad, Zenghua Fan, Zhiguang Sun. "... <1%

103 Publication

"Advances in Mechanical Coating", Springer Science and Business Media LLC, 2025 <1%

104 Publication

Amini, Ezatollah. "Elucidation of the Factors Affecting the Production and Propert... <1%

105 Publication

Hyeon-Tae Im, Dae Ha Kim, Ryun-Ho Kwak, Sung-Min Park, Nam-Seok Kim, Kwan... <1%

106 Publication

Ioan Doré Landau, Rogelio Lozano, Mohammed M'Saad, Alireza Karimi. "Chapter ... <1%

107 Publication

J. Lima, S. R. Sousa, A. Ferreira, M. A. Barbosa. "Interactions between calcium, pho... <1%

108 Publication

Jaikishan Sambharia, Harlal Singh Mali. "Recent developments in abrasive flow fi... <1%

109 Publication

Jinwei Liu, Xin Zeng, Peng Zhang, Xiang Peng, Deping Yu. "Counterion-Driven Mec... <1%

110 Publication

Leeladhar Nagdeve, V.K. Jain, J. Ramkumar. "Nanofinishing of freeform/sculpture... <1%

111 Publication

Lokesh Kumar, Ashish Goyal, Vimal Kumar Pathak. "Prediction and optimization o... <1%

112 Publication

Mbelle, Margaret Ntombizodwa. "Evaluation of the Implementation of the School... <1%

113 Publication

Mitsuo Niinomi. "Recent research and development in titanium alloys for biomed... <1%

114 Publication

Murat Sarıkaya, Munish Kumar Gupta, Italo Tomaz, Danil Yu Pimenov et al. "A sta... <1%

115 Publication

Nguyen Duy Trinh, Nguyen Minh Quang, Le Thi Phuong Thanh, Nguyen Tien Tun... <1%

116 Publication

Prabhat Ranjan, R. Balasubramaniam, V. K. Jain. "Analysis, design and synthesis o... <1%

117 Publication

S. Karthikeyan, B. Mohan, S. Kathiresan, G. Anbuchezhiyan. "Effect of process par... <1%

118 Publication

S. Usha Rani, V.V. Anusha Thampi, D. Kesavan, S. Ramanathan, M. Kamaraj. "An in... <1%

119 Publication

Shadab Ahmad, Yebing Tian, Zhen Ma, Cheng Qian, Xiangyu Yuan. "Effect of mag... <1%

120 Publication

Shadab Ahmad, Yebing Tian, Zhen Ma, Faiz Iqbal, Cheng Qian. "Exploring multi-co... <1%

121 Publication

Sheng, Xia. "Development of a Modeling and Analysis Procedure to Predict Flow-I... <1%

122 Publication

Sheth, Saurin Mukundbhai. "Investigation of Machining Process Parameters in th... <1%

123 Publication

Shuai Long, Jiang Zhu, Yiwan Jing, Si He, Lijia Cheng, Zheng Shi. "A Comprehensiv... <1%

124 Publication

Solanki, Amitkumar Bharatkumar. "Implementation of Quality Tools and Optimiz... <1%

125 Publication

Song, Guangchao. "Magnetic-Field Assisted Finishing Process (MAF) on Mold Steel... <1%

126 Publication

Tanmoy Das, Tanima Bhattacharya. "Evolution of Low-Dimensional Biosensors in ... <1%

127 Publication

Ungan, Güler Gülîzar. "Characterization of the MG Doped CA-P Compounds Electr... <1%

128 Publication

Walaa Abd-Elaziem, Moustafa A. Darwish, Atef Hamada, Walid M. Daoush. "Titani... <1%

129 Publication

Wang, Meng. "Joining vacuum high pressure die cast aluminum alloy a356 subjec... <1%

130 Publication

Xuenan Li, Huiting Shi, Shengqiang Yang, Wenhui Li, Xiuhong Li. "Finishing mech... <1%

131 Publication

Yanfang Qin, Hongjian Zhao, Chao Li, Jinbin Lu, Jining He. "Effect of heat treatme... <1%

132 Publication

Yazhou Hu, Hongshui Wang, Donghui Wang, Baoe Li, Chunyong Liang. "High-perf... <1%

133 Publication

Yifei Wu, Keming Wan, Jianhua Lu, Changyong Yuan, Yuwei Cui, Rongquan Duan, ... <1%

134 Publication

Yogendra Kumar, Harpreet Singh. " Effect of sintering routes on CIP/EIP – Al O c... <1%

135 Publication

Zeeshan ur Rahman, Lebin Thomas. "Industrial and Environmental Microbiology"... <1%

136 Publication

Zenghua Fan, Zihao Yang, Xiang Zhang, Jun Gao, Yebing Tian. "Material removal b... <1%

Integrated Chemical Treatment and Magneto-rheological Finishing of Titanium Alloy for Biomedical Applications

THESIS

Submitted in partial fulfillment of the requirements for the award of the degree of

DOCTOR OF PHILOSOPHY

In

Mechanical Engineering

By

Fadia Ahmed Abdullah Naji

(ROLL NO- 2K22/PhD/ME/06)

Under the Supervision of

(Prof. Qasim Murtaza)
(DTU, Delhi)

(Prof. M.S. Niranjan)
(DTU, Delhi)

Department of Mechanical Engineering

DELHI TECHNOLOGICAL UNIVERSITY

(Formerly Delhi College of Engineering)

Shahbad Daulatpur, Main Bawana Road, Delhi-110042, India

January, 2026

CERTIFICATE

This is to certify that the thesis entitled **"Integrated Chemical Treatment and Magneto-rheological Finishing of Titanium Alloy for Biomedical Applications"** being submitted by **Fadia Ahmed Abdullah Naji**, **Roll No. 2K22/PhD/ME/06** to the Delhi Technological University, Delhi, for the award of the degree of **Doctor of Philosophy** is a bonafide record of original research work carried out by her. She has worked under our guidance and supervision, fulfilling the requirements for the submission of this thesis, which has met the requisite standard. The results of this thesis have not been submitted, in part or in full, to any other University or Institute for the awarding of any degree or diploma.

Prof. Qasim Murtaza
Department of Mechanical Engineering
(Delhi Technological University, Delhi)

Prof. M.S. Niranjan
Department of Mechanical Engineering
(Delhi Technological University, Delhi)

CANDIDATE'S DECLARATION

I**, Fadia Ahmed Naji**, hereby certify that the work being presented in the thesis entitled "Integrated Chemical Treatment and Magneto-rheological Finishing of Titanium Alloy for Biomedical Applications" in partial fulfillment of the requirements for the award of the Degree of Doctor of Philosophy, submitted in the Department of Mechanical Engineering, Delhi Technological University is an authentic record of my work carried out during the period from July 2022 to September 2025 under the supervision of **Prof. Qasim Murtaza** and **Prof. M.S. Niranjan.** I have not submitted the matter presented in the thesis for the award of any other degree of this or any other Institute.

Fadia Ahmed Naji

(Roll No- 2K22/PHD/ME/06)

DEDICATED TO

THE SOUL OF MY FATHER

" O Allah, have mercy on my father and make his grave a garden from the gardens of Paradise."

ACKNOWLEDGEMENTS

"الحمد والشكر لله أولاً وآخراً "

I gratefully acknowledge the support and guidance of my supervisor throughout this research.

I would also like to express my gratitude to everyone who helped me in any way, whether directly or indirectly, in the process of completing this thesis work. In addition, I would like to take this opportunity to express my heartfelt appreciation to my family for the unwavering love, encouragement, and guidance they have provided me throughout my life. Last but certainly not least, I would like to offer my heartfelt appreciation to the Almighty for everything.

Fadia Ahmed Naji

PREFACE

Titanium and its alloys are widely used in biomedical implants owing to their exceptional biocompatibility, corrosion resistance, and mechanical strength; however, their inherent hardness, low wear resistance, and chemical inertness present significant challenges in achieving the required surface finish and ensuring long-term functionality. To overcome these limitations and develop high-quality, damage-free, and functional implant surfaces, this research uses an eco-friendly chemical combination of citric acid and hydrogen peroxide for surface modification of Ti alloys. First, a finishing process of Ti64 alloy was developed using a chemo-mechanical magneto-rheological (CH-MR) process to enhance the surface finish. Second, a surface modification of Ti64 alloy by thermochemical process (THCP) to improve the mechanical properties, biocompatibility, and bioactivity. The contents of the thesis are as follows:

First chapter: -

This chapter introduces Ti alloys, highlights their applications in biomedical implants, and classifies surface finishing techniques, with particular emphasis on nano-finishing processes to achieve superior surface quality for implant components. It further outlines the existing challenges and research gaps in improving the surface roughness of Ti alloys and presents the motivation for undertaking the present study.

Second chapter:-

This chapter provides a critical review of the literature on the CMMRF, examining its process parameters, research trends, challenges, and limitations. It includes the chemical reagents used in etching processes, associated changes in surface characterization, constraints of nano-finishing methods, and comparative evaluations of finishing techniques and processing times.

Third chapter: -

This chapter formulates the problem statement, identifies the research gaps through comprehensive analysis, and clearly defines the study objectives. It also outlines the methodology for effectively addressing these objectives.

Fourth chapter: -

This chapter presents the materials and methods, detailing the substrate, eco-friendly reagents, and the mechanism of surface modification. It further describes the statistical analysis used to optimize process parameters to minimize surface roughness (Sa) and provides the specifications of the equipment used for characterization.

Fifth chapter: -

This chapter presents the results and discussion in two parts. Part I focuses on the surface modification of Ti64 alloy by THCP. Part II focuses on the integrated chemical treatment with CH-MR of Ti64 alloy to improve the finishing process. In this part, the CH-MR process parameters were optimized using RSM by a CCD to minimize Sa.

Sixth chapter: -

This chapter presents the conclusions of the investigation into the surface modification of Ti64 alloy by TCHP, and the finishing process by the CH-MR process, followed by a discussion of the future scope of the present work.

TABLE OF CONTENTS

Title **Page No.**

CERTIFICATE I

DEDICATED TO..... III

ACKNOWLEDGEMENTS IV

PREFACE

....V

TABLE OF CONTENTS VII

LIST OF FIGURES XI

LIST OF TABLES XV

LIST OF ABBREVIATIONS XVI

ABSTRACT

.....XVIII

CHAPTER 1: INTRODUCTION 1

1.1 Introduction to Titanium and Its Alloys 1

1.2 Titanium and Its Alloys in Biomedical Applications 3

1.3 Finishing Process Classifications 7

1.3.1 Mechanical Finishing Processes 9

1.3.2 Chemical Finishing Process (CP) 19

1.3.3. Hybrid Finishing Processes 23

1.4 Comparison of Nano-Finishing Processes for Ti Alloys..... 27

1.5 Summary..... 29

CHAPTER 2: LITERATURE REVIEW 30

2.1 Introduction 30

2.2 Chemical Magneto-rheological Finishing (CMMRF) Process..... 34

2.2.1 Review of Chemical-Mechanical Finishing Process (CMP) 36

2.2.2 Review of Magneto-rheological (MR) Finishing 42

2.3 Research Trends in the (CMMRF) Process..... 46

2.4 Challenges and Limitations 49

2.5 Comparison of finishing techniques and processing time..... 53

2.6 Summary..... 55

CHAPTER 3: PROBLEM FORMULATION 56

3.1 Problem Statement..... 56

3.2 Research Gaps:..... 58

3.3 Research Objectives: 59

3.4 Methodology..... 60

CHAPTER 4: MATERIALS AND METHODS 62

4.1 The Substrate Materials: 62

4.1.1 Titanium alloy..... 62

4.1.2 Magnetorheological Fluid (MR)..... 63

4.1.3 The Chemical Materials..... 64

4.2 Surface Preparation 65

4.3 Surface Modification of Ti64 Alloy by THCP..... 66

4.4 The Surface Finishing by the CH-MR Process 68

4.4.1 The CH-MR process mechanism..... 68

4.4.2 Design of Experiments..... 69

4.4.3 Machining Process..... 71

4.5 The Characterizations 73
4.5.1 Surface Morphology 73
4.5.2 Mechanical Properties 73
4.5.3 Corrosion Characterization 77
4.5.4 The Biocompatibility 78
CHAPTER 5: RESULTS AND DISCUSSION 80
5.1 Surface Modification by THCP 80
5.1.1 Surface Morphology 80
5.1.2. Mechanical Properties 87
5.1.3 In Vitro Hemocompatibility 92
5.1.4 The Corrosion Behavior 93
5.1.5 The Bioactivity 96
5.1.6 Summary 101
5.2 Surface Finishing by CH-MR Process 102
5.2.1 Experimentation 102
5.2.1.2 Regression Model 105
5.2.3 Influence of the Process Parameters on the Sa 108
5.2.4 Process Parameters Optimization 113
5.2.5 Surface Roughness (Sa) Analysis 115
5.2.6 Summary 119
CHAPTER 6: CONCLUSIONS AND FUTURE SCOPE 120
6.1 Conclusions 120
6.2 Future Scope of Work 124
REFERENCES 126

RESEARCH PUBLICATIONS 162

CURRICULUM VITAE 164

LIST OF FIGURES

Fig.1. 1 Densities of various metals 2
Fig.1. 2 Ti alloy phases and their attributes 3
Fig.1. 3 Application of Ti alloy in implants in the entire body: b) The implants need nano-finishing 5
Fig.1. 4 Mechanical properties of Ti alloys compatible with human bones 6
Fig.1. 5 The requirements for metal implants 7
Fig.1. 6 Classification of finishing processes 8
Fig.1. 7 Timeline of the development of the advanced nano-finishing processes 9
Fig.1. 8 Classification of the abrasive flow finishing process 10
Fig.1. 9 AFF process schematic diagram [79,80] 11
Fig.1. 10 MFAF process setup, surface roughness, and effect of process parameters on the Sa [91,93] 13
Fig.1. 11 MRF, AFF, and MRAF process the relationship 14
Fig.1. 12 MRAF process schematic diagram [100–102] 15
Fig.1. 13 R-MRAFF Schematic diagram with the femoral knee in four different points faces [108,110] 17
Fig.1. 14 BEMRF Process Mechanism with Surface profiles a) before and b) after finishing [69] 19
Fig.1. 15 Schematic of the layered structure of titanium alloys (a) before (native oxide) and (b) after chemical [125] 21
Fig.1. 16 Schematic diagram of the CP and ECF process [118,133] 22
Fig.1. 17 ZYGO surface roughness and topography a) before, b) after the CMP process [131] 24
Fig.1. 18 3D profile and morphology for surface (a) before and (b) after ECFAP [138] 25
Fig.1. 19 UAMAF process setup and 3D profile of surface roughness and micrograph [70]. 27
Fig.1. 20 Comparison of nano-finishing techniques (Ti alloys)

[21,69,70,80,102,108,138,149–151] 28

Fig.2. 1 Timeline of the development of the CMMRF process [61]. 35

Fig.2. 2 The number of publications on CMMRF processes. (Data retrieved from the Web of Science on 03/04/2024) 36

Fig.2. 3 Effect of chemical process passivation on different materials [60,156,165,169]..... 38

Fig.2. 4 A diagram illustrating the components of the MR finishing in the CMMRF process..... 44

Fig.2. 5 An optical image of MR finishing a) without a magnetic field and b) under the effect of a magnetic field and shear strain [195,196]..... 44

Fig.2. 6 CMMRF magnetic abrasive preparation for MR finishing: a) the conventional sintering (SMA), and b) Composite magnetic abrasives (CMA) [150,200]..... 45

Fig.2. 7 Comparison of Sa values over time through different advanced nano-finishing processes [62,91,111,150,156,217,218]..... 54

Fig. 3. 1 Methodology..... 61

Fig. 4. 1 Ti64 alloy surface morphology, with the metal elements compositions and XRD..... 64

Fig. 4. 2 Surface preparation process of Ti64 alloy 65

Fig. 4. 3 Schematic representation of the novel process procedure for surface modification of Ti64 alloy by environmentally friendly chemicals..... 67

Fig. 4. 4 Schematic diagram of the CH-MR finishing process mechanism..... 69

Fig. 4. 5 CNC machine with Setup tool (a), MR finishing under the effect of the magnetic field, and without the influence of the magnetic field (b)..... 72

Fig. 4. 6 Scanning Electron Microscope attached with an EDS detector. 73

Fig. 4. 7 Vickers Hardness Machine (Duramin-40 M1 (ASTM E384) 74

Fig. 4. 8 Linear Reciprocating tribometer (ASTM-G133)..... 76

Fig. 4. 9 Surface roughness tester (Taylor-Hobson) 77

Fig. 4. 10 Potentiostat/Galvanostat Device..... 78

Fig. 5. 1A) FESEM image of surface morphology of Samples A.a) without modification,

A.b) (with pH5), A.c) (with pH7), A.d) (with pH9), and (B) the average particle size diameter for the surface modification (group A) 82
Fig. 5. 2 EDS spectra with the composition (W%) of Ti64 alloy (group A), a) before processing, b) after processing (with pH 5), c) after processing (with pH 7), and d) after processing (with pH 9) 84
Fig. 5. 3 Cross-sectional morphology of the deposited layer on the Ti64 alloy (a), b) EDS analysis of the layer on the surface 85
Fig. 5. 4 FTIR spectrum for samples Group (A) (a), and b) the formula of the chemical solution used in the process 86
Fig. 5. 5 The microhardness tester of sample group (A): a) the microhardness tester, b) the microhardness of sample group A 88
Fig. 5. 6 Surface characterization of Samples (Group A), a) the average surface roughness, b) contact angle, c) roughness profile, d) the adhesion test, and e) the ISO Class: 2/ASTM Class: 3 B. 89
Fig. 5. 7 (a) Schematic of linear tribometer with sample, b) the wear rate of samples (group A), c) the friction coefficient (COF) of samples (group A) 92
Fig. 5. 8 The hemolysis test on the samples (group A) (a), b) the result of the hemolysis ratio (%) for samples (group A) 93
Fig. 5. 9 Surface Morphology of Ti64 alloy samples (group B) by optical microscopic images at 1000× magnification (a); (b) Potentiodynamic polarization curves for samples group B 95
Fig. 5. 10 EDS spectra of samples (group B) with FESEM micrographs showing the hydroxyapatite grown on the surface, a) before processing, b) after processing (with pH5), c) after processing (with pH7), d) after processing (with pH9) 98
Fig. 5. 11 The cross-section of the Ti64 alloy surface modification (a); FTIR spectra of samples after chemical modification and immersion in HBSS for 15 days with pH values (5,7, and 9) 100
Fig. 5. 12 Optical microscopy along with FESEM for the formation of the oxide layer by chemical treatment with eco-friendly chemicals on Ti64 alloy, a) with (pH 5), b) with (pH 7), and c) with (pH 9) 103
Fig. 5. 13 a) Cross-section for the oxide layer on the Ti64 alloy, b) EDS images for the

growth of the oxide layer with (pH5), c) with (pH 7), and d) with (pH9). 105
Fig. 5. 15 Graphs for response surface regression analysis: Normal probability plot (a), Pareto chart for standardized effect (α = 0.05) (b) 108
Fig. 5. 16 The main effect plot for CH-MR process parameters on the Sa (a) and the pie chart for the percentage contribution of various significant factors (b) 109
Fig. 5. 17 Interaction effects of Sa vs. pH value, RS, and WG with the contour plot. 110
Fig. 5. 18 Interaction effects of Sa vs. WG and RS with 3D plot surface and contour plot. 111
Fig. 5. 19 The interaction plot of Sa vs. C and WG with the contour plot 112
Fig. 5. 20 Plot optimization for Sa with CH-MR process parameters 114
Fig. 5. 21 Roughness profile for Ti64 alloy before and after the CH-MR process 115
Fig. 5. 22 SEM images of Ti64 alloy before the CH-MR process (a), and after CH-MR with optimal parameters (b), AFM image for Ti64 alloy before the CH-MR process (c), and after CH-MR with optimal parameters (d) 116
Fig. 5. 23 XPS spectra of Ti64 alloy surface sequence elements (a) after eco-friendly treatment, and after the CH-MR process (b) high-resolution spectrum Ti 2p, and (c) O 1s 118

LIST OF TABLES

Table 2. 1 Different chemical reagents are used for etching processes on various materials. 39
Table 2. 2 Various Nano-finishing Processes in Biomaterials. 40
Table 2. 4 The change of surface characterization of different materials by the (CMMRF) process..... 47
Table 2. 5 The limitations of various nano-finishing processes on different materials..... 50
Table 2. 6 Nano finishing of various metals and alloys by the CH-MR finishing process 52

Table 4. 1 Composition of Ti64 alloy..... 61
Table 4. 2 Properties of Ti64 alloy 62
Table 4. 3 MR finishing compositions..... **63**
Table 4. 4 The surface modification sample groups..... 65
Table 4. 5 Coded and actual values of the ch-mr process parameters. 69
Table 4. 6 The CCD experimental runs and resulting Sa of ch-mr finishing of Ti64 alloy 69

Table 5. 1 electrochemical parameters of Ti64 alloy samples (group b)..... 93
Table 5. 2 ca/p atomic ratio (at%) of Ti64 alloy (group b) after soaking in the HBSS for 15 days 96
Table 5. 3 Analysis of Variance (anova) for sa 105
Table 5. 4 The experimental and predicted sa values for ch-mr optimal sa 113

LIST OF ABBREVIATIONS

SYMBOL	ABBREVIATIONS
AFF	Abrasive Flow Finishing
AFM	Abrasive Flow Machining
ASTM	American Society for Testing and Materials
BEMRF	Ball End Magneto-rheological Finishing
CP-TI	Commercially Pure Titanium
CP	Chemical Finishing Process
CR	Corrosion Rate
CUMAF	Chemo Ultrasonic Assisted Magnetic Abrasive Finishing
CMP	Chemical Mechanical Process
CMMRF	Chemo-Mechanical Magneto-rheological Finishing
CH-MR	Integrated chemical followed by Magneto-rheological Finishing
CIPS	Carbonyl Iron Particles
MPa	Mega Pascal
GPA	Giga Pascal
WCA	Water Contact Angle
FMAB	Flexible Magnetic Abrasive Brush
MFAF	Magnetic Field-Assisted Finishing Process
MAF	Magnetic Abrasive Finishing
MRAFF	Magneto-rheological Abrasive Flow Finishing
MR	Magneto-rheological Fluid

MRF	Magneto-rheological Fluid Finishing
MRAH	Magneto-rheological Honing Finishing
MRJF	Magneto-rheological Jet Finishing
MRR	Material Removal Rate
UAMAF	Ultrasonic Assisted Magnetic Abrasive Finishing
R-AFF	Rotational abrasive Flow Finishing
R-MRAFF	Rotational Magneto-rheological Abrasive Flow Finishing Process
ECP	Electrochemical Finishing Process
ECFAP	Electrochemical Process Assisted by a High-speed Flow of Abrasive Particles
PBS	Phosphate Buffered Saline solution
SMA	Sintering Magnetic Abrasives
SIC	Silicon Carbide
SA	The Roughness of Surfaces
Δ SA	Change in the Surface Roughness
SEM	Scanning Electron Microscope
THCP	Thermochemical process
FE-SEM	Field Emission-Scanning Electron Microscope
FTIR	Fourier Transformed Infrared Spectroscopy
XRD	X-ray Diffraction
EDS	Energy Dispersive Spectrometry
XPS	X-ray Photoelectron Spectroscopy

ABSTRACT

Nano-finishing processes have transformed industrial surface finishing by offering significant opportunities to enhance surface integrity, particularly in biomedical applications. With the rising demand for artificial implants, expectations and standards for surface roughness are continually increasing. Achieving a consistent nanoscale finish remains a critical challenge, especially for replacement implant components such as femoral, knee, elbow, and hip joints, which must comply with ISO 7206-2:2011/AMD 1:2016 standards. Ti-6Al-4V (Grade 5) alloy is widely used in biomedical implants due to its superior combination of strength, toughness, corrosion resistance, biocompatibility, and relatively low density. Its α+β microstructure further enhances adaptability for biomedical applications. However, conventional finishing methods are effective for macro- and micro-scale finishing but are insufficient for achieving nanoscale precision, often leading to surface flaws such as cracks. To overcome these limitations, advanced finishing techniques such as magneto-rheological finishing (MRF) and abrasive flow finishing (AFF) have been developed. While they improve precision, challenges persist, including low finishing rates, microcrack formation, surface degradation, and reliance on hazardous chemicals, which raise concerns about safety and the environment. Future processes must therefore be more efficient, sustainable, and capable of achieving nanoscale precision without compromising material integrity or biocompatibility.

This thesis develops two advanced processes for surface modification of Ti64 alloy for biomedical implant applications by sustainable, eco-friendly chemicals, including citric acid, Hydrogen peroxide, and Sodium hydroxide. Firstly, a novel thermochemical process (THCP) was developed, followed by simulated mineralization in Hank's Balanced Salt Solution (HBSS) to enhance the mechanical properties, biocompatibility, and bioactivity of Ti64 alloy. The study investigates the effects of eco-friendly chemicals on surface characteristics by

evaluating their ability to modify surfaces and determining the optimal pH value. The findings demonstrated that the modification effectively enhanced the Ti64 alloy's mechanical properties, with a significant increase in average microhardness of approximately 71% and a reduction in wear rate of approximately 64.29%, compared to the untreated Ti64 alloy. The surface modification with pH (5, 7, and 9) revealed absorptive properties, as evidenced by a contact angle below 90 °, indicating a hydrophilic surface that enhances cell attachment to biomaterials. After soaking Ti64 alloy in HBSS, a uniform coating layer of approximately 20.5 μm formed, leading to increased bioactivity, as evidenced by a Ca/P ratio of 1.67, comparable to that of hydroxyapatite in human bone. The hemolysis ratio of 0.027% at pH 7 indicates minimal Red Blood Cell (RBC) lysis and increased biocompatibility. The corrosion rate was enhanced with pH (5,7 and 9) approximately (1.975×10^{-2}, 1.078×10^{-2}, and 1.615×10^{-2}) mm/year, respectively. These findings indicate that the novel process at neutral pH (7) is optimal for surface modification, as it is the most effective at enhancing the biocompatibility and bioactivity of the Ti64 alloy, making it suitable for biomedical implants.

Secondly, an advanced finishing process using a hybrid chemical process to oxidize and soften the Ti alloy surface, followed by a magnetorheological fluid (CH-MR) to achieve nanoscale roughness with reduced processing time and enhanced surface quality. To systematically evaluate and optimize the influence of CH-MR process parameters, a Central Composite Design (CCD) under Response Surface Methodology (RSM) was employed. CCD combines factorial or fractional factorial points, axial points, and center points to develop a quadratic model for predicting and optimizing process responses. In this study, CCD was used to investigate the effects of critical parameters of pH value, working gap (WG), rotational speed (RS), and current (C) on the surface roughness (Sa) of Ti64 alloy. Analysis of Variance (ANOVA) revealed pH as the most influential parameter (19.14% contribution), followed by WG (15.73%), RS (12.85%), and C (9.93%), while the remaining variation was attributed to parameter

interactions. Optimization yielded a minimum Sa of 38.20 nm after 30 minutes of finishing under the optimal parameters of pH of 5, a WG of 0.5 mm, an RS of 150 rpm, and a C of 3.5 A.

Surface morphology and integrity were assessed using Field Emission Scanning Electron Microscopy (FESEM) and Atomic Force Microscopy (AFM), confirming a significant reduction in surface roughness and improvements in quality, with fewer surface defects. X-ray Photoelectron Spectroscopy (XPS) further elucidated the finishing mechanism, linking surface oxidation states to enhanced chemical-mechanical synergy. These characterizations validated the CH-MR process's ability to improve surface roughness and confirmed the absence of contamination or subsurface damage, both of which are crucial for biomedical and aerospace applications.

CHAPTER 1: INTRODUCTION

This chapter presents an overview of Titanium and its alloys in biomedical applications, covering their properties, significance, and applications as implant materials. It also discusses the classification of surface finishing techniques, with a focus on nano-finishing methods, and concludes with a summary of key insights

1.1 Introduction to Titanium and Its Alloys

Titanium (Ti) and its alloys are widely used as biomaterials in human body implants, such as those for shoulder, knee, and hip joints [1–3]. These biomaterials have excellent mechanical properties and biocompatibility compared with other metals, making them suitable for medical implants [4–6]. Stainless steel and cobalt-chrome alloys are considered primary metals for orthopedic implants due to their mechanical properties and lower corrosion rates. However, Ti and its alloys have replaced them due to their superior properties, such as inertness toward tissues and bodily fluids [4,7–9]. In addition, after the implantation of Ti and its alloys, no toxic elements are released [10,11].

Ti and its alloys are widely recognized for their unique mechanical and lightweight properties. Fig. 1.1 illustrates the densities of different light and heavy metals [12]. Ti alloys weigh around 56% less than stainless steel, despite having twice the yield strength and a 25% greater ultimate tensile strength [13]. They are widely used in various applications due to their remarkable specific strength and approximately 4.5 g/cm^3 density. They have a high tensile strength of around 1400 MPa at ambient temperature and, on heating, exhibit noticeable reactivity with other substances [13,14]. In addition to having a lower Young's modulus than certain other metals, Ti alloys have several other beneficial properties that make them very useful in various applications [4,7].

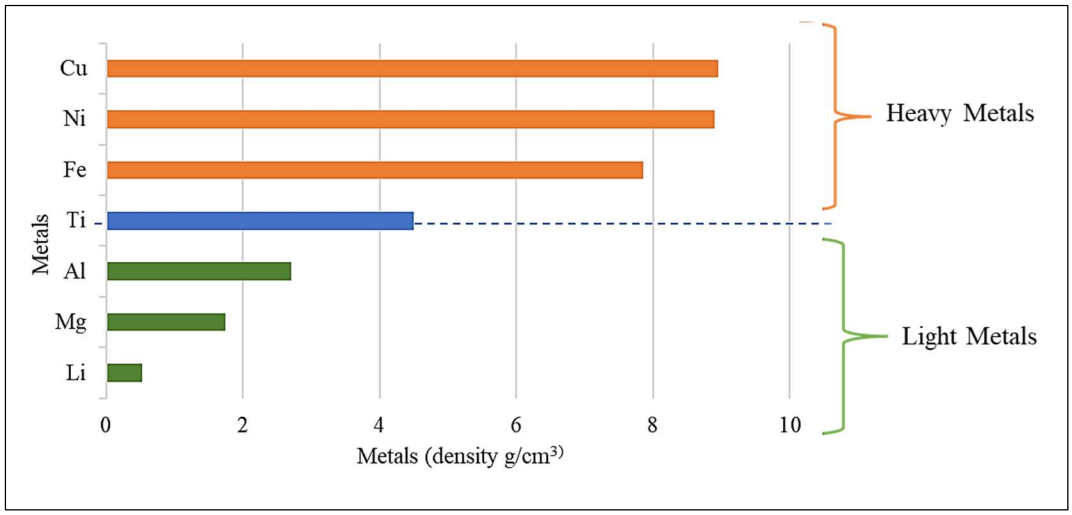

Fig.1. 1 Densities of various metals

It is essential to understand their mechanical characteristics to evaluate their suitability for applications in aerospace, automotive, and biomedical implants [15]. There are three classifications of the microstructure of Ti alloys: alpha (α), near beta (β), and alpha + beta (α + β), as shown in Fig.1.2. The phase β crystalline structure is face-centered cubic, while the phase α crystalline structure is hexagonal close-packed [16]. At higher temperatures, α-stabilizers such as aluminum, oxygen, and nitrogen promote phase development. On the other hand, β stabilizers, which include metals such as nickel, vanadium, niobium, tantalum, molybdenum, chromium, copper, and iron, maintain the β phase stable at lower temperatures. In their study, Nakai et al. emphasized the stabilizing influence of hafnium and zirconium on two different phases, α and β, within a Ti alloy [17].

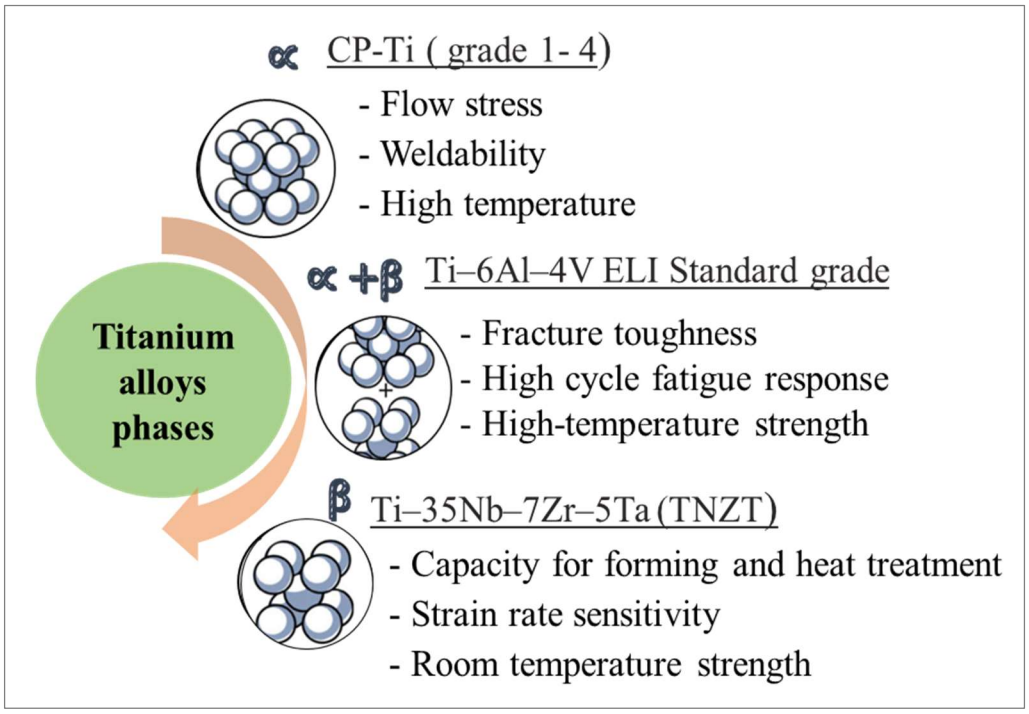

Fig.1. 2 Ti alloy phases and their attributes

1.2 Titanium and Its Alloys in Biomedical Applications

William Gregor first discovered Titanium in 1791, and it was later identified in 1795 by Martin Heinrich Klaproth; it is named after the Greek Titans. Metallurgist William Kroll invented the Kroll process in 1946 to simplify the extraction of significant volumes of pure Ti, even though there is a lot of Titanium in the Earth's crust [18]. Titanium-based medical, surgical, and dental device development began after World War II. Numerous studies have investigated the various applications of Ti alloys across industries, including the production of engines for the aerospace sector [19–22], as well as chemical, nuclear [9], military [23], marine [24], and medical applications [4,25–28].

Fig. 1.3 discusses Titanium and its alloys in biomedical implants in the human body, such as arthroplasty, dental implants, and craniofacial and maxillofacial implants [26], with the primary focus on the implant parts that need the nano level of finishing, such as shoulder, femoral knee, hip, and elbow joints (Fig. 1.3 (b)). Alloy CP-Ti is used in dental and orthopedic implants [29–31].

However, its use is limited to implant parts such as bone screws, hip implants, and plates. To overcome its limitations, Ti alloy grade 5 (Ti64) is extensively used on other implant parts [28,32–34] due to its better biocompatibility with the human body and higher wear resistance [35,36], (Ti-6Al-7Nb) alloy is used in dental, cardiovascular, and joint implants [37], and (Ti-15Mo-5Zr-3Al) alloy is used in surgical implants [38,39]. Moreover, the (Ti–30Nb–3Ag) alloy is used in orthopedic and dental applications, offering enhanced antimicrobial and corrosion resistance [40]. In addition, (NiTi) alloy is used in an implant with shape memory to improve wear resistance and pseudo plasticity [41].

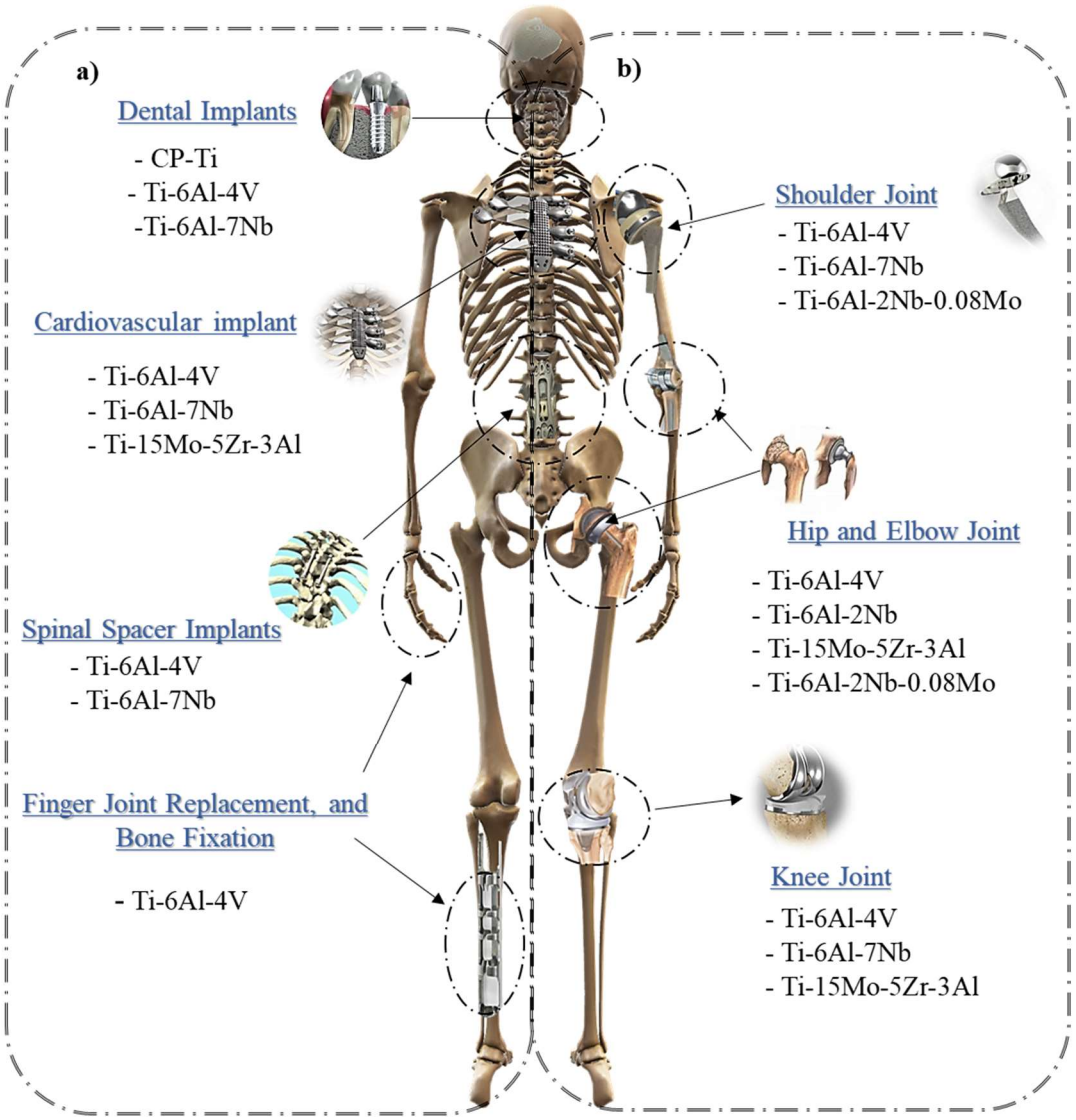

Fig.1. 3 Application of Ti alloy in implants in the entire body: b) The implants need nano-finishing

Ti alloys are a better choice for orthopedic applications requiring hard-tissue replacement due to their lower elastic modulus and reduced stress shielding [42]. Fig. 1.4 shows the yield strength, ultimate strength, and Young's modulus for Ti alloys and bone [43,44]. A biomaterial's Young's modulus should be close to that of a cortical bone used as a benchmark bone for better results, because the possibility of resorption tends to increase if Young's modulus greatly exceeds that of the benchmark bone [45].

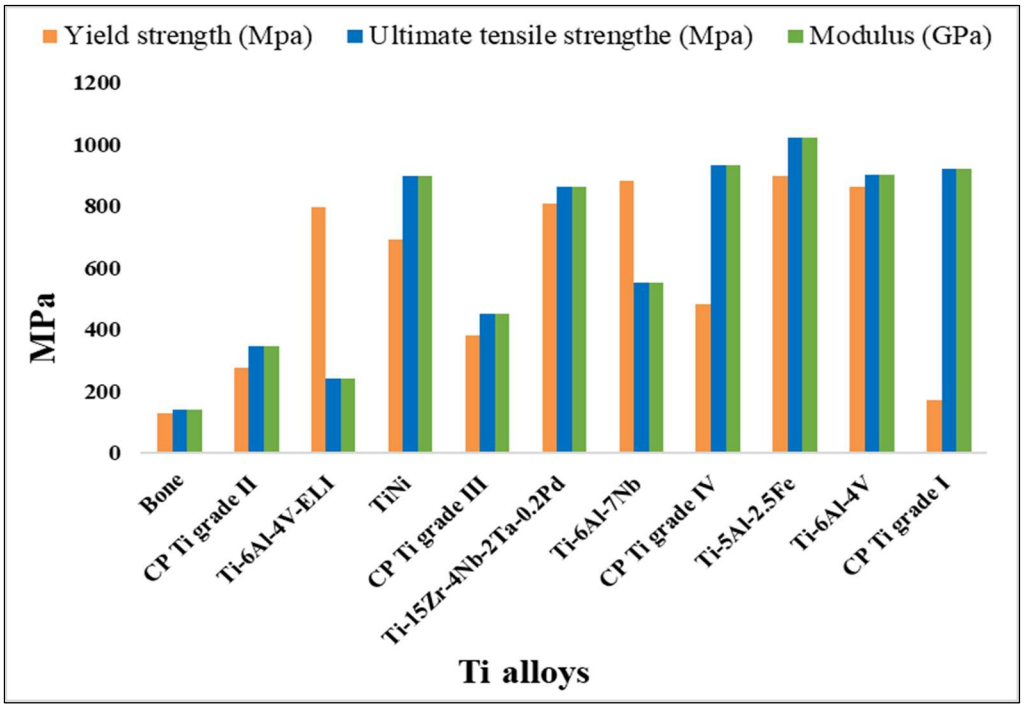

Fig.1. 4 Mechanical properties of Ti alloys compatible with human bones

The selection of biomaterial alloys for biomedical applications is crucial in ensuring the success of medical devices and implants, as well as biocompatibility, mechanical strength, corrosion resistance, and surface characteristics [46]. Moreover, studying the tribological properties of biomedical materials is crucial to making biomedical implants and equipment last longer by reducing wear and friction [47]. Fig. 1.5 depicts the requirements for a metal implant. Ti alloys are considered more compatible and have little toxicity due to the natural formation of a protective oxide layer that shields the metal from further oxidation and offers strong corrosion resistance compared to other metal alloys [3]. Moreover, several investigations can be conducted, such as evaluating the corrosion resistance of Ti64 and Ti-6Al-7Nb alloys in a Phosphate-buffered saline (PBS) solution to assess how these alloys perform in a physiological simulation environment. Ti-6Al-7Nb alloy displayed better corrosion resistance than Ti64 alloy, which is attributed to niobium's superior corrosion resistance compared to vanadium [48]. Moreover, the implant's success depends on morphological compatibility, which

encourages bone cell growth at the implant site; mechanical compatibility, which allows stress transfer between the implant and live tissue; and biological compatibility, which ensures the implant is not hazardous to surrounding tissues [49,50].

64

Biocompatibility and osseointegration are crucial for the effectiveness and longevity of orthopedic implants, as they describe the materials' ability to interact with the biological environment and influence various forms of bone formation. They are classified into three types: "biotolerant," which encourages remote osteogenesis; "bioinert," which facilitates contact osteogenesis; and "bioactive," which promotes bonding osteogenesis [51].

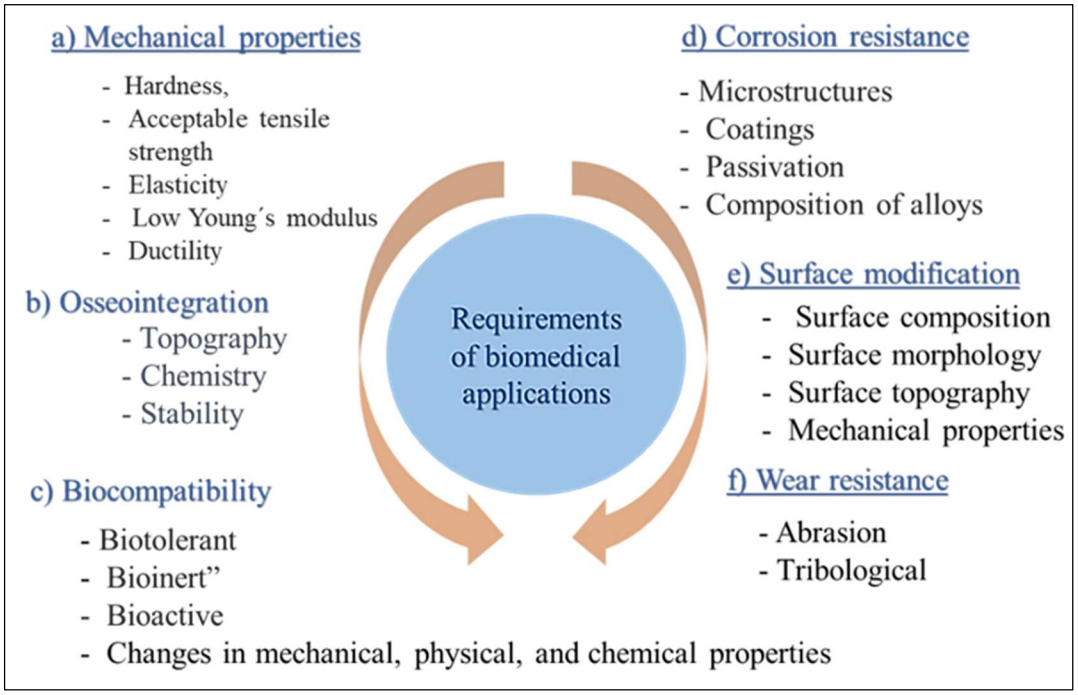

Fig.1. 5 The requirements for metal implants

1.3 Finishing Process Classifications

There are two surface-finishing processes, as shown in Fig. 1.6: traditional and nontraditional. Traditional machining methods, such as grinding, lapping, chemical etching, and blasting, provide a good surface finish. However, these processes are less effective at accurately finishing complex surfaces [52] , due to

a lack of control over the force [53] and the high pressure that may damage the polished surface [54], resulting in more flaws on the final surfaces [55]. Nontraditional machining is a collection of operations employing electrical, thermal, chemical, and mechanical, or a hybrid of these methods, to overcome the limitations of conventional machining [56]. These methods remove materials from a surface with high accuracy, providing good surface smoothness and complex geometries in machined parts without burrs or residual stresses [56].

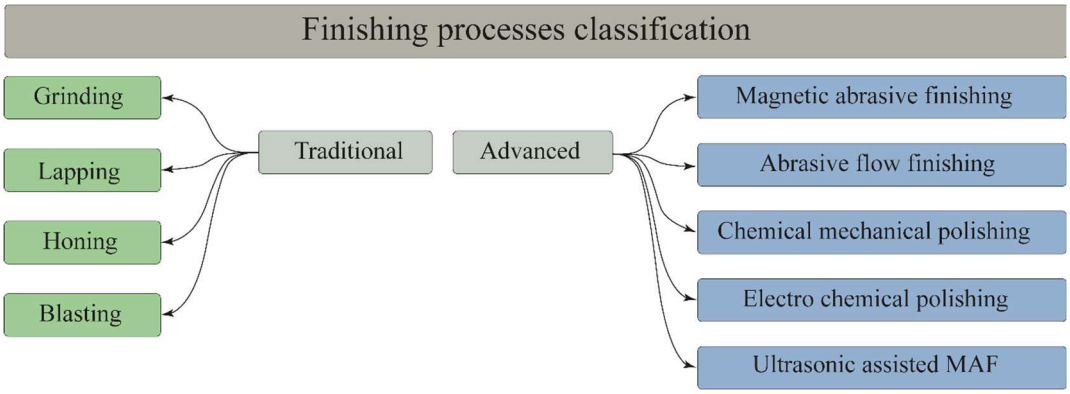

Fig.1. 6 Classification of finishing processes

Nano-finishing processes are advanced finishing techniques that enhance surface integrity. Surface integrity refers to the condition and characteristics of a machined surface that affect its functional performance. Surface integrity comprises two main components: the outer topography, commonly referred to as surface finish, and the inner subsurface layer, which encompasses the microstructure, mechanical properties, and residual stresses [57]. Surface integrity is strongly influenced by topography and mechanical properties, which, in turn, significantly affect stress distribution and tissue adhesion. Enhancing functional performance and aesthetics is particularly crucial in biomedicals, where roughness plays a significant role [58]. On the other hand, hybrid advanced finishing processes such as Chemo-mechanical magneto-rheological finishing (CMMRF), Chemo Ultrasonic Assisted Magnetic Abrasive Finishing (CUMAF), Electrochemical process assisted by a high-speed flow of abrasive particles

(ECFAP), and MFAF have been developed to integrate the benefits of both traditional and nontraditional processes [56,59,60] to overcome their limitations and efficiently produce finishing freeform parts with more complex shapes with high-quality surfaces [61,62].

The history of advanced finishing processes involves several decades, starting with the invention of MRF in 1963 by Jacob Rabinow. Then, Kordonski and his research team developed the MRF in the late 1980s [63–65] and gradually developed novel approaches, including AFM, ECP, R-MRAF, and BEMRF, as shown in Fig. 1.7 [61]. As a result of this ongoing development, significant improvements in precision, surface quality, and material-specific finishing have been achieved, thereby meeting the evolving demands of various industrial applications [61,66–72].

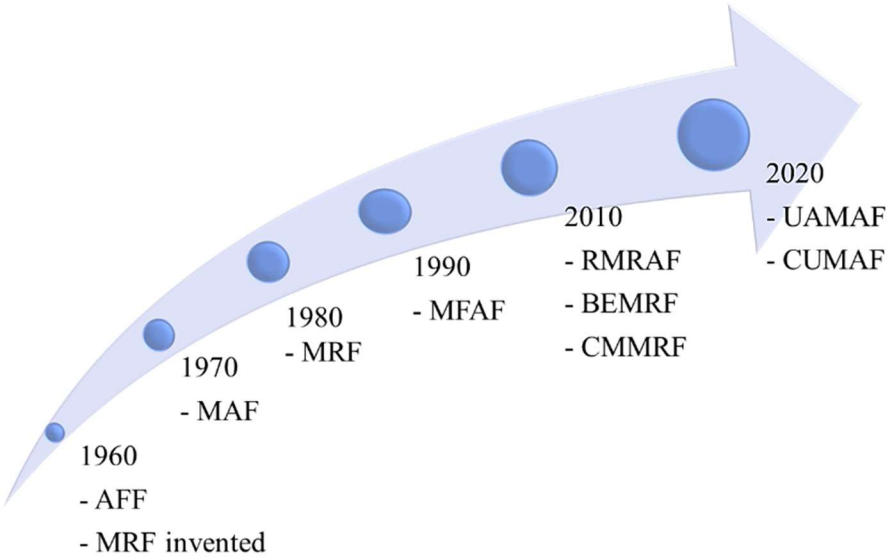

Fig.1. 7 Timeline of the development of the advanced nano-finishing processes

1.3.1 Mechanical Finishing Processes

Mechanical finishing processes are advanced finishing techniques for achieving accurate micro- to nano-scale surface finishes. The processes that stand

out among these are (AFF), (AFF), (MFAF), (MRAFF), (MAF), and (R-MRAFF). These processes significantly aid in achieving precise surface finishes, which are essential for various biomedical applications, by using magnetic forces to control abrasive particles and achieve the desired finish.

1.3.1.1 Abrasive Flow Finishing Process (AFF)

AFF is an advanced finishing process invented in the 1960s by Extrude Hone Corporation for deburring cylinder-shaped blocks [73]. This process has become the most advanced finishing method, based on the configuration and motion of the media cylinders. AFF can be divided into four categories, as shown in Fig. 1.8: one-way AFF, two-way AFF, multi-way AFF, and orbital AFF. In each category, showcasing a variety of capabilities for obtaining desired surface finishes [74].

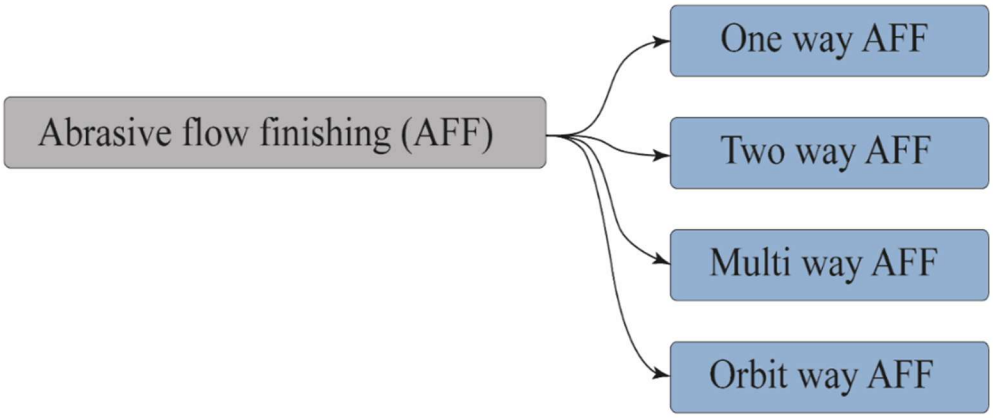

Fig.1. 8 Classification of the abrasive flow finishing process

Fig. 1.9(a) illustrates the working principle of AFF, which involves various elements, including tooling, machine parts, fixtures, a specific abrasive, the composition of the flow-machining media, and process conditions [75]. The abrasive grain must be at least 20% harder than the workpiece to be considered an abrasive [76]. Extrusion pressure is applied by hydraulic cylinders, which causes normal and axial stresses on the abrasive particles. While the axial force allows the abrasive to move axially and effectively remove material from the surface, the regular force pushes into the work surface [77]. Hiremath et el. 2016 [78] used

Visco-elastic polymer in conjunction with abrasive particles in a particular ratio to create a semi-solid medium under pressure; this medium is extruded through or over the surface to achieve a desired surface finish, as shown in Fig. 1.9 (c), surface morphology for the workpiece before, and after finishing by AFF processes [79].

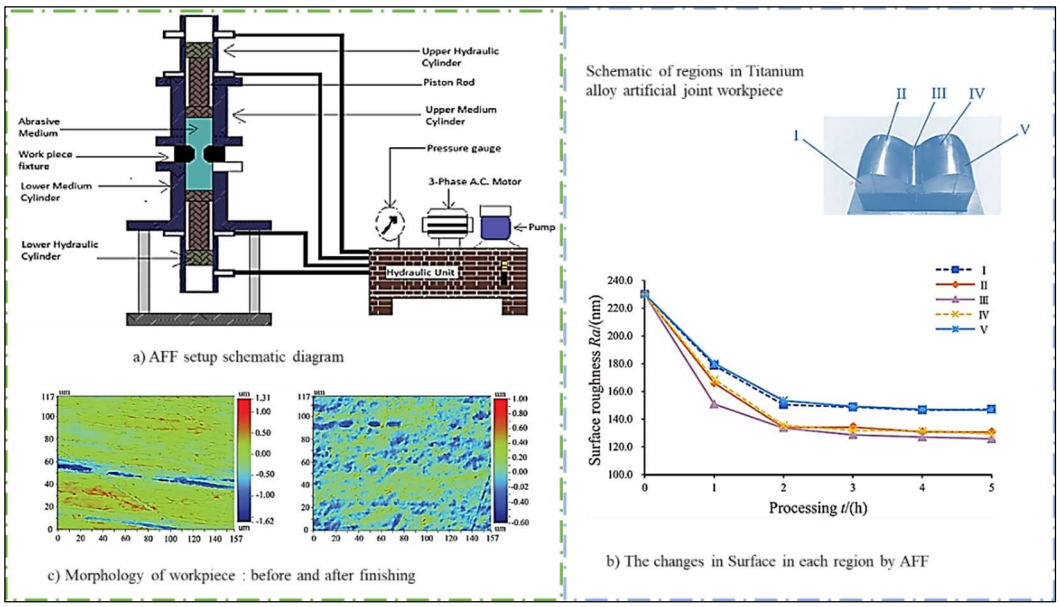

Fig.1. 9 AFF process schematic diagram [79,80]

The AFF process can effectively polish, deburr, and radius difficult-to-finish materials [81], achieving a high-quality surface finish for many complex geometries in various manufacturing parts, such as bolt head dies and turbine blades [11, 98, 101]. In the medical industry, the AFF process produces different biomedical parts manufactured with Ti alloys, including heart valves, dental crowns, and knee, hip, and elbow joints [23, 101–103]. It produced a low Sa of 39 nm. in the hip joint, improved tribological features, reduced friction between the prosthetic hip ball and socket, and minimized implant wear and tear [84]. Moreover, it enhances the implant surface's wettability and surface finish, thereby reducing the likelihood of bacterial adhesion on the implant surface [85]. AFF produces good surface finishes, and the interaction between processing time and abrasive particle size significantly influences the machining process, as shown in Fig. 1.9(b) [80]. However, the finishing takes a long time. Sankar (2009)

developed an (R-AFF) process to address this issue, thereby enhancing performance, improving surface finishing capabilities, and reducing time. In the (R-AFF) process, the workpiece is rotated while the abrasive-filled medium oscillates. The combined motion extends the contact routes of the active abrasive particles, resulting in longer shearing actions. Adjusting the medium's velocity and rotation speed can create a crosshatch pattern on the workpiece's surface. The abrasive particles are subjected to tangential, radial, and axial forces [86].

1.3.1.2 Magnetic Field-Assisted Finishing Process (MFAF)

The conventional AFF process has been extended to MFAF by adding a magnetic field to enhance surface analysis capabilities [87]. Fig. 1.10 (a) depicts the tool with MRF. The MFAF process uses ferromagnetic abrasive particles to sort magnetic materials using magnetic force. These ferromagnetic abrasives cause microchipping and microplowing on the surfaces [88]. Qian et al. (2020) [67] categorized the finishing process by MAF, MRF, and MRAFF based on different finishing media, bonded or unbound abrasive, and MRF. In industrial biomedicals, finishing capillary tube components with small diameters presents a significant challenge due to their size. These tubes require high-precision nano-finishing to meet the demanding requirements of modern biomedical and implant parts. Therefore, the MFAF process has produced an internal capillary tube (inner diameter = 0.4 µm) [108, 109]. Barman and Das (2018) [91] studied the effects of the MFAF process on surface finish and reported an improvement in the ΔSa by approximately 83.33%. The Sa has been reduced from 120 to 20 nm (Fig. 1.10 (c)). AFM image topography at high resolution has provided extensive information about the surface shape at the nanoscale [92]; the surface was smoother, with lower peak and valley heights than the initial surface, which had scratches, high peaks, and deep valleys. In addition, Barman and Das (2019) [93] developed a novel MFAF tool to achieve nano-finishing of bio Ti alloy, with the final Sa being 10 nm from the initial Sa = 0.12 µm (Fig. 1.10 (d)) with a very high percentage reduction (approximately Sa 98.21%) in the surface roughness. Furthermore, it examined the impact of abrasive particle concentration on surface finishing and

found that both the initial roughness and the abrasive particle concentration notably influenced the finishing rate. However, a parallel toolpath demonstrated a superior surface finish (ΔSa 93.3%) compared to the spiral toolpath (ΔSa 71.4%). ISO 7207-2:2011 was also established as a standard for surface roughness of semi-permanent implant materials [94]. The optimal process parameters for achieving the best surface finish are a rotational speed of 1200 rpm, a working gap of 1 mm, and a finishing time of 6.30 hours, as shown in Fig. 1.10b.

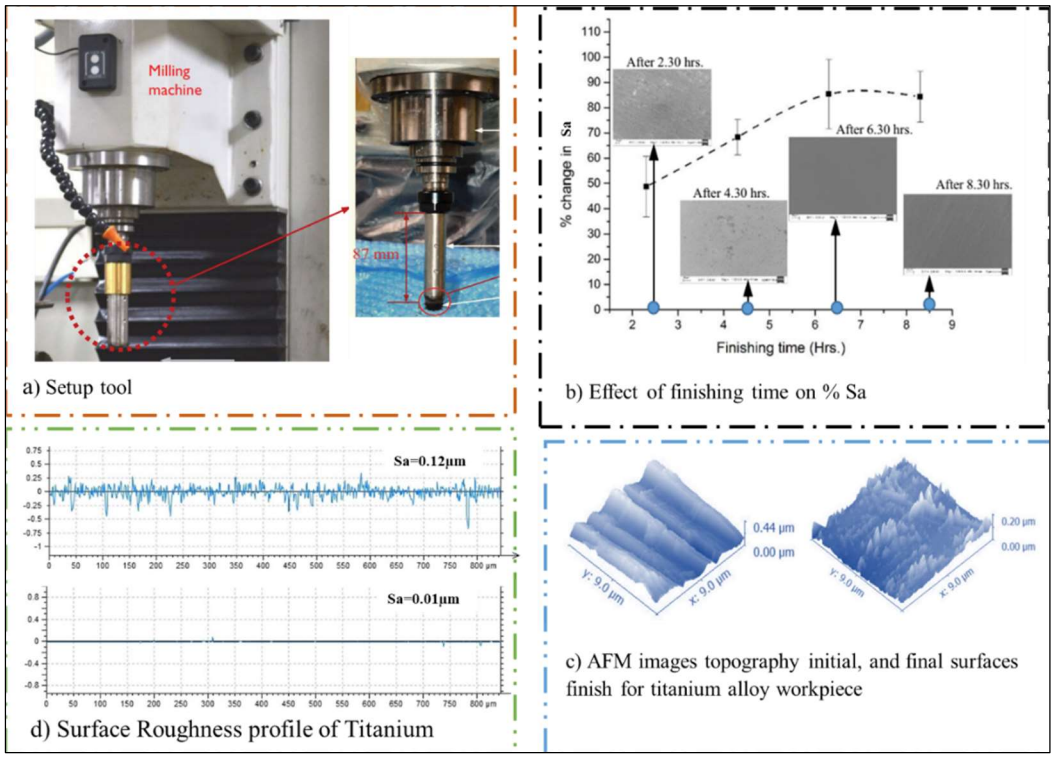

Fig.1. 10 MFAF process setup, surface roughness, and effect of process parameters on the Sa [91,93]

FESEM images reveal the microstructure of the Ti64 alloy before and after the MFAF finishing process. The original surface exhibits scratches, and after finishing, the surface microstructure reveals reduced surface flaws and improved surface quality (Fig. 1.10a).

MFAF is an effective method for manufacturing biomedical implants. It combines magnetic fields and abrasive particles to enhance the surface quality and

mechanical properties of implants, thereby improving their performance and longevity [67]. During the machining of Ti64 alloy, the MAF process tools helped improve dimensional accuracy and overall surface integrity and considerably reduced ΔSa by 50%–60% [95].

1.3.1.3 Magneto-rheological Abrasive Flow Finishing Process (MRAFF)

The MRAFF process, a variant of the MAF process, utilizes the same AFM setup. However, it distinguishes itself by using MRF rather than a conventional polishing medium. Additionally, the MRAFF process introduces an external magnetic field as an additional element in the finishing procedure. Fig. 1.11 depicts the relationship of MRAFF with AFM and MRF. Moreover, these innovative modifications offer the potential for further improvements in surface finishing and polishing efficiency, making the MRAFF technique a promising advancement in the field of advanced finishing [96–98].

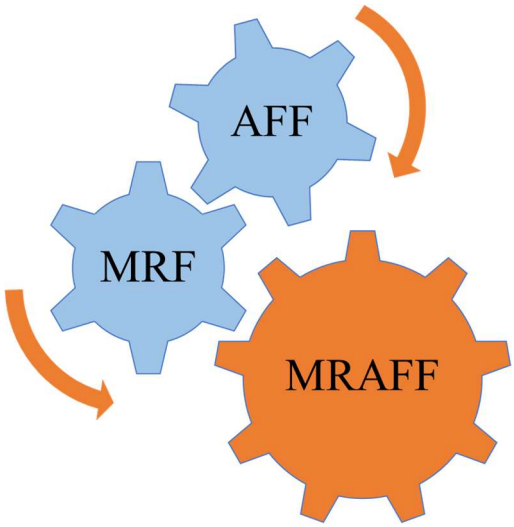

Fig.1. 11 MRF, AFF, and MRAF process the relationship

MRAFF is an efficient surface-finishing process that produces extremely flat, detailed 3D features. This process uses MRF, which was developed and recognized by [99], enabling diverse practical applications due to its intelligence and ease of management. Exposure to magnetic fields can cause a liquid to change state to a solid. Chain-like structures align in the direction of the magnetic field

when a magnetic field is applied, resulting in significant changes in the rheological properties of the MRF [54]. Fig. 1.11(A) graphically depicts the MRF behavior, specifically the shear force. This shear force, resulting from the combined magnetic and centrifugal forces, plays a crucial role in smoothing the surface undulations of Ti alloys.

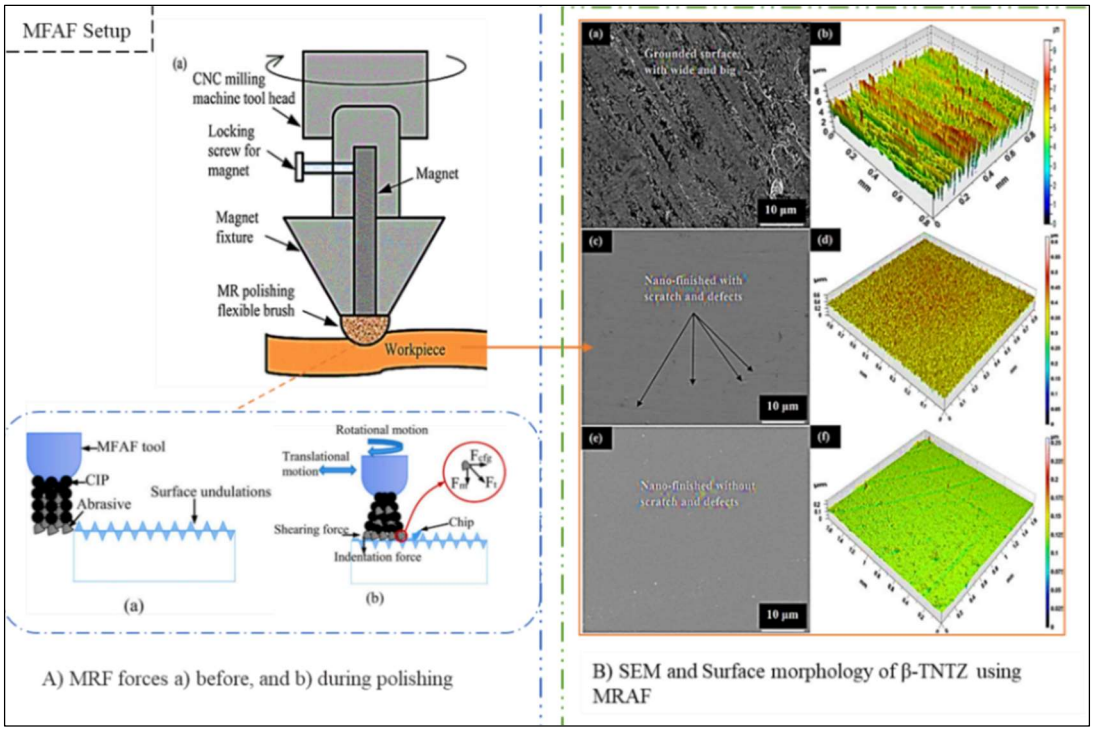

Fig.1. 12 MRAF process schematic diagram [100–102]

The MRAFF process yields a satisfactory surface finish in the biomedical field, particularly on the surface of Ti alloys, and improves surface morphology [103]. Singh et al. (2020) [104] studied the effect of nano-finishing of a Ti-Nb-Ta-Zr alloy using the MRFAF process and the improvement in the biological functionality of the surface. The ΔSa increased by over 95%, from 1.121 µm to 46 nm, making the surface smoother. On the other hand, Baghel et al. (2015) [105] studied the MRAFF process to achieve the optimum surface roughness of implant dental crowns by using MRF containing 15% (SiC), with 37% CIPs, 8% glycerin, and 40% water to get Sa.0.008 µm from initial Sa 1.43µm. In addition, Prakash et al. (2021) [102] studied the effects of the MRAF process on the β-TNTZ alloy

surface. The Sa noticeably decreased by ΔSa 97.68 %, resulting in a minimum surface roughness of about 9 nm. The surface roughness was quantified using Talysurf CCI Lite, a three-dimensional (3D) Surface Profilometer equipped with a white-light interferometer, and TalyMap Platinum 6.0 software. The final morphology of the processed specimens was examined using Atomic Force Microscopy (AFM) and Field Emission Scanning Electron Microscopy (FE-SEM) with a JEOL 7600F [102]. Fig.1.12 (B) displays the SEM image and 3D surface map of the ground β-TNTZ samples. Based on the SEM image, the grinding process resulted in prominent, wide scratch marks. The grinding operation achieved a Sa value of 0.550 µm, and the 3D surface plot confirms the formation of elevated ridges and depressions. The specimen after MRAF demonstrates a notably higher level of clarity and smoothness than the grounded surface [102]. The MRAFF process is widely used in numerous research fields [61,106]; however, it has certain limitations. One issue is the uneven polishing of the component because the magnetic flux density is distributed unevenly along the workpiece profiles. Rotational motion is introduced into the workpiece or magnet to mitigate this limitation. This rotation mitigates the effects of spatially varying magnetic fields, enhancing the surface finish and material removal rate (MRR) [82].

1.3.1.4 Rotational-MRAFF Finishing Process (R-MRAFF)

As mentioned earlier, the R-MRAFF is the MRAFF process with the addition of rotational motion [82]. It is used for polishing various freeform surfaces with extreme precision, including those made of complex materials such as cemented carbide, Titanium, nickel-chromium, and stainless steel [107]. In biomedicals, a particular application is to finish the knee joint implant with the R-MRAFF process [92, 132, 133]. The primary objective of these finishing processes is to combine magnetic fluid and high hydrodynamic pressure. The workpiece's axial and rotational movements (Fig. 1.13(A)) are simultaneously regulated, resulting in an increasing finishing rate. The Taylor Hobson surface analyzer's final Sa value, previously 35.3 nm, was reduced to 26 nm, indicating a

notable improvement in surface quality and smoothness. The 3D images in Fig.1.13 (B) (a-d) depict the surface topography of the knee joint on face 1 and face 2. These images were obtained using 3D-AFM and illustrate the surface texture before and after completion. Due to the constraints of 3D-AFM and the significant curvature of faces 3 and 4, measuring the surface texture on these faces was not feasible. During repeated finishing at various pressures, it was observed that the high peaks on faces 1 and 2 were eliminated and flattened. The study found that the area roughness of face 1 significantly improved, reducing it from an initial value of 362 nm to a final value of 6.64 nm. Similarly, face 2 also showed improvement, reducing the initial area roughness from 335 nm to 17 nm. [108,110].

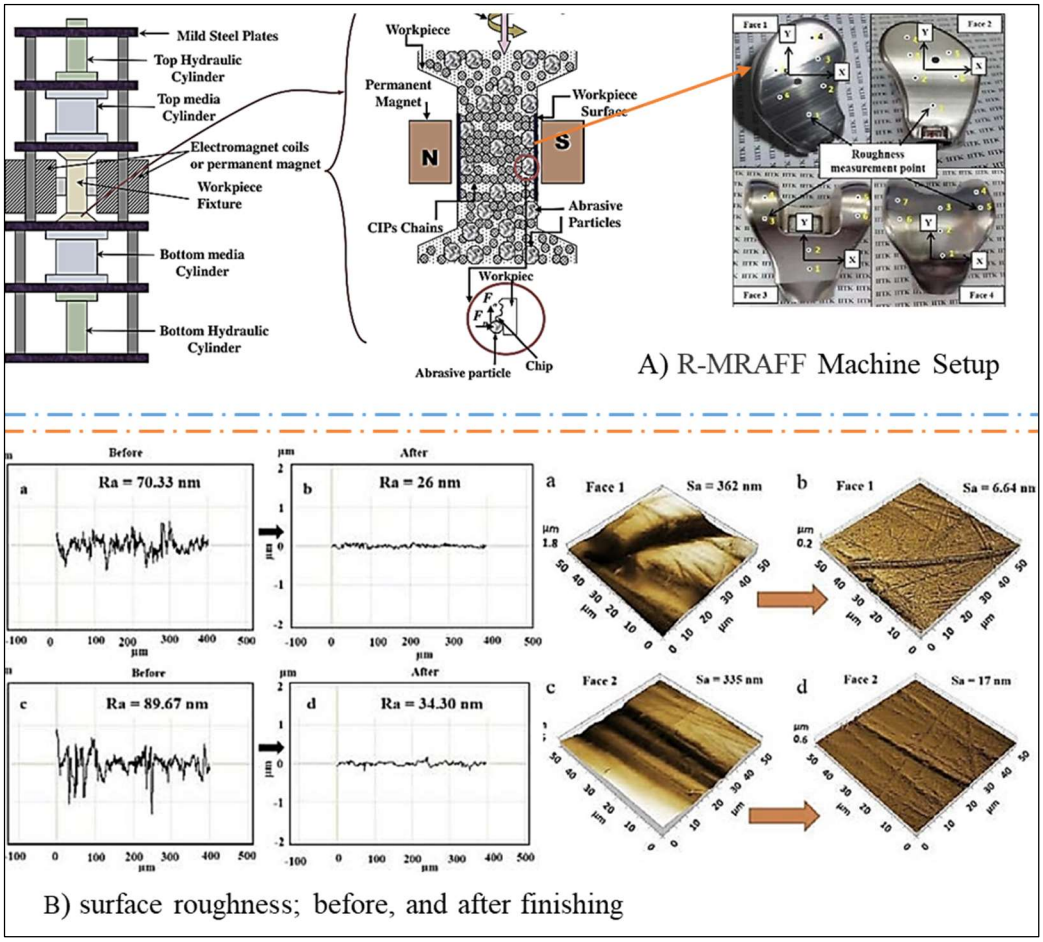

Fig.1. 13 R-MRAFF Schematic diagram with the femoral knee in four different points faces [108,110]

The R-MRAFF process improves the exterior surface, and the surface's topographical features influence the stability and long-term effectiveness of the implant [109]. Using an abrasive material such as SiC with a mesh size of 2000, extrusion pressure of 15 bar, finishing cycles of 1600, and rotational magnet speed at 150 (rpm). Moreover, surface roughness was achieved between 35 nm and 78 nm. Higher extrusion pressure breaks down CIPs chains and reduces the finishing action between the abrasive particles [112]. Nagdeve et al. (2019) [111] conducted a nano-finishing process, R-MRAFF, on the femoral component of a knee joint using a novel tool to achieve a surface polish in the range of Sa 78 nm to 89 nm. Despite the effectiveness and high-quality finishing achieved with the R-MRAFF process, it becomes more complicated and expensive the first time, as a separate setup is required for each component [82]. To address this issue, a process known as Ball-End Magneto Rheological Finishing (BEMRF) has been developed.

1.3.1.5 Ball end Magneto rheological Finishing (BEMRF)

The BEMRF process uses MRF, an intelligent fluid that changes viscosity in a magnetic field, to finish 3D surfaces. The principle of the BEMRF depends on the ability of CIPs' bonding strength to bind around the non-magnetic abrasive in MRF because CIPs are cross-linked clusters [113]. MRF adheres to the edge of a magnetic polishing tool to produce a flexible end-form polishing tool [114]. The BEMRF process can polish intricate structures, such as concave, convex, spherical, and freeform geometries, thanks to its ability to run on three- or five-axis CNC machines, enabling accurate and effective polishing [115]. The abrasive is subjected to two forces during finishing: normal force from the magnetic field and shear force from the MRF. Therefore, when the tool spins, the gripping abrasives in contact with the workpiece surface perform finishing by removing roughness peaks, as shown in Fig. 1.14 [69].

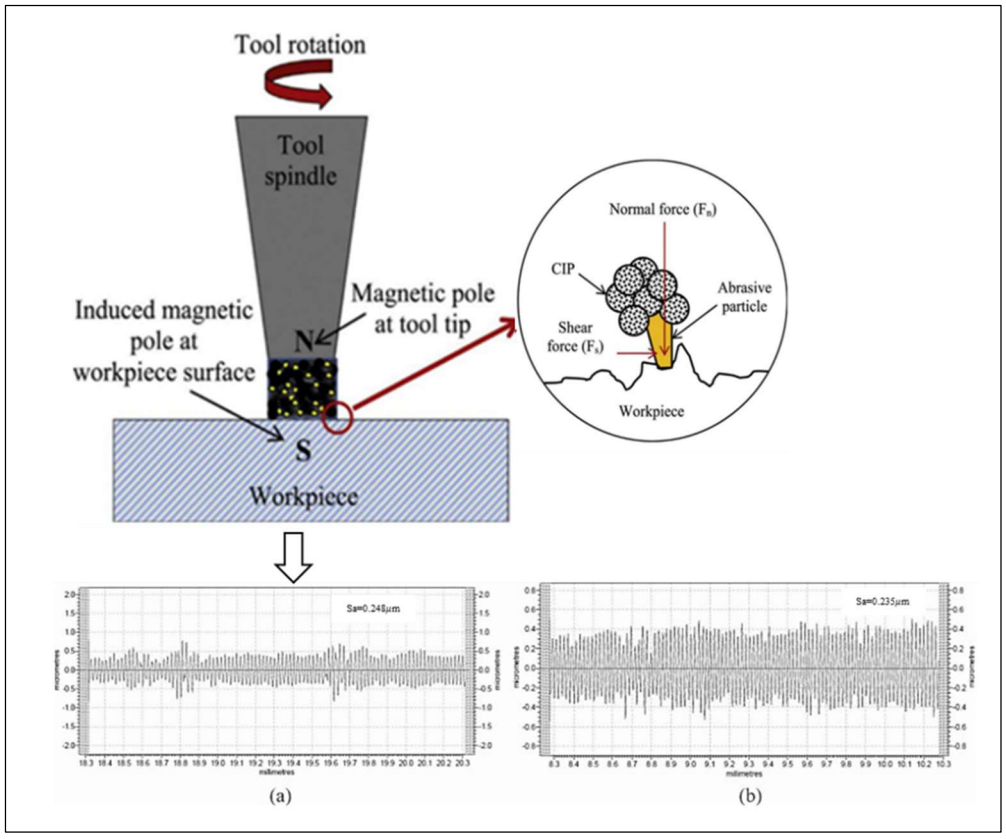

Fig.1. 14 BEMRF Process Mechanism with Surface profiles a) before and b) after finishing [69]

The BEMRF process has significant potential for surface polishing and finishing applications in the biomedical industry due to its capability to produce high precision, consistency, and control for parts. Bhavsar and Unune (2018) [116] carried out the BEMRF process on Ti-4Al-6C using a combined MRF comprising 8 µm CIPs and SiC abrasive. The base medium contained 100 ml of distilled water, 3 ml of hydrofluoric acid (HF), and 6 ml of nitric acid (HNO_3) to achieve a Sa value of approximately 500 nm.

1.3.2 Chemical Finishing Process (CP)

Chemical treatments involve surface modification at the interface between metal surfaces and solutions, resulting in various surface modification methods, including acid treatment, hydrogen peroxide (H_2O_2) treatment, alkali and heat

treatments, and sol-gel coatings. These treatments improve the bioactivity of Ti implants [47]. The CP is an effective process that offers accurate surface topography by producing highly smooth surfaces, thereby enhancing functionality and improving mechanical performance [35]. In the biomedical field, the chemical finishing of biomaterials, such as Ti alloys, involves treatment at the point where the components meet the surface-modifying solution [117]. A high-quality surface can be achieved by combining corrosive oxidation action with a polishing liquid to refine the surface quality by reducing the distance between peaks and valleys of the character [118].

Furthermore, CP enhances wear and improves corrosion resistance [119] by precisely controlling chemical parameters, such as the type of agents, concentration, and temperature. One of the CP processes, polishing, is a chemical treatment that mainly uses treatments with acids, alkalis, and H_2O_2 [117], sulfuric acid [120], hydrofluoric acid [121], or different acid mixtures frequently used, such as sulfuric acid/hydrochloric acid or hydrofluoric acid/nitric acid solutions [122–124]. Therefore, it is possible to precisely control the surface physicochemical properties and topographies of these treatments to promote osteogenic cell adhesion and proliferation [125,126], apatite precipitation [127], and the expression of bone-related genes and proteins [128].

On Titanium alloys, CP forms a passivation film comprising rutile and anatase on the alloy surface. Titanium alloys typically have three layers: TiO (the inner layer in contact with the metal), Ti_2O_3 (the intermediate layer), and TiO_2 (the outer layer), as shown in Fig. 1.15 [117]. This process enhances the surface integrity of the implant material by removing oxides and impurities, thereby improving its performance and overall effectiveness. During the CP process, the suboxides transform TiO, thereby restoring the layered structure. The presence of the oxide film contributes to Titanium's stability, inertness, corrosion resistance, and biocompatibility [129,130].

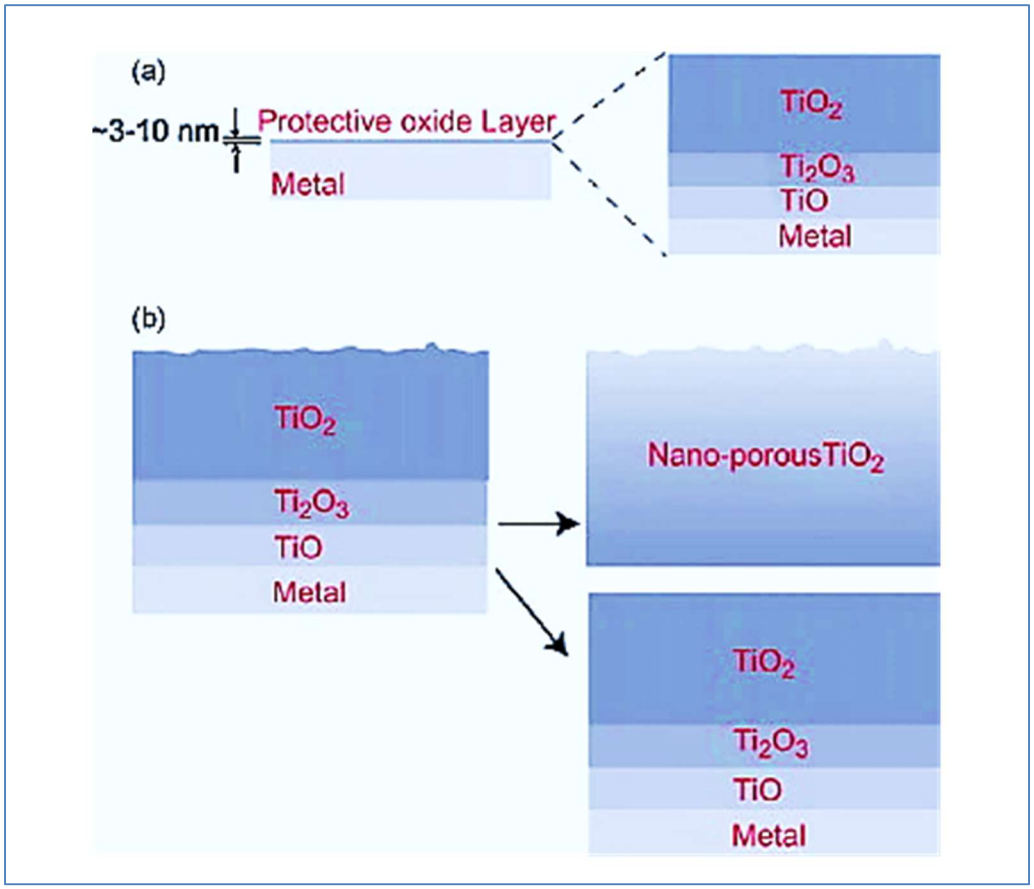

Fig.1. 15 Schematic of the layered structure of titanium alloys (a) before (native oxide) and (b) after chemical [125]

CP processes are known for their simplicity and versatility, enabling the treatment of small parts and intricate shapes, including narrow tubes, large openings, meshes, and curved surfaces. Y. Zhang et al. (2019) [118] conducted an experiment by CP on the Ti-6Al-4V alloy with an initial Sa value of 8.04 µm. After treatment with CP one-step polishing, the Sa was 2.48 µm; after the second polishing step, it was 2.13 µm (Fig. 1.16C). In addition, Zhang et al. (2018) [131] developed a CP process using a more accurate Ti-6Al-4V alloy to achieve a high surface finish and enhance biomedical compatibility, using H_2O_2, malic acid, silica, and deionized water as reagents. Similarly, Khodaei and Hossein Kelishadi (2018) [132] used H_2O_2 on a Ti alloy to treat implant surfaces, aiming to improve osseointegration.

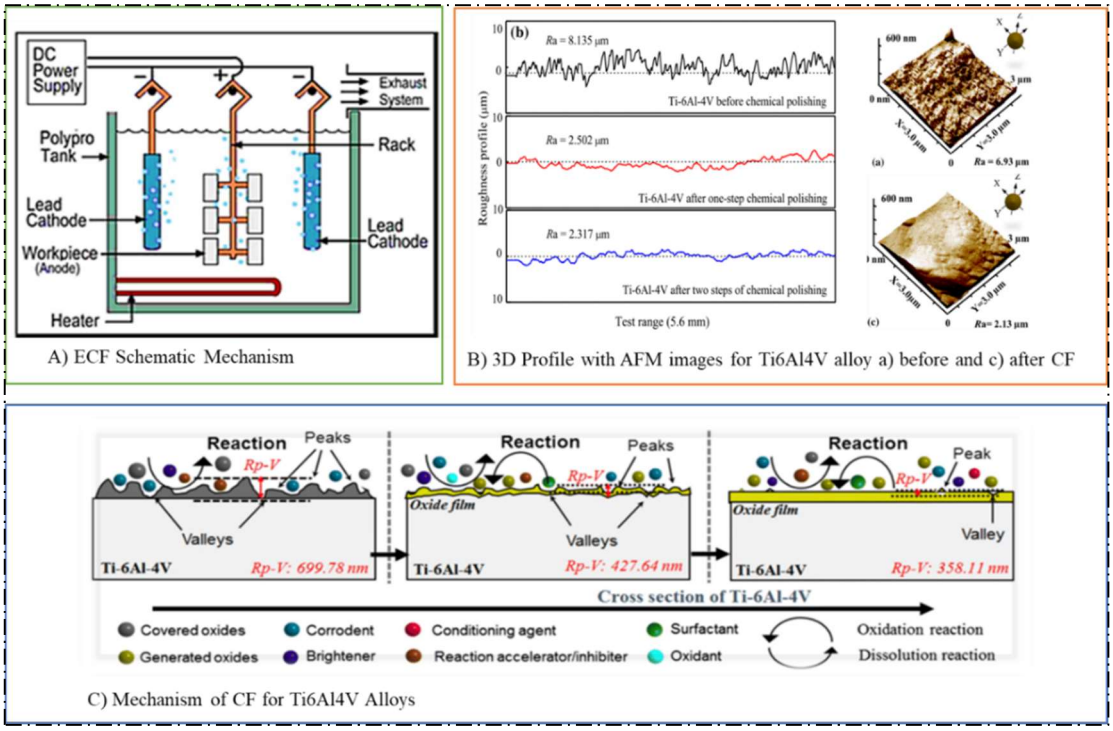

Fig.1. 16 Schematic diagram of the CP and ECF process [118,133]

One of the CP processes, the ECF, uses an electrical circuit. This procedure is straightforward to perform and can polish multiple components simultaneously. Nevertheless, the intricate interaction renders the chemical polishing process difficult to regulate. Alternatively, the CP fluid leads to ecological contamination [101]. ECF is preferred in some applications that demand greater accuracy and a superior finish. As shown in Fig. 1.17(A), during ECF, the workpiece and insoluble metal are treated as the anode and cathode, respectively [133].

Additionally, Ti alloys can be subjected to ECF for various applications. However, numerous variables influence this process, complicating the determination of the optimal processing settings. Ashikur Rahman Khan (2017) [134] examined the effects of several parameters on the changing surface roughness of Ti5Al2.5Sn alloy, including discharge current, voltage, pulse-on time, pulse-off time, polarity, electrode material, and cleansing pressure.

110

1.3.3. Hybrid Finishing Processes

The hybrid finishing process has emerged as a promising strategy to enhance nanofinishing effectiveness. Classical nano-finishing techniques are combined with other processes, such as CMF, ECP, and UMAF, to improve finishing performance and meet the growing demands of various industries. However, further research is still needed on the hybrid finishing process for Ti alloys [101]. These hybrid processes can produce ultra-fine, high-surface-area materials with improved surface quality and enhanced biocompatibility.

1.3.3.1 Chemical Mechanical Finishing Process (CMP)

A novel hybrid approach called CMP precisely modifies surface roughness, enabling the creation of controlled nano- or micro-roughness or nanoscale smoothness as needed. CMP is used to modify Ti alloy surfaces, improving their overall quality and performance [131]. The Ti oxide layer, a naturally occurring coating with a thickness of 3-10 nm, as shown in Fig. 1.15, is a protective coating. However, supplementary oxidation procedures are used to maintain its wear properties and biocompatibility. The continuous, pore-free oxide layer prevents spontaneous Ti-ion dissolution in biomaterial implants [125,135]. The CMP slurry significantly affects surface roughness [101]. Kaushik et al. (2014) [136] used a mixture of emulsified oil and H_2O_2 to chemically and mechanically polish a Ti alloy, achieving a smooth surface with a surface roughness (Sa) of 40 nm. Ozdemir (2016) [135] investigated CMP to improve the surface roughness of Ti alloys using two slurries: one containing 3 wt% H_2O_2 and 5 wt% Al_2O_3, and the other without H_2O_2, at pH 4. It was discovered that CMP might be successfully utilized in implants to prevent bacterial growth by forming a protective oxide layer.

On the other hand, Liang et al. (2016) [137] used a slurry for CMP that contained colloidal silica (SiO_2) with a diameter of about 110 nm and 30 wt.% H_2O_2. Also, Zhang et al. (2018) [131] developed a unique, environmentally friendly CMP slurry containing colloidal SiO_2 , H_2O_2 , malic acid, and deionized water; the slurry composition can be adjusted to produce a smooth layer on a Ti

alloy with a final Sa of 0.68 nm. Fig. 1.17 illustrates how ZYGO's optical equipment is used to precisely examine and evaluate surface characteristics of materials, measuring both surface roughness and topography.

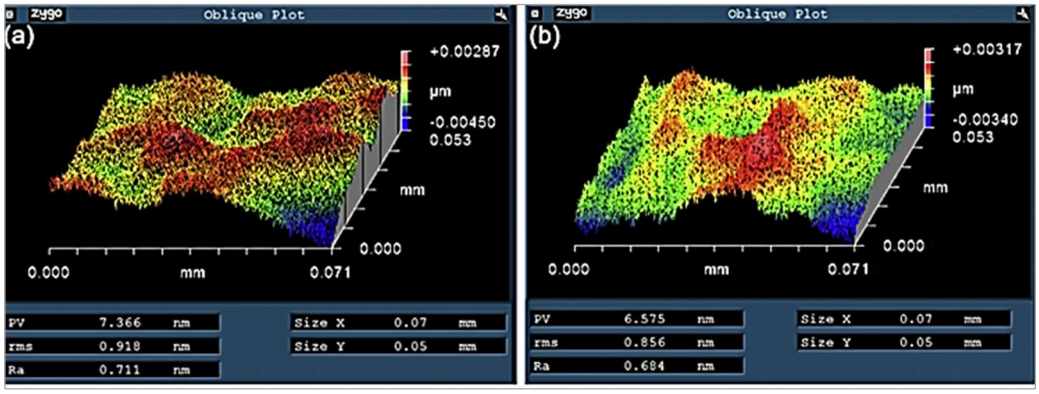

Fig.1. 17 ZYGO surface roughness and topography a) before, b) after the CMP process [131]

1.3.3.2. Electrochemical Finishing Assisted Abrasive Particles

The electrochemical finishing process (ECP) is an efficient, cost-effective, advanced technique for polishing complex, challenging materials. Ti alloy surfaces form a compact passivation coating using an environmentally friendly neutral salt solution as the polishing electrolyte. Nevertheless, this passivation layer affects the effectiveness of the polishing process and the surface's overall quality [138]. ECP is a technique that enhances the quality and modifies the surface of Ti and its alloys in biomedical applications by utilizing distinct electrochemical dissolutions between the convex and concave parts of the surface [139]. Simka et al. (2012) [140] analyzed the corrosion resistance of the Ti-13Nb-13Zr alloy using ECP and found that the sulfuric acid and ammonium fluoride bath performed best. Wang et al. (2021) [141] investigated ECP on Ti alloys in an acid-alcohol solution electrolyte, optimizing the process variables and achieving a surface roughness (Sa) of 0.3 µm. Liu et al. (2022) [138] studied ECP assisted by a high-speed flow of abrasive particles (ECFAP) on Ti6Al4V alloy, using 10% $NaNo_3$ as the electrolyte. The polishing effectiveness and surface quality are both

enhanced by the ECFAP procedure (Fig. 1.18). SEM investigation was performed to examine the surface morphology. It was shown that microcracks decreased after ΔSa reached 0.0953 μm under an ideal voltage of 3 V for 10 min. This improvement reduced the frequency of scratches.

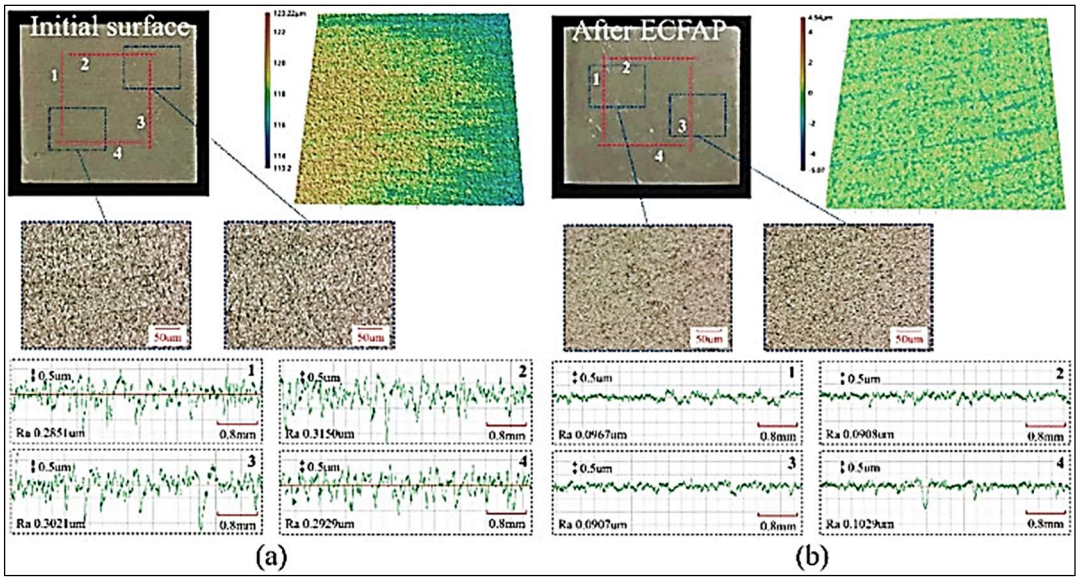

Fig.1. 18 3D profile and morphology for surface (a) before and (b) after ECFAP [138]

1.3.3.3 Ultrasonic-Assisted Magnetic Abrasive Finishing (UAMAF)

Ultrasonic-Assisted Magnetic Abrasive Finishing (UAMAF) is a hybrid surface-finishing process that combines the concepts of Magnetic Abrasive Finishing (MAF) with ultrasonic vibrations, using magnetic particles in a fluid medium. The principle illustrated in Fig. 1.20(A) is that magnetic abrasive adheres to the workpiece surface due to magnetic forces. The MRR happens as the magnetic abrasive strikes and cuts the workpiece under the influence of the magnetic pole's rotation and ultrasonic vibration. Ultrasonic vibration improves abrasion depth and contact length, thereby increasing the material removal rate (MRR) and total machining effectiveness [70]. UAMAF improves surface finish and material removal rate (MRR) across various applications, including biomedical implants. Mulik and Pandey (2011, 2010) [142,143] conducted UAMAF to improve the MRR and surface finish from microchipping and

nanoscratching of a workpiece, achieving a Sa of 0.022 µm. In addition, Chen (2019) [144] carried out UAMAF on the inner surface of a tube made of a nickel-based alloy, demonstrating that by finishing for 30 min. with an ultrasonic amplitude of 19 µm at a vibration frequency of 19 kHz, the surface roughness is reduced from Sa 2.4 µm to Sa 0.31 µm. Additionally, Zhou et al. (2015)[145] investigated UAMAF on a Ti alloy workpiece and reported that the surface residual stress changed significantly, whereas the initial measured stress was +280 MPa in tension. However, after undergoing UAMAF, the stress had changed to -20 MPa in compression. Moreover, Çelik et al. (2022) [146] experimentally investigated Ti6Al4V alloy workpieces via wire electrical discharge machining. They found that a thick white layer was deposited on the surface, and Δthat Sa could be improved by Δ89% with UAMAF.

Similarly, Ma et al. (2022) [70] studied Ti alloy's characteristics through experimental comparisons of MAF and UAMAF; the results showed that UAMAF produced a final Sa 0.075 µm, which was improved by a ΔSa 59% compared to MAF, In addition, while evaluating the surface roughness, the process shows an enhancement in the surface integrity of the workpiece (Fig. 1.19B), The results indicate that the Sa obtained with UEAMAF is lower in comparison to that Sa with MAF process. Ultrasonic-assisted finishing processes can reduce the average surface roughness [147].

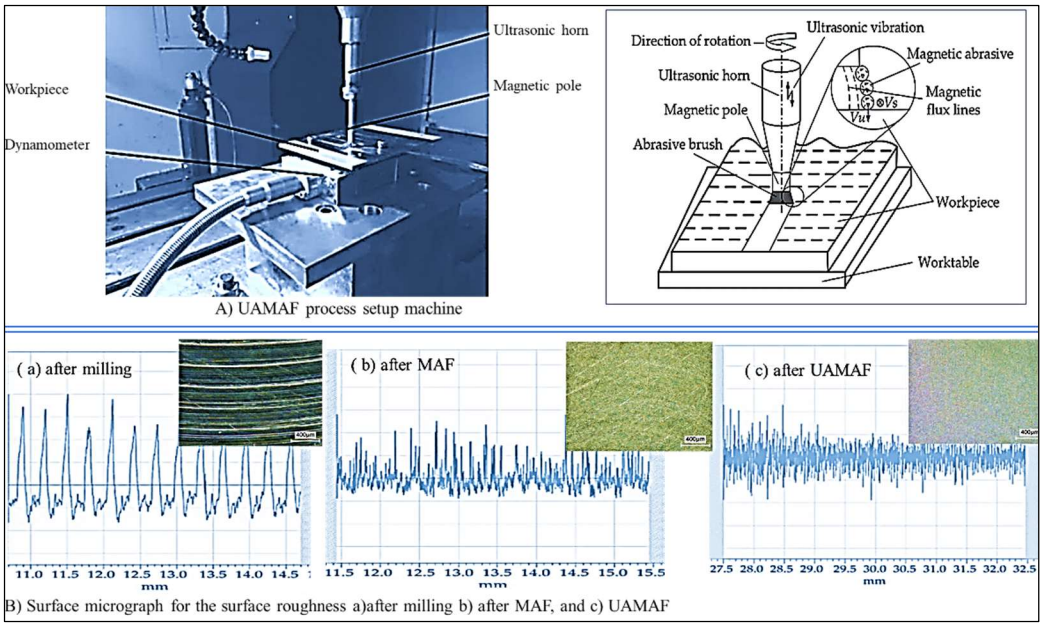

Fig.1. 19 UAMAF process setup and 3D profile of surface roughness and micrograph [70].

Another hybrid process, called Chemo Ultrasonic Assisted Magnetic Abrasive Finishing (CUMAF), combines Magnetic Abrasive Finishing (MAF) and Chemical Mechanical Polishing (CMP) with ultrasonic vibrations to achieve a nanoscale surface finish. Sihag et al. (2015) [148] investigated and analyzed the significant parameters of surface finishing procedures using CUMAF, with an initial Sa value of 0.3571 µm, which was reduced to 0.0617 µm.

1.4 Comparison of Nano-Finishing Processes for Ti Alloys

Fig. 1.20 compares the capability of nano-finishing techniques on Ti alloys to achieve the lowest Sa. MFAF demonstrates a considerable reduction in surface roughness, with a final Sa of 0.01 µm, which is significantly improved over the initial Sa of 0.56 µm. This remarkable surface smoothing demonstrates the effectiveness and accuracy of MFAF in producing smoother surfaces on intricately shaped components, making it a promising method for bio-implants. In addition, CMP in nanoscale surface engineering achieves a final Sa of 0.684 nm, starting from an initial Sa of 0.711 nm. CMP nano-scale precision is essential for sophisticated applications in nanoelectronics and high-precision optical devices.

The significant decrease in surface roughness underscores the accuracy and efficiency of these techniques in producing smoother and more polished surfaces, which are essential for bio-implants.

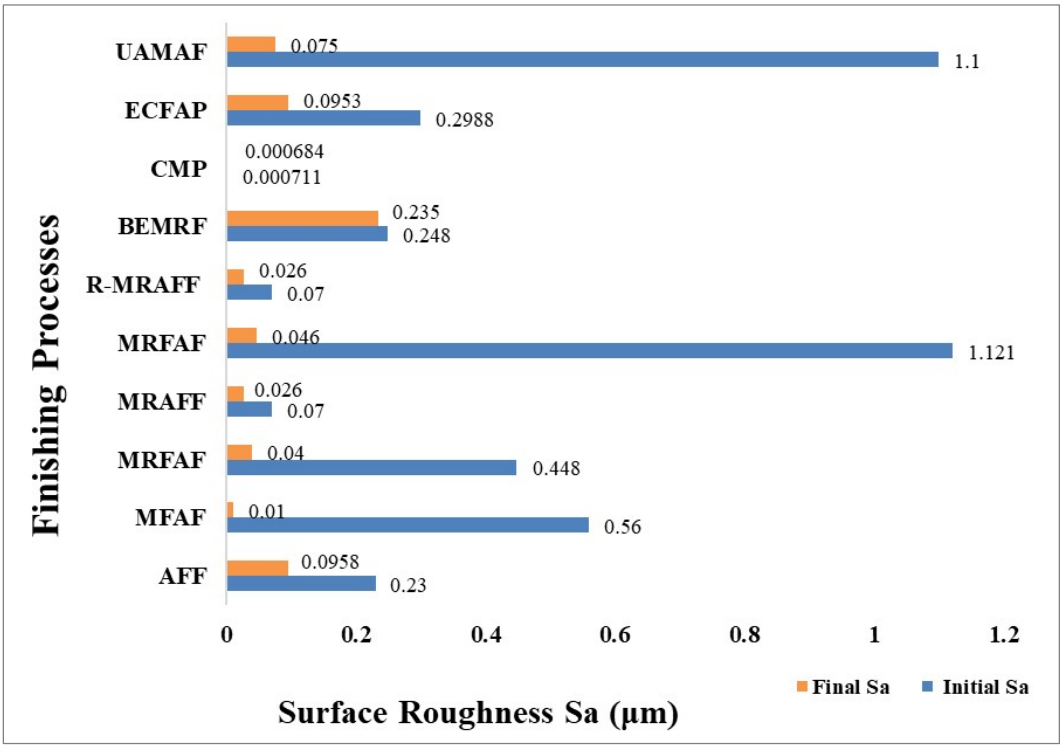

Fig.1. 20 Comparison of nano-finishing techniques (Ti alloys) [21,69,70,80,102,108,138,149–151]

1.5 Summary

Conventional finishing processes are less effective for 3D parts because they offer less force control and fewer constraints on tool movement, which can damage the polished surface and lead to more flaws and cracks. Therefore, advanced nano-finishing processes are developed to overcome the limitations of conventional finishing processes. Moreover, it's used to finish complex shapes with less roughness, enhancing surface integrity. Nano-finishing processes are advanced manufacturing processes that offer significant opportunities to improve surface integrity and reduce roughness across various industries, including marine, military, and medical applications. Titanium and its alloys are widely used in biomedical implants due to their exceptional biocompatibility and mechanical properties, which surpass those of other metal alloys. These alloys are extensively used to fabricate artificial implants such as elbow, hip, and femoral knee joints. The performance of these implants depends on surface integrity, which affects their longevity and functionality.

CHAPTER 2: LITERATURE REVIEW

This chapter presents a comprehensive review of the various types of surface treatments and the finishing process of Ti alloys. The timeline of the CMMRF process, principles and parameters, current research trends, and associated challenges and limitations.

2.1 Introduction

With the rising demand for advanced biomaterials in biomedical implants, surface modification is increasingly seeking sustainable materials and environmentally friendly methods to modify surfaces while preserving biocompatibility and functionality. Titanium (Ti) and its alloys have been widely used in biomedical applications, particularly in orthopedic and dental implants [152], owing to their exceptional mechanical strength, biocompatibility, and resistance to corrosion in physiological environments. These attributes are crucial for improving implant quality [153,154]. They assist in the attachment and growth of host tissues on their surfaces. However, like other metallic implants, Ti is liable to corrosion and wear, and its bio-inertness can sometimes slow the healing of surgical wounds [155]. Since postponing wound healing can lead to aseptic loosening and implant failure, particularly in chronic conditions like diabetes and osteoporosis, it requires additional surgical procedures [156].

The bio-inert nature helps avoid bacterial attachment and subsequent infections in surgical wounds [157]. In addition, a spontaneous oxide layer, typically 2-5 nm thick, forms upon exposure to air or oxygen [158]. This dense oxide layer, which adheres firmly to the underlying alloy, is chemically inert in many environments, providing outstanding corrosion resistance [159,160]. However, Ti alloys can corrode in very reactive environments [161]. Surface modification suggests a potential solution by enhancing the thickness of the oxide layer [162–164], thereby mitigating these concerns. Surface modification

techniques encourage oxidation reactions, either chemical or electrochemical, to augment the protective oxide layer [165]. Different techniques for surface alteration of Ti alloys include mechanical, chemical, and physical processes [35].

Surface modification via chemical processes enhances biocompatibility by increasing oxide thickness and reducing defect density [166–168]. Surface modification by chemical processes typically uses acids or alkalis due to their accessibility, cost-effectiveness, and ease of implementation [168]. Recent studies have focused on enhancing the bioactivity of biomaterials to facilitate direct bone-implant integration through chemical surface modifications [14]. Zhao (2020) demonstrated that combining alkali heat treatment, induction heating, and acid etching enhances Hydroxyapatite formation on the alloy surface [169].

Yao (2019) [170] investigated acid-alkali solutions to create nanoscale surface textures on porous Ti alloy, aiming to improve bioactivity and bone regeneration. Kokubo (2010) [171] experimented with alkali (NaOH) and applied heat to induce apatite formation on Ti alloy surfaces, which were used in clinical trials for hip joints and spinal fusion devices. In addition, Gostin (2013) [172] experimented on Ti alloy by a process including sand-blasting and etching using strongly oxidizing acidic solutions such as hydrofluoric acid: nitric acid (HF: HNO_3) or sulfuric acid: hydrogen peroxide (H_2SO_4: H_2O_2), known for their potent nano-scale corrosion initiation on alloy surfaces. However, acids such as hydrochloric acid (HCl), sulfuric acid (H_2SO_4), and nitric acid (HNO_3) pose hazards to human health and the environment, highlighting the need for safer, environmentally friendly alternatives in surface modification.

Although it is challenging to modify the surface of Ti alloys using environmentally friendly, safe chemicals free of hazardous substances, this study addresses these concerns by developing a novel thermochemical process that uses eco-friendly chemicals, such as hydrogen peroxide (H_2O_2) and citric acid ($C_6H_8O_7$).

H_2O_2 has been investigated for its potential use in biomedical implants,

specifically in modifying the surface properties of biomaterials. It is frequently employed in processes to improve the compatibility and activity of biological systems. Khodaei (2018) [132] used H_2O_2 for oxidation to treat the surfaces of Ti dental implants. Moreover, its efficacy against bacteria stems from its oxidizing properties [173]. Although the reaction between H_2O_2 and Ti alloys forms Ti-peroxyl gels, these gels promote apatite deposition on Ti surfaces, making them advantageous for orthopedic implants. Also, a significant outcome of mechanical property changes is the formation of a nanocrystalline surface layer that is hardened by treatment [174].

$C_6H_8O_7$ has a low pH and can affect cellular activity on the Ti surface at high concentrations. Verdeguer (2022) [166] demonstrates that $C_6H_8O_7$ improves the biological reactivity and corrosion resistance of Ti surfaces. $C_6H_8O_7$ at a 20 % concentration effectively resists corrosion, and at a 40 % concentration, it kills microorganisms. Additionally, $C_6H_8O_7$ enhances corrosion resistance and releases ions into the surrounding environment, necessitating careful evaluation of long-term performance [166]. Previous studies, such as those by Fernández-Garrido et al. (2024) [251], used $C_6H_8O_7$ with H_2O_2 for surface decontamination of dental implants and to control bacterial infections. Mirdamadi et al. (2022) [175] studied the impact of post-heat treatment in terms of crystal phase structure on the surface characteristics of Ti grade 2 by H_2O_2. In addition, Cordeiro et al. (2021) [176] applied $C_6H_8O_7$ to alter the surface of Ti alloy's physical and biological properties. Wheelis et al. (2016) [177] used $C_6H_8O_7$ with H_2O_2, chlorhexidine gluconate, tetracycline, doxycycline, sodium fluoride, peroxyacetic acid, and treatment with carbon dioxide laser to apply on dental implants. However, this study develops eco-friendly chemical formulations, including citric acid, hydrogen peroxide, and sodium hydroxide, specifically designed to enhance the surface properties of Ti alloys for biomedical implant applications.

Nano-level surface finishing is crucial for high-performance materials in advanced manufacturing and biointerface applications, as it enhances wear and corrosion resistance, and biocompatibility by producing flawless, smooth surfaces

at the nanometer scale [178,179]. Ti alloy grade 5 (Ti64) is widely used in industries such as aerospace, petrochemicals, medical devices, and automotive manufacturing [20,23], accounting for its exceptional strength-to-weight ratio, corrosion resistance, and biocompatibility [5,26,33,130,154]. However, it is considered one of the most challenging materials to machine, and achieving ultra-smooth surface finishes remains difficult, as surface imperfections can undermine fatigue resistance, wear performance, and functionality due to high cutting temperatures, tool wear, and the formation of a built-up edge [180,181].

Traditional finishing techniques induce microcracks and surface degradation, resulting in macro- to micro-level roughness [54]. These techniques involve energy-intensive processes or hazardous chemicals, contradicting global sustainability goals. Advanced techniques achieve exceptionally smooth surfaces with high precision, such as Abrasive flow machining (AFM) [80], Magneto-rheological (MR) finishing [182], Magnetic abrasive finishing (MAF) [95,183], Magnetic field-assisted finishing (MFAF) [184], and ultrasonic-assisted magnetic abrasive finishing (UAMAF) [146]. Zhang (2019) [80] conducted AFM experiments on Ti64 alloy in artificial joints. The surface roughness Sa decreased from 230 nm to 95.8 nm after 5 hr. of finishing. Additionally, it enhances surface integrity by reducing surface grooves and peaks. Tian et al. (2020) [150] used the MAF process to finish Ti64 alloy with improvement in the final Sa by almost 94 % (from 1.195 μm to 0.073 μm) with the optimal process parameters of spindle rotation of 900 (rpm), rotary speed 160 (r/min), and working gap 0.7 (mm) to achieve a significant improved in the surface quality with only 90 min. of finishing. Also, Tien et al. (2022) [185] used the MR-assisted abrasive process to finish the Ti64 alloy. The abrasives contain Carbon iron particles (CIPs) (20-30 μm) and Alumina (Al_2O_3) with a size of 30 μm, and optimized process parameters are achieved using a hybrid algorithm, resulting in a 37.5% reduction in ΔSa. Additionally, Barman et al. (2019) [93] investigated the Ti64 alloy by the MFAF process. By optimizing the process parameters, a tool speed of 901 rpm and a working gap of 0.60 mm achieved a Sa of 11.32 nm in a finishing time of 4.30

hours.

Based on the research above, Ti64 alloy is a hard material that requires a longer finishing time to achieve the desired surface roughness (Sa). To address this challenge, an advanced hybrid finishing technique, the chemo-mechanical magneto-rheological process, was developed, offering high-precision finishing while significantly reducing time, cost, and energy consumption. Conventional polishing chemicals typically rely on corrosive acids such as HNO_3, HF, H_2SO_4, or HCl, which pose hazards to human health and the environment. To overcome these limitations, this study develops an advanced, eco-friendly finishing process using chemical magneto-rheological finishing to minimize surface finish, reduce finishing time, and enhance surface quality.

2.2 Chemical Magneto-rheological Finishing (CMMRF) Process

In recent decades, numerous attempts have been made to develop a hybrid advanced finishing process. Fig. 2.1 shows the development timeline for these. The MR finishing was first introduced in the 1970s by Kordonski's team at the Institute of Heat and Mass Transfer in the former Soviet Union for machining [186]. In 1992, (MR) finishing was introduced to achieve high-precision, controlled surface finishing [187]. Although AFF uses pressure, and MAF employs a magnetic field to aid the finishing process, both methods are relatively slow at reducing finishing time and improving (Sa) [188]. Later advancements, including R-MRAFF, BEMRF, MRAFF, MRJF, and CMMRF processes, incorporated magneto-rheological principles [96,189–191]. These improvements enhanced the rheological properties of the fluids under magnetic fields, introducing rotational motion and offering significant advantages for finishing complex geometries [192].

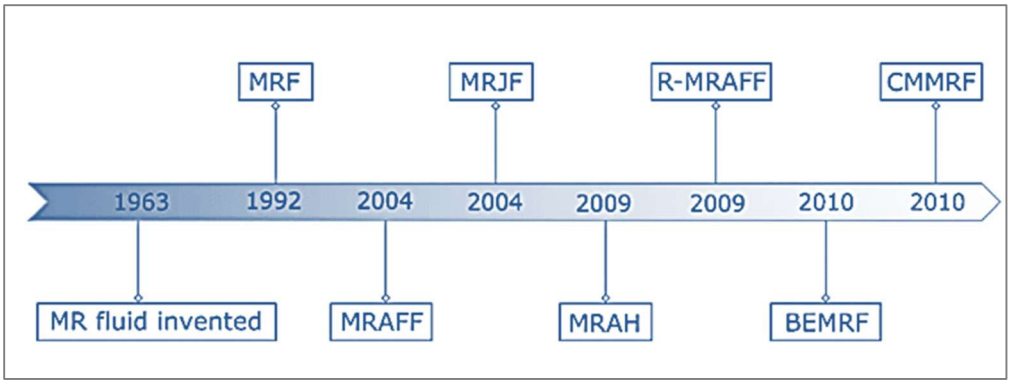

Fig.2. 1 Timeline of the development of the CMMRF process [61].

Chemical-mechanical finishing (CMP) was developed as an efficient nanofinishing process that combines chemical assistance with mechanical abrasion. In this technique, the reaction of chemicals passivates the surface to form an oxide layer, followed by random abrasive polishing. CMP is widely used in industry to polish metals and non-metals to an atomic-level finish [193]. However, this process has several limitations, including the size and shape of the workpiece, the polishing pad's limited flexibility, and its limited lifespan.

A hybrid advanced finishing process called Chemo-mechanical Magneto-Rheological Finishing (CMMRF) was developed to overcome these limitations. This process combines the principles of chemical polishing and (MR) finishing. CMMRF offers significant advantages, including achieving nanometre surface finishes on hard metals while overcoming the drawbacks of CMP and MRF processes, such as improved precision for complex surface features and reduced processing time [102,111,194–196]. It is primarily utilized in semiconductor manufacturing to create highly polished integrated circuits [197]. The surface is enhanced with superior polishing rates, high surface quality, improved repeatability, extended pad lifespan, and greater process flexibility. Additionally, this technique achieved a surface finish of 0.5 nm on silicon [198,199]. Furthermore, a Sa of up to 2.5 nm has been achieved on a copper alloy by utilizing the CMMRF technique, as recently reported [199].

The publications on CMMRF processes began in 2010 and have increased

significantly over the last decade, as shown in Fig. 2.2, providing insight into its growing significance in advanced nano-finishing processes. Therefore, by analyzing publications on CMMRF research across industries such as electronics, automotive, medical, and aviation, it's clear that this technology is gaining popularity and improving the precision, durability, and performance of vital components. The existing literature on this process has a limited number of publications. However, it is important to consider implementing this process in manufacturing due to its economic advantages, time-saving benefits, and reduced effort required. This gap in the literature serves as the inspiration for this work.

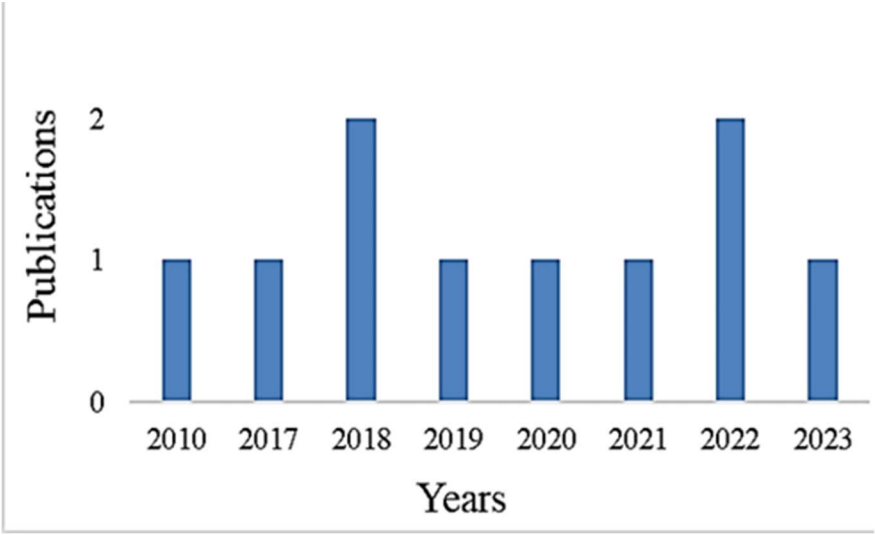

Fig.2. 2 The number of publications on CMMRF processes. (Data retrieved from the Web of Science on 03/04/2024)

2.2.1 Review of Chemical-Mechanical Finishing Process (CMP)

The chemical finishing process is a surface treatment that primarily involves acid, alkali, and hydrogen peroxide treatments [1]. It involves chemical reactions at the interface between the materials and the solution for surface modification [200]. The acid treatment removes the oxide film formed on the material's surface, adsorbs contaminants, and improves the surface roughness of the implant material. Some standard chemical solutions used for the surface treatment are hydrofluoric acid [121], Sulfuric acid [120], hydrochloric acid [201], or mixed with other

solutions such as sulfuric acid, hydrochloric acid, hydrofluoric acid, or nitric acid [122–124]. Chemical processes were primarily used to create a soft passivation layer that protects the underlying material during finishing. The material removal process involves both chemical reactions and mechanical abrasion during the chemical process. The effect of chemical solutions on different workpieces, such as Ti alloy, copper, and tungsten, and the development of a protective layer on various metals due to chemical reactions throughout the finishing process (Fig. 2.3). This layer can be easily removed by employing abrasives. During surface finishing, it is imperative to remove waste particles, as any undissolved particles tend to accumulate on the workpiece's surface, either as the same metal or its oxides. This phenomenon improves the effectiveness of mechanical abrasion and the rate of elimination, leading to the production of abrasions on the smooth surface [60]. The metal undergoes dissolution in the MR finishing due to oxidation, forming ions upon contact with a chemical etchant, as depicted in Fig. 2.3 (a); the oxidation of the workpiece surface also enhances mechanical abrasion. The reaction between Murakami's reagent (The sodium hydroxide NaOH and potassium ferricyanide ($C_6N_6FeK_3$) are dissolved in distilled water) and the Co binder forms Co $(OH)^{3-}$, CO^{2+}, and CO_3O_4. The interaction between MR finishing and WC-Co leads to the formation of CO_3O_4. Tungsten trioxide (WO_3) exhibits greater malleability and susceptibility to mechanical abrasion.

On the other hand, in the chemical treatment of Ti alloys, a passivation film forms on the alloy surface, comprising rutile and anatase. Ti alloys typically have three layers: TiO (the inner layer in contact with the metal), Ti_2O_3 (the intermediate layer), and TiO_2 (the outer layer), as shown in Fig. 2.3 (b) [117]. This procedure modifies the surface integrity while removing the oxide film and contaminants. The suboxides are changed into TiO_2 throughout the chemical polishing process, causing the layered structure to be re-established. The oxide film helps make Ti stable, inert, corrosion-resistant, and biocompatible [129,130]. Similarly, the passivation layers are formed in the workpiece using chemical reactions with Ammonia and Glycine, converting the superficial layer into a passivated layer.

13

The chemical process used in copper production is shown in Fig. 2.3(c) [202].

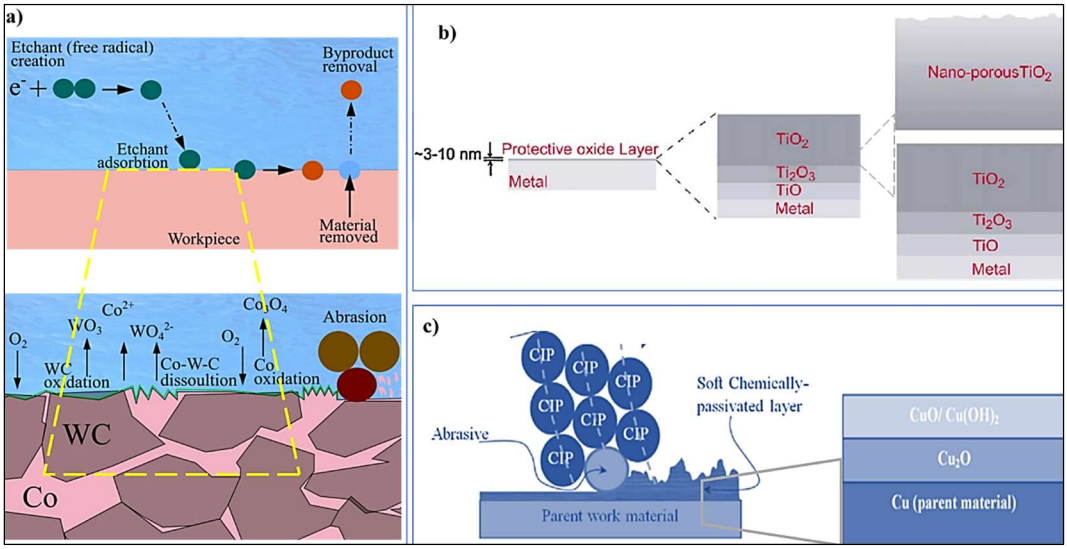

Fig.2. 3 Effect of chemical process passivation on different materials [60,190,199,203]

To achieve the intended outcomes, many substances necessitate the utilization of suitable reagents, such as acidic or alkaline solutions. Chemical finishing benefits individuals working in the domains of education and engineering, as well as professionals involved in processing materials and microfabrication [204].

Table 2.1 presents the chemical reagents utilized in various materials, which ultimately result in a textured surface. Additionally, we provide the composition of certain chemicals used through controlled dissolution, which is employed to selectively remove material from the surface of a substrate, thereby producing a patterned or textured surface. To enhance functionality and improve mechanical performance, nano-finishing with assisting chemical action is a surface treatment procedure that provides the correct surface topography. This is accomplished by providing a surface finish that smooths the surface. This procedure generates ultra-smooth textures while simultaneously improving surface quality by enabling precise control over chemical factors, such as agent type, concentration, and pH [205].

Table 2. 1 Different chemical reagents are used for etching processes on various materials.

References	Materials	Reagent	Constituents
Barman and Das(2018b) [91]	Titanium alloy	Keller's reagent	Glycerol (8%), Hydrofluoric acid (1.17%), Nitric acid (2.33%),
Gouné et al. (2012)[207]	Steels	Kroll's reagent	NaOH (40 g), $NaNO_3$(15 g), H_2O (60 g)
Lee et al. (2022)[208]	Copper alloy	Piranha's reagent	The mixture consists of H_2O (50 ml), NH_4OH (50 ml), and H_2O_2 (10-50 ml).
Han et al. (2022)[209]	Silver alloys	Ammonium persulphate	The mixture contained H_2O (100 ml), $(NH_4)2S_2O_8$ (10 g), and KCN (10 g).
Kim et al. (2018)[210]	Tungsten carbide	Murakami's reagent	Sodium hydroxide (10 g), potassium ferricyanide (10 g), and water (100 ml)
Agbonlahor et al.(1986) [211]	Zinc alloys	Palmerton's reagent	Chromium (III) oxide (20 g.), sodium sulfate (1.5 g.), and H_2O (100 ml),
Bae et al. (2020)[212]	Gold alloys	Aqua regia solution	Nitric acid (40 ml) and hydrochloric acid (60 ml)
Jovičević-Klug et al. (2021) [213]	Al-alloy	Nital's reagent	Nitric acid (1-5 ml) with ethanol (95-99 ml)

Nano-finishing processes have garnered substantial attention in materials engineering and manufacturing, particularly in the medical field, due to their

ability to refine surface roughness at the nanoscale. Table 2.2 illustrates various nano-finishing processes for Ti alloy, examining surface roughnesses with different MRF types and various process parameters.

Table 2. 2 Various Nano-finishing Processes in Biomaterials.

Reference	Titanium Alloys	Finishing Processes	MRF	Findings
L. Zhang et al., (2019) [80]	Ti alloy artificial joint surface	AFF	The MRF includes SiC abrasive particles ranging from 8 to 18 µm, and their concentration ranges from 0.1 to 0.2.	The Sa reduced from 230 nm. to 95.8 nm. After finishing time for 5 hr. under the condition that the abrasive particle diameter is 18-8 µm and the abrasive particle concentration is 0.1. Less Sa is achieved by taking more time to finish and having smaller abrasive particle sizes with a higher concentration.
Barman and Das, (2018) [206]	Bio-titanium free form.	MFAF	MRF type (I), CIPs, and abrasive particles with HF, HNO_3, and deionized water as the base medium. MRF type (II), CIPs, and abrasive particles in the base medium of H_2O_2 and deionized water.	The surface roughness with MRF type (I) is (Sa = 10 nm.), and the improvement is approximately ΔSa = 98.21%). The surface roughness with MRF type (II) is (Sa =70 nm), which is approximately (ΔSa of 89.06%). High SA is affected by the addition of chemicals.
Fan et al., (2019) [184]	Biomaterial	MFAF	The MRF is SiC particle size (150 µm), and CIPs size (250 µm)	Achieved Sa=46 nm from the initial Sa=1.121 µm, which improved ΔSa by 95 %.
Barman and Das, (2018) [91]	Femoral knee implant	MFAF	The MRF is CIP (40 vol%) with size (8µm), and diamond abrasive particles (7.1 vol%) of size 6 µm in the base medium.	Achieved Sa = 20 nm., from the initial Sa=120 nm. To ensure implant performance, the operating gap, rotation speed, and time should be between 0.6 and 0.8 mm, 1100 to 1200 rpm, and 5.5 to 6

				hr, respectively.
Barman and Das (2019) [93]	Bio-implant	MFAF	The MRF is CIPs size (8 m), 40%, and magnetic abrasive diamond powder 3.5% powder (6 m), combined with 91.7% distilled water, 2.7% hydrofluoric acid (HF), 5.5 % nitric acid (HNO_3).	The final Sa is 10 nm. under the condition parameter of 1200 rpm, a 1 mm gap, and 6.30 hr, -The parallel toolpath produces a superior surface texture roughness to the spiral toolpath.
Fan et al. (2020) [183]	Bio-materials	MAF	MRF contains CIPs size (250μm) and SiC particle size (150 μm)	Reduce Sa from 1.17 μm to 54 nm under the experimental conditions of a 0.8 mm working gap, 15000 mm/min of feed rate, and 900 rpm of spindle rotation.
Tian et al., (2020) [150]	Bio-medicals	MAF	MRF contains CIPs (size 250 μm), SiC particles size 150 μm. with a weight ratio (9:1, and Lubricant oil.	The Sa reduced from 1.195 μm to 0.073 μm, representing an improvement of Sa about 94% under the ideal finishing conditions: 900 rpm spindle rotation, 160 r/min rotary table speed, and a 0.7 mm working gap.
Tien et al., (2022) [185]	Ti6Al4V alloy	MRFAF	MRF contains CIPs size (20 –30 μm.) and (Al2O3) size of 30 μm.	The surface quality significantly improved by ΔSa 37.5% (final Sa 0.04 μm) through the optimized cutting parameters determined by the hybrid algorithm and Taguchi experimental analysis.
Peng et al., (2021) [214]	Titanium alloy tubes	MRF	MRF contains CIPs size 18 μm, diamond size 20 μm, and Glycerol with Deionized water as a basis.	The Sa reduced from 0.251 to 0.191 μm after 600 cycles and removed 0.0012 g of material.
Kumar et al., (2015) [109]	Ti6Al4V alloy	MRAF	MRF contains CIP, SIC, and base medium of paraffin	The knee joint's surface was polished to a smoothness comparable to that of a mirror during the finishing process,

			oil.	with the final surface roughness (Sa) ranging from 78 to 35 nm.
Prakash et al., (2021) [102]	TieNbeTaeZr (β-TNTZ)	MRAF	MRF contains CIP Iron (Fe); size ~ 25 mm and Diamond; size ~ 2 mm	The improvement in Sa is around ΔSa 97.68 %, with a minimum surface finish of about 9 nm.
Singh et al. (2020) [104]	β-TiNbTaZr Alloy	MRFAF	MRF contains CIPs (Fe size ~25 µm) from 30-40% vol.	The finishing process improved by approximately ΔSa 95% from the starting value of Sa 1.121 µm, resulting in a final Sa of 46 nm.
Nagdeve et al., (2018) [108]	Replica of the knee joint.	R-MRAFF	The MRF (CIPs) particles range in size from 1 to 2 µm. and 10 %, and the abrasive boron carbide (B4C), size (4-9 µm), in 6% grease and 54% paraffin oil.	The Sa values of the femoral component exhibited variations across different faces, ranging from 190.4 to 79.5 nm on face 1, 85.3 to 72.3 nm on face 2, 202.7 to 85.7 nm on face 3, and 121.7 to 89.3 nm on face 4.
Bhavsar and Unune, (2018) [116]	Ti4Al6C	BEMRF	MRF contains CIPs grade (8µm) and SiC with a base medium of 3 ml of hydrofluoric acid (HF), 6 ml of nitric acid (HNO_3), and 100 ml of distilled water.	The tool rotational speed and gap distance were the primary determining factors in achieving a surface finish of up to Sa 500 nm, and were influenced by parameters such as mesh size and abrasive concentration.

2.2.2 Review of Magneto-rheological (MR) Finishing

Rabinow (1948) [215] developed magneto-rheological (MR) in the late 1940s. It consists of a 0.5 -10 µm suspension of ferromagnetic particles [216]. MR finishing is a smart material because it changes its properties in response to a magnetic field, which may be reversed throughout a carrier fluid that may consist of synthetic mineral oil [217], hydrocarbon oil [218], glycol [219], or water [220]. The compositions of MR fluids range from 20% to 80% in weight. (MR) Finishing can

instantly change from a fluid to a semi-solid or plastic form in reaction to a magnetic field. Field-dependent yield stress indicates viscoelastic behavior in semi-solid fluids [221]. Due to its distinctive features, MR finishing is used in various applications, including dampers, brakes, clutches, automotive suspensions, hydraulic valves, flexible fittings, and artificial muscles [222].

Numerous researchers in nano-finishing are using MR finishing [33,63,72,223,224]. The MR finishing in the CMMRF process is a mixture of multiple crucial elements, as shown in Fig. 2.4, that work together to enhance its distinct abilities to achieve precise surface finishing. MR finishing uses magnetic particles containing iron or an iron alloy that react actively to external magnetic fields. The particles are suspended in a liquid based on thickness and heat resistance. These liquids conduct magnetic particles. Surfactants and stabilizers stabilize and disperse fluids. A magnetic field can also reversibly improve viscosity and yield stress [111,192]. In their initial state, without a magnetic field, the magnetizable particles remain disordered inside the carrier fluid. Abrasive particles become lodged inside the CIPs chains. Fig.2.5 (a) [225]. When a magnetic field is applied, the particles align along the magnetic field lines, as shown in Fig. 2.5 (b) [112].

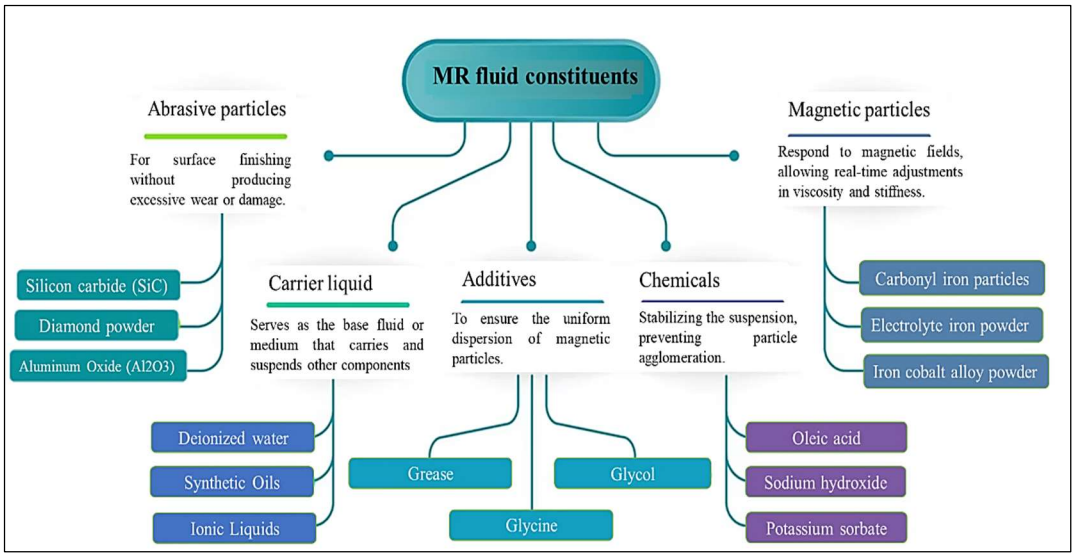

Fig.2. 4 A diagram illustrating the components of the MR finishing in the CMMRF process

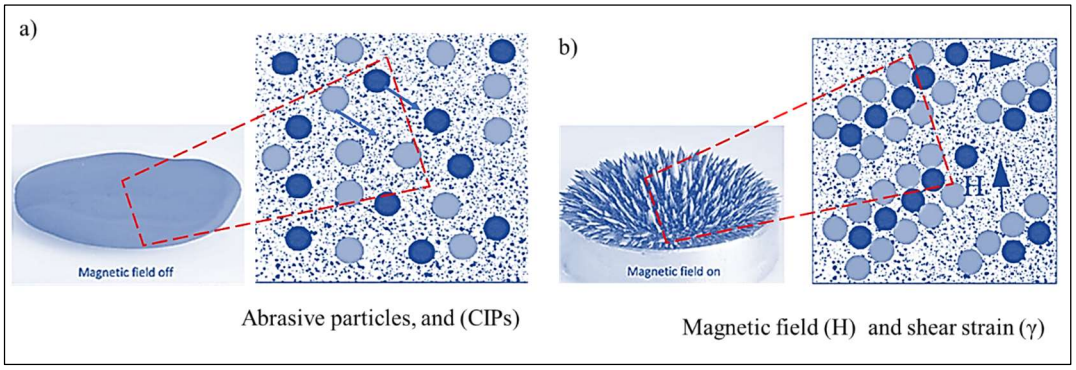

Fig.2. 5 An optical image of MR finishing a) without a magnetic field and b) under the effect of a magnetic field and shear strain [226,227].

MR finishing involves a rapid transition from liquid to solid, using abrasives and magnetic particles for precise surface removal and modification. Magnetic abrasives are essential for nano-cutting and modifying rheological characteristics [228,229]. The preparation of magnetic abrasives in MR finishing involves various approaches, which are conventional sintering magnetic abrasives (SMA) and the formation of composite powders that bond ferromagnetic material and abrasives, as shown in Fig. 2.6. Previously, the most often used for preparing magnetic abrasives were simply combined, as shown in Fig.2.6(a), which was preferred

because of their easy preparation [230]. However, the magnet's rotational speed creates a significant centripetal force that blows loosely mixed powder away from the work zone during surface finishing, thereby limiting its efficiency [98], as well as forming surface imperfections on the metal surface due to the combination of abrasive particles. Consequently, using a simple mixture of magnetic abrasives is less efficient and requires an extensive finishing process [224].

Additionally, it is time-consuming and costly [231]. To overcome this limitation, bonded magnetic abrasives in the form of composite powder are utilized [232]. Composite magnetic abrasives CMA are produced through gel-based, adhesive-based, mechanically alloyed, and plasma spraying processes [233]. CMA Microwave sintering is considered the most effective method for producing composite magnetic abrasives; it produces higher characteristics and finer microstructures using less energy [200] and significantly affects the material removal rate (MRR) compared to conventional mixed abrasives. The CMA enhances the surface roughness Sa of Al-6061 alloy by 34% after finishing, compared to a simple mixed abrasive. Additionally, the MRR can be increased by up to 50 % [231].

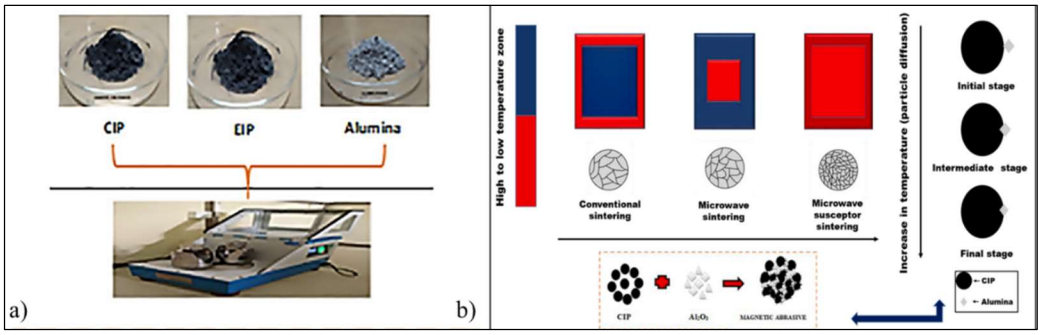

Fig.2. 6 CMMRF magnetic abrasive preparation for MR finishing: a) the conventional sintering (SMA), and b) Composite magnetic abrasives (CMA) [150,231].

Another type of MR finishing, combining magneto-rheological and shear thickening effects, offers excellent adaptability and processing efficiency. It enables the formation of magnetically enhanced particle clusters, resulting in

stronger holding forces on abrasive particles and achieving a nano-level surface finish [234]. Finishing by shear thickening improves the Sa by 77% to 79.0 nm from 337.6 nm for 1 hour, erasing all workpiece surface scratches [235]. The selection and precise constituents for MR finishing, as well as the preparation methods, affect the precision and efficiency of the CMMRF process, enabling the achievement of exceptional surface finishes in an advanced nano-finishing process.

2.3 Research Trends in the (CMMRF) Process

Recently, the CMMRF process has proven its precision in finishing large metal electronics and optical products [236]. It can be used for high-quality finishing machining of workpiece surfaces, with applications in aerospace, chip manufacturing, joint production, power electronics, and semiconductor fields [205]. CMMRF is employed to achieve final processing of semiconductor wafers, achieving a Sa of up to 2 nm [237]. Surface roughness ensures impeccably smooth surfaces, which are vital for the optimal performance and reliability of microchips and integrated circuits [197]. The application of CMMRF in the refinement of implants and surgical equipment. The procedure enhances a material's ability to interact with living tissues and reduces the likelihood of infection by creating surfaces that prevent germs from adhering to them [154]. In aviation, CMMRF is essential to finishing jet engine components, including turbine blades. The method ensures that these parts have smooth, flawless surfaces that can withstand harsh conditions, thereby improving their aerodynamic performance and longevity [137].

Table 2.3 presents an analysis of surface integrity alterations induced by the CMMRF process on various materials, utilizing instruments such as Taylor Hobson surface analyzers for surface roughness measurement, SEM, and FESEM for microstructure and topography analysis. Talysurf measures the surface roughness profile, providing a 2D representation, while AFM provides a 3D surface profile, or topography, correlated with peaks and valleys in both 2D and

3D images.

Table 2. 3 The change of surface characterization of different materials by the (CMMRF) process

Analysis of the change in the surface characterization.	**Before the (CMMRF) process**	**After the (CMMRF) process**
Materials: **Aluminum alloy (Al-6061)** The workpiece before and after the CMMRF process finishing; the 2D surface profile measures the change in surface roughness. The initial Sa is 351 nm, and the final Sa is 59 nm [231].	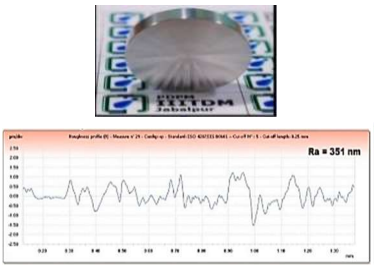	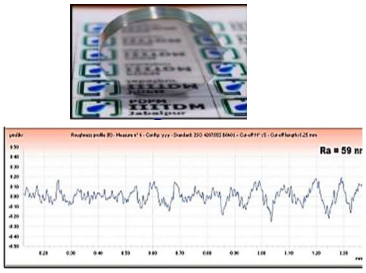
Materials: **Al-6061** The initial and final surfaces observed by scanning electron microscopy (SEM) showed reduced surface texture, and grinding marks on the finished surface disappeared after the CMMRF process [231].	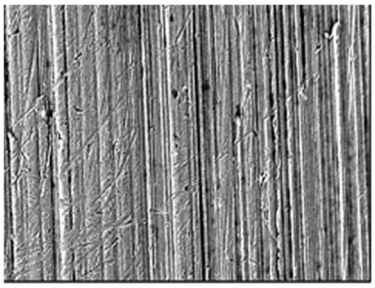	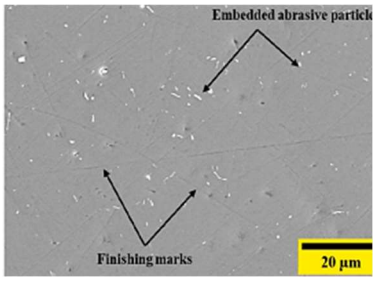
Materials: **Tungsten Carbide-Cobalt (WC-Co)** Optical microscopic images of the finishing Tungsten Carbide-Cobalt (WC-Co) cutting edge before and after the CMMRF process, showing a (Sa) reduction from 312.87 nm to 34.50 nm [60].	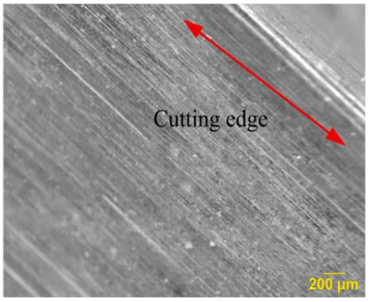	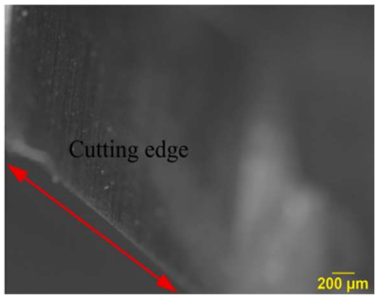

Materials: Aluminum alloy (Al 6061-T6) The 2D roughness profile shows an initial surface roughness of 50 nm after lapping. After the CMMRF process, the final (Sa) is 8.4 nm [190].	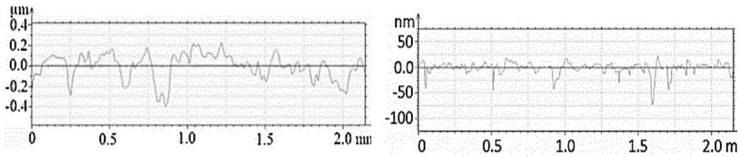
Materials: Aluminum alloy (Al 6061-T6) 3D topography shows the initial and final surface topographies after the CMMRF process, with fewer peaks [190].	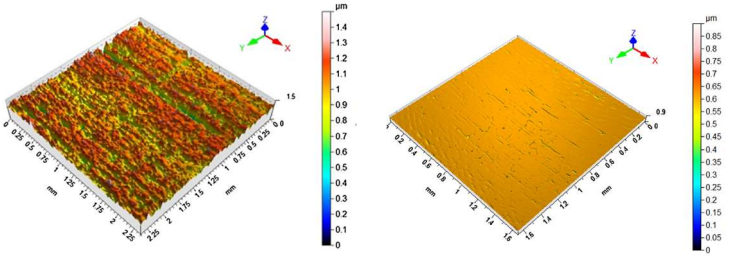
Materials: Aluminum (Al) The surface topography before and after the CMMRF process shows the final fine surface, with the surface texture and lines removed. The final result of (Sa) is 2.23 nm [238].	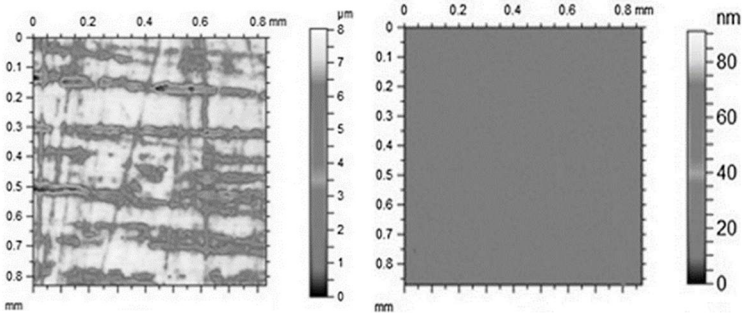
Material: Silicon wafer Scanning electron microscopy (SEM) and atomic force microscopy (AFM) images of the polished surface demonstrate the consistent and accurate execution of the polishing technique, with no visible scratch marks after the CMMRF process [224].	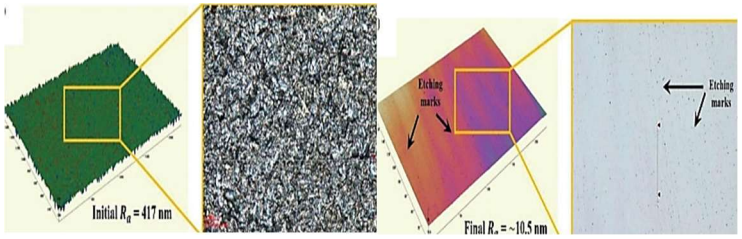

Materials: Silicon wafer Si (100)

The reduction of Sa using a 3D optical profilometer (Model: Zeta-20, Zeta Instruments) with a resolution of 0.2 nm and an accuracy of ±1%. The initial Ra is 417 nm, reduced to the final Sa is 2.432 nm [224].

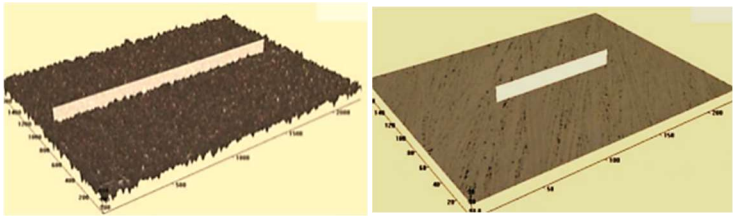

Materials: Aluminum alloy

The 2D profile shows the change of Ra values from the initial (Sa) 559 nm to 90 nm. AFM examination revealed the presence of surface peaks on the initial Ra and no peaks in the final Ra. Also, the surface is free of defects after the CMMRF process [239].

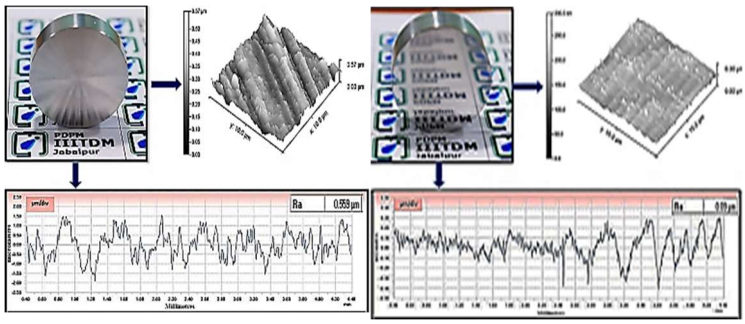

The CMMRF has extensive applications across various metals. It could provide nano-finishing surfaces on various materials, as the microelectronics and optics industries require components with high precision and minimal surface defects [240], which are utilized in advanced technologies [241] in different forms, sizes, and with varying levels of accuracy for efficient operation [242]. For instance, the final Sa value for finishing Aluminum alloy using the CMMRF process is 8.4 nm at a finishing time of 50 minutes [72], which is better than the surface finish of Aluminum by the CMP process [243].

2.4 Challenges and Limitations

Advanced nano-finishing processes, such as BEMRF, MRFF, CMMRF, R-MRAFF, and AFF, improve surface roughness. Still, challenges remain, including extended processing times, high operational costs, and varying effectiveness across materials. Table 2.4 summarizes the restrictions on nano-finishing methods for different materials. Despite its advanced capabilities, each process has

limitations that can restrict its efficacy and applicability. The advanced nano-finishing method CMMRF faces challenges in processing both ferrous and non-ferrous materials, managing MR finishing for brittle materials, and addressing environmental concerns, including waste disposal and chemical handling. It increases complexity and cost and may limit the ability to handle challenging, complex-geometry surfaces.

Table 2. 4 The limitations of various nano-finishing processes on different materials

References	Finishing process	Materials	The Sa results	Limitations
Saraswathamma et al. (2015) [244]	BEMRF	Silicon	Reduction in the Sa from 457nm to 89.8 nm. The ΔSa = 80 %	The process may take longer to achieve the desired surface finish. The heat to the magnetic coil reduces the (MR finishing) viscosity. There is a requirement for a consistent replacement of the MR fluid. Setup is costly.
Khan and Jha (2017)[114]	BEMRF	Copper	Reduced the Sa from 65.90 to 38 nm with a 42.34 % improvement	
Khan and Jha (2019) [245]	BEMRF	Copper	Reduce the Sa from the initial Sa = 97.10 nm to the final Sa = 26.40 nm.	The process may have limitations in achieving the desired surface finish for delicate or fragile materials.

Sidpara and Jain (2012a) [62]	MRFF	Stainless steel	Reduce the Sa from 97 nm to the final Sa of 28 nm	The time required to finish is longer. Particle segregation within a fluid. The process setup may be complex. Finishing a component's interior or complicated external surface is not appropriate.
H. Z. Liang et al. (2016) [237]	CMMRF	Single crystal (SiC)	Reduce the Sa from 50 nm to the final Sa of 2 nm.	A nonuniform corrosion layer on the (SiC) wafer is observed when there is a more significant concentration of iron particles. Handling chemicals in the polishing media can be hazardous.
Nagdeve et al. (2019)[111]	R-MRAFF	Co-Cr-Mo alloy	Reduce the Sa from 172 nm to 78 nm.	The time required to finish is high. Increased frictional heat alters the viscosity of MR fluid. CIPs change structure when MR fluid interacts with container walls. Increased rotating speed causes setup vibrations, resulting in diminished finishing performance.

Subramanian, et al. (2016) [84]	AFF	Co–Cr alloy	Reduced the Sa from 200 nm to 100 nm.	Machines and abrasives increase operational costs (machines and abrasives) Achieving smooth surface textures is complex. Insufficient fluid velocity. The time required to finish is very long.

Many successful attempts have been made to finish different metals and alloys using CH-MR finishing, as shown in Table 2.5. However, only a limited number of studies have investigated the application of the CH-MR process for nano-finishing hard materials such as Ti64 alloy.

Table 2. 5 Nano finishing of various metals and alloys by the CH-MR finishing process

References	**Materials**	**MR finishing / Chemicals**	**Findings**
Kumar (2023) [231]	Aluminum 6061	Sintering routes on CIPs and composite abrasive of Al_2O_3 / H_2O_2	A significant improvement of 34% in Sa was achieved, reaching 59 nm, and a 50% increase in material removal rate (MRR) was realized by optimizing the process parameters to a tool speed of 297.87 rpm, a working gap of 1.48 mm, and a finishing time of 57.45 minutes.
Tian (2022) [246]	Fused silica components	MR is CIPs and abrasive of cerium oxide / NaOH (PH~14)	Reduce the Sa from 208.4 to 12.3 nm and increase MRR by 287% with the optimal process

			parameters: polishing gap of 0.1 mm, feed speed of 0.03 mm/s, and pH value of 14.
Rajput (2022) [60]	Tungsten carbide in a cobalt (WC-Co)	MR is CIPs in distilled water with Diamond/ Murakami's reagent, a (NaOH, and potassium ferricyanide (C6N6FeK3).	Reduce the Sa from 312.87 nm to 34.50 nm. The ΔSa without and with Murakami's reagent in the MR is 43.12 % and Sa 88.97 %, respectively, for a constant finishing time.
Ghai (2018) [238]	Al-alloy	MR is CIPs, and (Glycol+Glycine), / (Citricacid+Ammonia)	The Sa was reduced to below 2 nm, and further improvements were achieved by refining the process parameters. The best result is the Sa (0.597 nm).
Srivastava (2021) [224]	Silicon wafer (100)	MR is CIPs, Alumina, Glycerol /(NaOH), (H_2O_2), Marshall's acid salt ($K_2S_2O_8$), and Caro's acid salt ($KHSO_5$)	Reduced the Sa to 4.225 nm in a polishing time of 60 min. The Sa is affected by CIP concentration, working gap, slurry flow rate, and polishing speed.

2.5 Comparison of finishing techniques and processing time

Fig. 2.7 compares various nano-finishing techniques, including CMMRF, MFAF, BEMRF, MAF, R-MRAFF, MRFF, and AFF, to evaluate the Sa value and associated finishing times. MFAF and BEMRF achieve high surface finish with moderate finishing times, making them promising for high-precision applications. MAF, known for its high surface finish potential, exhibits higher final roughness despite its short processing time. R-MRAFF and MRFF exhibit longer finishing times, with final roughness values of 78 nm and 28 nm, respectively; however, their extended processing times may hinder industrial scalability. Overall, these techniques offer promising solutions for high-precision applications.

Among the processes, the CMMRF process demonstrates exceptional efficiency when applied to aluminum alloy, decreasing the required finishing time. The minimum Sa value is 8.4 nm after 50 minutes of finishing, indicating that the combined action of chemical and magnetorheological processes can significantly improve surface quality in a comparatively short time.

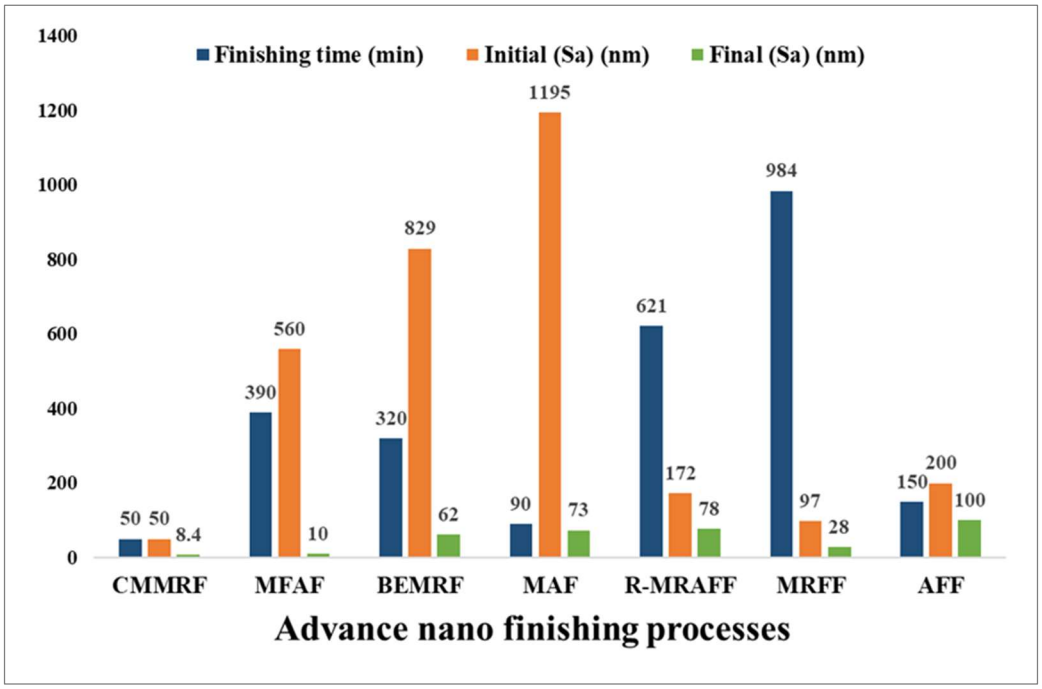

Fig.2. 7 Comparison of Sa values over time through different advanced nano-finishing processes [62,91,111,150,190,247,248]

2.6 Summary

In this chapter, we reviewed the finishing of Ti alloys using the chemo-mechanical magnetorheological finishing (CMMRF) process. This process is a cost-effective, efficient finishing technique used in high-precision industries, such as electronics, automotive, medical, and aviation, to achieve ultra-smooth surfaces with strict dimensional tolerances. It combines chemical and magneto-rheological processes for precise surface control. The CMMRF process involves a chemical reaction to form a passivation layer on the surface, followed by mechanical abrasion under a magnetic field to refine surface roughness, achieving precise nanoscale surface finishes. Magnetic abrasives can be prepared using traditional SMA sintering or composite CMA processes. This chapter covers the literature studies on CMMRF, discussing the process, its mechanism, properties, current research trends, and challenges in improving surface quality. It highlights that the procedure significantly enhances surface finishing, achieving a minimum Sa of 8.4 nm in just 50 minutes, with the finishing time having a significant impact on the outcome.

CHAPTER 3: PROBLEM FORMULATION

Based on a critical review of the literature, this chapter formulates the problem statement, identifies the research gaps, and defines the study objectives. Furthermore, it outlines the methodology used to effectively address these objectives.

3.1 Problem Statement

Surface finish is vital for biomedical implants, especially those used to replace femoral cups, knee joints, and hip joints. Moreover, it improves the implant's longevity and performance [178]. According to projections, the most in-demand implant parts are those used in spinal, knee, and hip replacement procedures. By the end of 2030, the expected increase in total hip replacements is projected to be 174% (reaching 572,000 procedures). Moreover, total knee arthroplasties are expected to grow by 673% from the current rate (3.48 million procedures) [4].

The primary tribological issue in artificial joints, such as knee and hip joints, is wear and the resulting wear debris, which can trigger infections and unfavorable tissue reactions, ultimately leading to the gradual deterioration of the prosthetic components [249–252]. However, surface treatment of Ti alloys enhances biocompatibility, corrosion resistance, and fatigue life, thereby reducing friction between implants and abutments [8,253].

Recently, researchers have sought to achieve higher-quality implant surfaces by using surface treatment methods, such as chemical etching, abrasive finishing, or laser sintering, to enhance mechanical and biofunctional properties [1,3,25,130,254–256].

The primary considerations regarding surface integrity pertained to the following:

i. topographical attributes such as textures, waviness, and surface roughness,

ii. mechanical properties that are influenced, such as residual stresses and hardness, and

iii. metallurgical conditions encompassing microstructure, phase transformation, grain size, shape, inclusions, etc. [181].

The significant impact of surface roughness on the interaction between the implant and the surrounding tissue at the micro- or nanoscale level has also been demonstrated [13,106]. Furthermore, surface nano-finishing and modification of Ti64 alloys are crucial in preventing the release of toxic elements from Ti alloys, such as vanadium and aluminum [257]. For nano finishing level in implants, according to ISO 7206-2: 2011/AMD 1:2016, the maximum surface roughness average (Sa) and maximum roughness total (St) are the quality control parameters for surface finish; also, Sa shall not be greater than 0.5 µm and St not greater than 1 µm [258–260] to prevent excessive wear from producing particles [258].

Various finishing processes have been developed to achieve high accuracy and meet medical requirements. These processes aim to enhance surface roughness and quality, ensuring optimal performance and compatibility across various medical fields. Ti alloys, especially Ti64 alloy, are widely used in biomedical applications due to their remarkable attributes, such as a high strength-to-weight ratio, outstanding corrosion resistance, and excellent biocompatibility. Nonetheless, achieving the necessary surface quality and bioactivity in these alloys is a significant challenge. Surface roughness and chemical characteristics are crucial in determining the functional performance of biomedical implants, as they affect cell adhesion, osseointegration, and wear resistance. Traditional finishing methods often fail to meet these rigorous standards while also ensuring environmental sustainability and cost efficiency.

MRF finishing is advantageous for achieving exceptional surface finishes because it provides precise control of material removal at the micro- and nanoscale. Nonetheless, the efficacy of MRF in processing Ti alloys is constrained by their intrinsic hardness and suboptimal machinability. Moreover, although chemical treatments can enhance the bioactivity of Ti alloys, their integration with mechanical finishing techniques for optimal performance remains inadequately investigated. A notable deficiency in surface engineering for biomedical applications is a lack of an environmentally sustainable, synergistic method that integrates chemical treatment and material recovery facilities for Ti alloys.

Traditional finishing techniques such as grinding, lapping, and blasting are often ineffective in producing the required nanoscale surface qualities. Furthermore, these processes can induce material degradation, residual stresses, and surface cracking, especially in high-performance titanium alloys. As a result, there is a pressing need for advanced nano-finishing techniques that can enhance the surface integrity of Ti64 without compromising its bulk mechanical properties.

The objective of this research is to develop a novel process for Ti64 alloy for biomedical applications.

3.2 Research Gaps:

The literature review has led to the identification of the following research gaps:

1. Most research has used hazardous chemicals, such as hydrofluoric and nitric acid, in the finishing process; however, we need to focus more on eco-friendly MR fluid.
2. There is a need to investigate Ti64 alloy after surface modification regarding its biocompatibility, bioactivity, and corrosion resistance for biomedical implants.
3. There is very little research on the surface modification of Ti64 alloy for biomedical applications.
4. A limited number of experimental investigations have been reported in the

literature on the finishing of Ti64 alloy by the chemo-mechanical magnetorheological process.

3.3 Research Objectives:

In light of the gaps, as mentioned earlier, the present investigation aims to complete the following objectives:

1. To develop an eco-friendly Chemo mechanical MR finishing process (CM-MR) for Ti64 alloy for biomedical implant applications.
2. To develop a novel process for surface modification of Ti64 alloy by eco-friendly chemicals to improve the mechanical characteristics, bioactivity, and biocompatibility.
3. To analyse the effect of CM-MR process parameters on the surface roughness (Sa) of Ti64 alloy and optimize them for enhanced surface finish.
4. To evaluate the surface roughness of Ti64 alloy after finishing and analyze the influence of integrated CH-MR process parameters on its quality.

This research aims to address this gap by developing an eco-friendly chemical as a sustainable solution that advances surface engineering for biomedical implants. Integrates chemical treatments with magnetorheological finishing to achieve a nanoscale surface finish on Ti64 alloy, optimizing the process parameters and evaluating their effects on reducing surface roughness. Additionally, it develops a thermochemical process to enhance the bioactivity, biocompatibility, and overall performance of biomedical implants.

This study aims to enhance surface engineering for biomedical implants by overcoming the limits of current techniques and introducing a novel, sustainable alternative.

3.4 Methodology

This chapter outlines the experimental methods used in the present study, which are structured into two complementary sections aimed at enhancing the surface properties of Ti64 alloy for biomedical implant applications (Fig. 3.1).

The first section focused on THCP, in which Ti64 specimens were chemically pretreated with eco-friendly reagents, then heat-treated and immersed in Hank's Balanced Salt Solution (HBSS). This sequence was designed to investigate surface integrity, bioactivity, and biocompatibility under simulated physiological conditions, with surface characterization performed using FTIR, FESEM, and EDS.

The second section utilizes the CH-MR process, which combines chemical pretreatment for oxidation and softening with MR finishing using CeO_2 abrasives and CIPs under a magnetic field. Key process parameters, including pH, spindle speed, working gap, and current, were systematically studied using a central composite design (CCD) and optimized using response surface methodology (RSM) to minimize surface roughness (Sa). Characterization techniques, including AFM, FESEM, and XPS, confirmed improvements in nanoscale surface quality.

Together, THCP and CH-MR established an integrated framework to enhance the biocompatibility, bioactivity, and finishing quality of Ti64 alloy, addressing critical requirements for long-term biomedical implant performance.

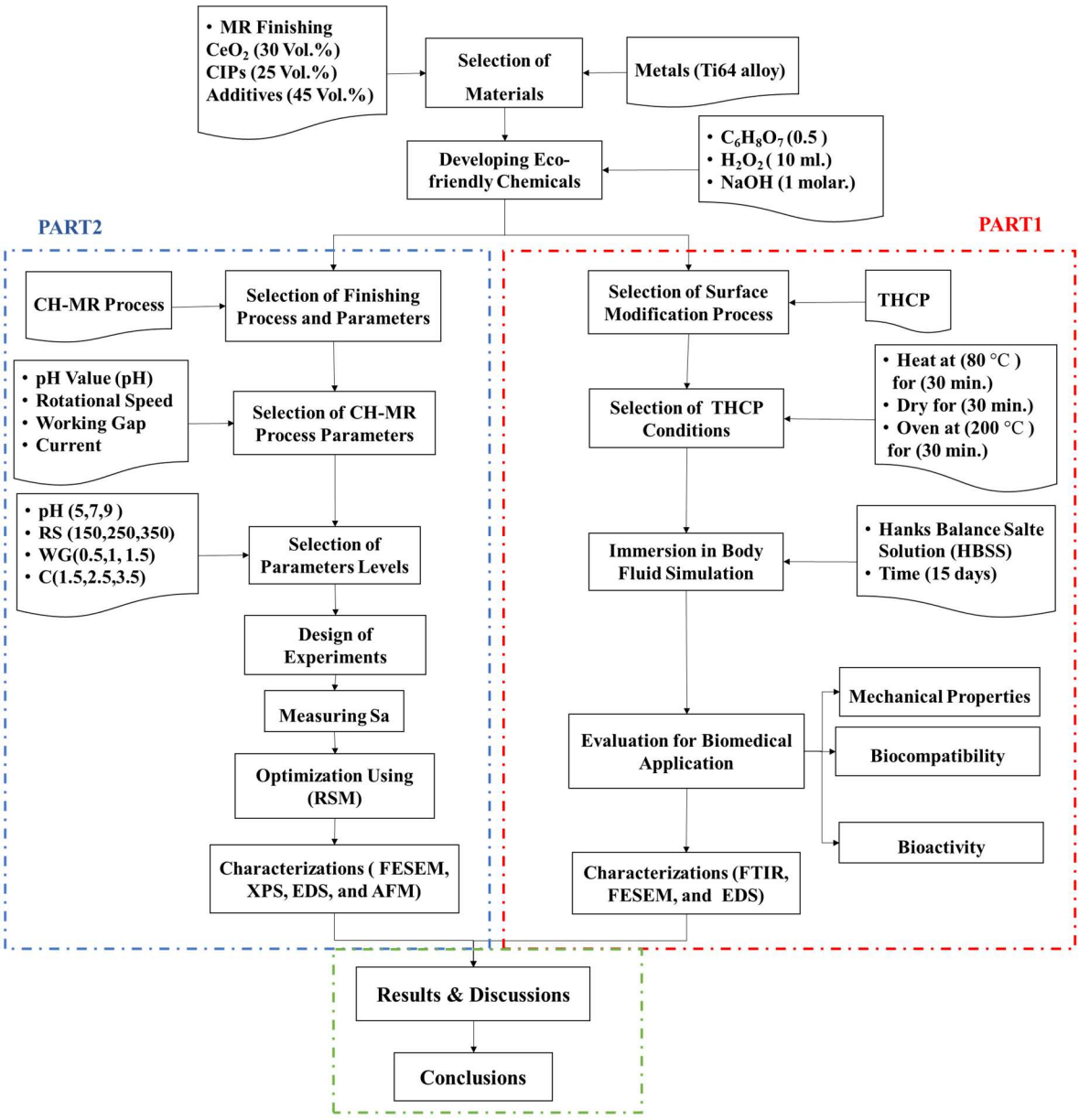

Fig. 3. 1 Methodology

124

CHAPTER 4: MATERIALS AND METHODS

This chapter presents the materials and methods, providing information on the substrate, eco-friendly materials, and the mechanism of surface modification. It further describes the statistical analysis used to optimize process parameters to minimize surface roughness (Sa) and provides the specifications of the characterization equipment.

4.1 The Substrate Materials:

4.1.1 Titanium alloy

Ti alloy grade 5 (Ti64 alloy) from PARSHWAMANI METALS Co. was selected due to its broad application in biomedical implants [3], which accounts for its excellent qualities [5], as shown in Table 4.2. The alloy composition is listed in Table 4.1. To improve the efficiency of the finishing process, we used wire EDM to cut the workpiece to the accurate dimensions of 25×10×5 mm. Subsequently, we perform grinding machining to refine the surface, followed by polishing with sandpapers of varying grit sizes, ranging from 400 to 2000 mesh. The workpiece is meticulously cleansed with distilled water and acetone.

Table 4. 1 Composition of Ti64 alloy

Elements	Percentage (%)
Carbon	0.08 %
Iron	0.25 %
Aluminum	5.50 %
Vanadium	3.80 %
Titanium	Balance

Table 4. 2 Properties of Ti64 alloy

Properties	**Value**
Density (g/cm^3)	4.429
Young's Modulus (GPa)	104
Melting Point (^{0}C)	1649
Tensile Strength (MPa)	897

4.1.2 Magnetorheological Fluid (MR)

The preparation of magneto-rheological (MR) finishing was achieved by mixing ferromagnetic particles (CIPs) and abrasives in a carrier fluid [261]. BASF manufactures the CIPs of the CS grade in Germany, and VEDAYUKT INDIA PVT manufactures Cerium oxide (mesh size 1200).LTD., and additives of carrier fluid of a mixture of glycerol and grease (Table 4.3) to prevent sedimentation of abrasive and ferromagnetic particles and ensure their soluble nature in water [96].

Table 4. 3 MR finishing compositions

MR constituents	**Purpose**	**(Vol. %)**
Ferromagnetic particle CIPs (CS grade size 5-15 µm) with a density of 7.8 g/cm³	CIPs manage MR finishing qualities in real time and reversibly through alignment and clustering.	30 %
Abrasive CeO_2 (1200 mesh size) with a density of 7.22 g/cm³	CeO_2 abrasive particles in the MR of surface polishing and abrading	25 %
Base Fluid Glycerol and deionized water	To prevent ferromagnetic and abrasive particles from sedimentation.	45 %

The characterization of the Ti64 alloy is illustrated in Fig. 4.1, which shows

the elemental composition and XRD patterns. The α-phase high-intensity peak, often observed at 2θ angles of 35° to 40°, is also shown. The β-phase, with its BCC structure, exhibits unique peaks, including the strongest (110) reflection at 2θ = 39°. These distinctive peaks distinguish between the two alloy phases.

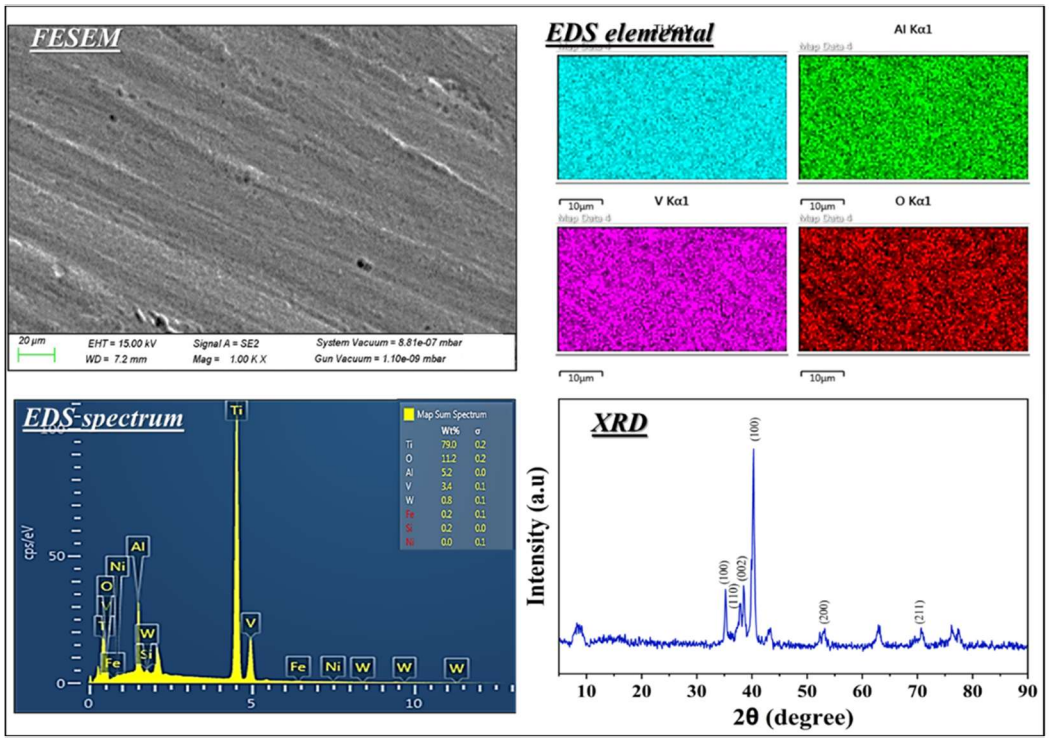

Fig. 4. 1 Ti64 alloy surface morphology, with the metal elements compositions and XRD

4.1.3 The Chemical Materials

The chemicals used include H_2O_2 (30% W/V, pH solution 1.8 – 1.12) from Thermo Fisher Scientific India Pvt. Ltd., $C_6H_8O_7$ (anhydrous) from Thermo Fisher Scientific India Pvt. Ltd., and NaOH (s SD Fine-Chem Limited). For in vitro test Hanks Balance solution (HBSS) was prepared composed of 8.0 g Sodium Chloride (NaCl), 0.4 g Potassium Chloride (KCl), 0.14 g Calcium Chloride ($CaCl_2$), 0.1 g Magnesium Sulphate ($MgSO_4$), 0.06 g Potassium Phosphate Monobasic (KH_2PO_4), 0.06 g Sodium Phosphate Dibasic (Na_2HPO_4), 1.0 g D - Glucose The components are dissolved in distilled water. The pH is adjusted to the required

level using NaOH or HCl to maintain a pH level of approximately 7.4, which is conducive to normal body functions.

The novel eco-friendly chemical solution was prepared by mixing 30 % (V) of H_2O_2 and 0.5 g of $C_6H_8O_7$ and using 1 Molar (Mol) NaOH to adjust the pH values (5, 7, and 9) at room temperature. The samples were submerged in a chemical solution mixture at room temperature for 30 minutes.

4.2 Surface Preparation

Fig. 4.2 outlines the process steps for preparing a metallic workpiece. Wire EDM was used to cut the workpiece to dimensions of 25 × 10 × 5 mm with high precision. Subsequently, grinding was performed to refine the surface, followed by polishing with sandpaper of varying grit sizes, ranging from 400 to 2000. Finally, thoroughly clean and rinse the sample with distilled water and acetone to eliminate contaminants, ensuring it is ready for further analysis or application.

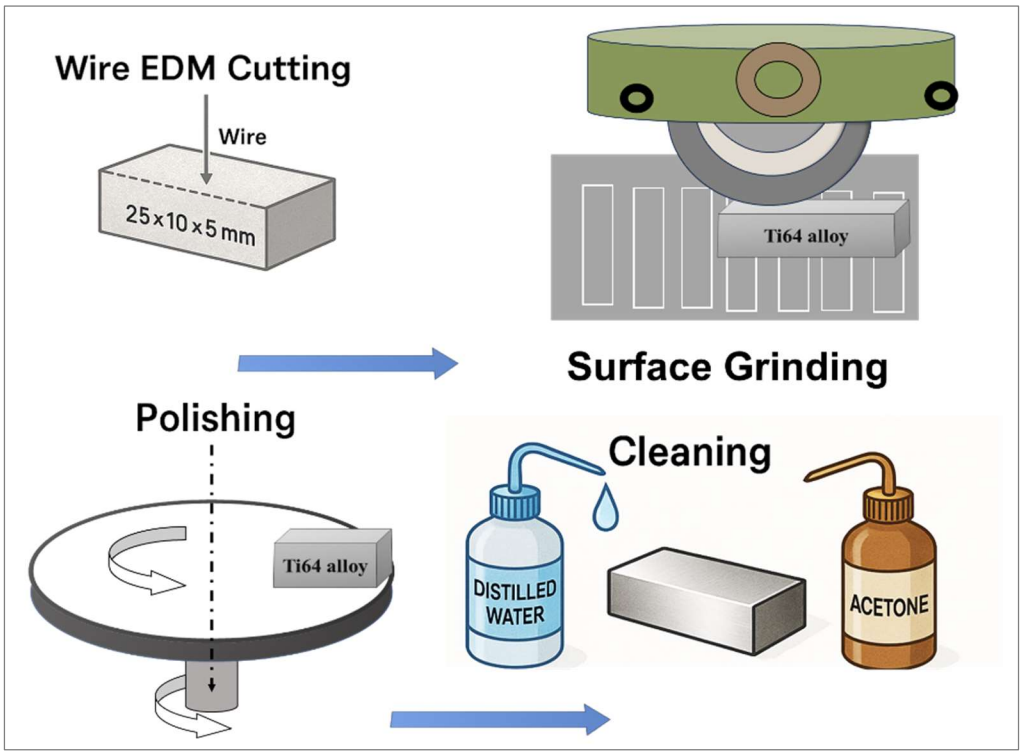

Fig. 4. 2 Surface preparation process of Ti64 alloy

4.3 Surface Modification of Ti64 Alloy by THCP

This study investigates chemical and heat treatments for surface modification of Ti64 alloy using H_2O_2 and $C_6H_8O_7$ as eco-friendly agents. The samples were separated into two groups, as indicated in Table 4.4. Group (A) consisted of samples treated with a thermochemical process, while one sample was left untreated as a control. Group (B) consisted of samples treated with a thermochemical process at different pH values (5, 7, and 9), followed by immersion in HBBS in vitro testing.

Table 4. 4 The surface modification sample groups

Ti64 alloy sample group	Ti64 alloy	Thermochemically treated	pH (value)	HBSS treated
Group (A)	Ti64 (0)	No	-	No
	Ti64 (1)	Yes	pH (5)	No
	Ti64 (2)		pH (7)	
	Ti64 (3)		pH (9)	
Group (B)	Ti64 (0)	No	-	Yes
	Ti64 (1)	Yes	pH (5)	Yes
	Ti64 (2)		pH (7)	
	Ti64 (3)		pH (9)	

The thermochemical surface modification procedure for Ti64 alloy is illustrated in Fig. 4.2. The chemical solution was prepared by mixing 30 % (v/v) (H_2O_2) with ($C_6H_8O_7$) and adjusting the pH to 5, 7, and 9 using a 1M (NaOH) solution at room temperature. Sample (group A) was then submerged in the solution and subjected to a heat treatment at 80 °C for 30 minutes. The samples were dried in a vacuum for 15 minutes. Subsequently, the samples were placed in a furnace at 200 °C for one hour and allowed to cool slowly within the furnace. The modified samples were immersed in HBSS for 15 days and designated as samples (group B).

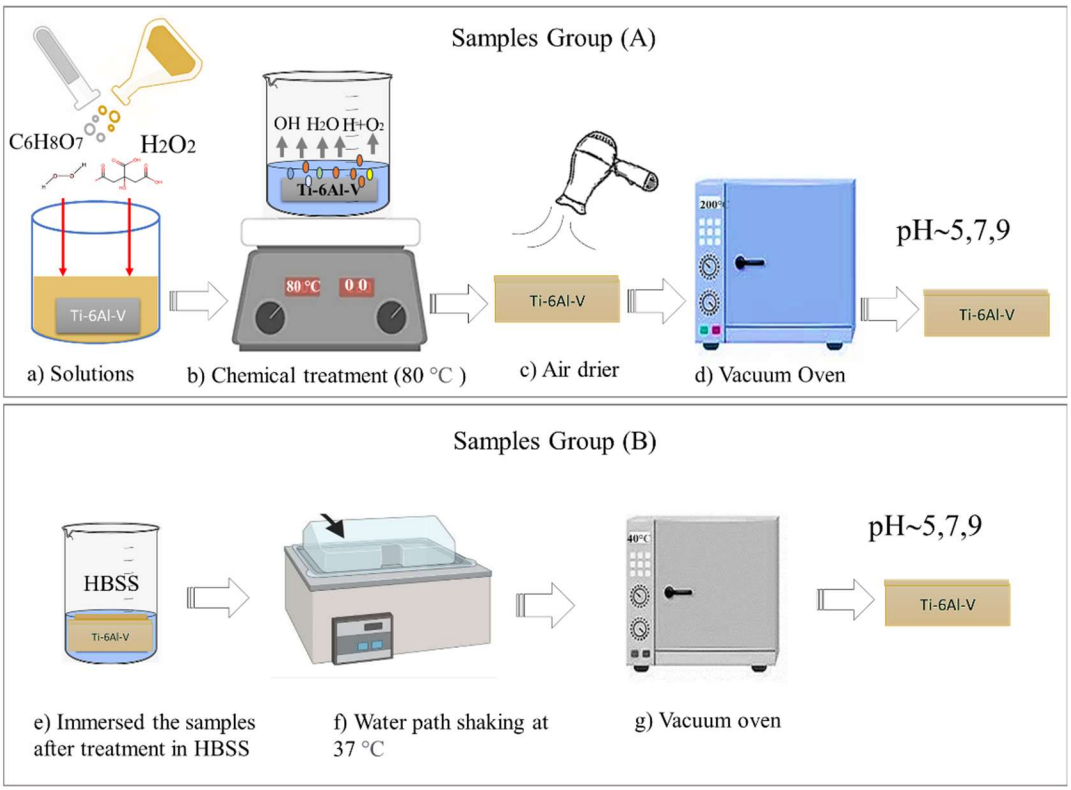

Fig. 4. 3 Schematic representation of the novel process procedure for surface modification of Ti64 alloy by environmentally friendly chemicals

The dissociation chemical represents the breakdown of Citric acid (CA) into protons (H^+) and its general base (M^{3-}) [262].

$$CA \rightleftharpoons 3H^+ + M^{3-} \quad (1)$$

The oxidation of Ti64 alloy by H_2O_2 promotes the formation of a layer on the surface; the reaction occurs as follows:

$$2Al + 3H_2O_2 \rightarrow Al_2O_3 + 3H_2O \quad (2)$$

$$V + 2H_2O_2 \rightarrow VO_2 + 2H_2O \quad (3)$$

$$Ti + 2\,H_2O_2 \rightarrow TiO^2 + 2H_2O \quad (4)$$

The reaction of the elements' oxides with protons

$$Al_2O_3 + 6H^+ \rightarrow 2Al^{3+} + 3H_2O \quad (5)$$

$$VO_2 + 2H^+ + 4H_2O \rightarrow [VO\,(H_2O)_5]^{2+} \quad (6)$$

Furthermore, H_2O_2 may react with Ti in the presence of citric acid [262].

$$Ti + 2H_2O_2 + 2H^+ \rightarrow TiO^{2+} + 3H_2O \quad (7)$$

4.4 The Surface Finishing by the CH-MR Process

4.4.1 The CH-MR process mechanism

The CH-MR process is a hybrid technique that uses chemical reactions to form passivation layers on Ti64 alloy surfaces, followed by magnetic-field-assisted mechanical abrasion to achieve a nanometric surface finish, thereby enhancing surface quality. Fig. 4.3 illustrates the mechanism of the CH-MR process. This process involves two significant steps: a chemical reaction that softens the substrate and facilitates the formation of an oxide layer on the surface (Fig. 4.3a), followed by mechanical abrasion for material removal. MR fluid is magnetized by a permanent magnet or electromagnet, creating a flexible polishing pad or brush [113]. Abrasive particles entangled in a chain of (CIPs) in MR fluid remove soft particles during surface finishing [262], making it easier to remove by MR finishing to improve MMR and surface quality, and eliminate wear marks [35], and decrease surface finishing time. The MR fluid exhibits increased rigidity in the presence of an external magnetic field, enabling the removal of surface irregularities through its relative motion with the workpiece [263].

(Fig. 4.3 b) illustrates the finishing action and feed direction on the workpiece. The amount of material removed from the workpiece surface by abrasives is governed by the bonding forces between the CIPs (carbonyl iron particles) within the finishing spot of the MR fluid. The finishing force F_F is generated by the finishing spot of the MR fluid on the workpiece surface. This force is a combination of the normal force Fn, which acts along the direction of magnetic lines of force, and the shear force Ft, which acts along the direction of the core rotation [113]. A permanent magnet was placed beneath the workpiece to enhance the magnetic flux density.

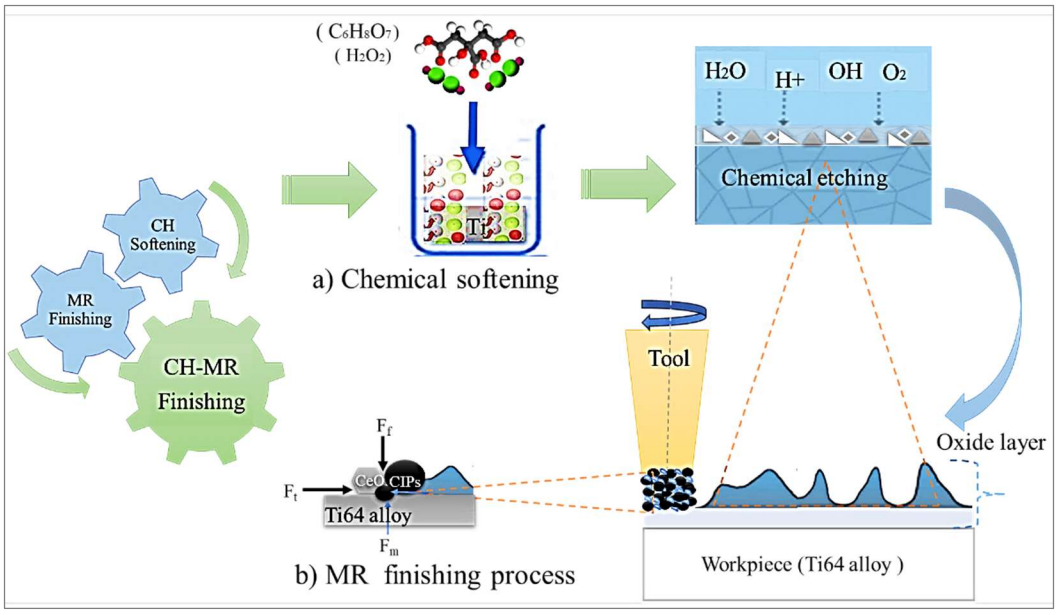

Fig. 4. 4 Schematic diagram of the CH-MR finishing process mechanism

4.4.2 Design of Experiments

In the hybrid CH-MR process, the final Sa depends on the machine parameters, working gap, feed rate, spindle speed, current, and type and specifications of the chemical [264]. This study utilizes eco-friendly materials with different pH values (acidic, neutral, and alkaline). The worktable feed rate is set to 25 mm/min, and four parameters are evaluated to determine the optimal Sa value for the best finishing conditions of the Ti64 alloy.

57

Experiments were conducted using a central composite design (CCD) to optimize the CH-MR process parameters and identify the optimal conditions for minimizing the Sa of Ti64 alloy using Minitab 22 software [265]. The process parameters range selection was based on initial experiments and literature studies [60,150,198]. For clarity, a four-parameter with a 3-level design was systematically tabulated in Table 4.5.

The CCD methodology statistically models linear, quadratic, and interaction effects between variables while minimizing the number of experiments, thereby maintaining statistical robustness and ensuring reliable

predictive outcomes [266].

Table 4. 5 Coded and actual values of the CH-MR process parameters.

S. no	Process parameters	Unit	Levels		
			-1	0	+1
1	pH value (pH)	No.	5	7	9
2	Working gap (WG)	(mm)	0.5	1	1.5
3	Rotational speed (RS)	(rpm)	150	250	350
4	Current (C)	(A)	1.5	2.5	3.5

A total of 28 experimental runs were systematically planned using a CCD and executed to develop a robust statistical model for predicting the final Sa, as shown in Table 4.6. This Table summarizes the experimental conditions and their corresponding output response. This study employed ANOVA to statistically analyze the influence of CH-MR process parameters on the surface roughness of the Ti64 alloy. After that, the mathematical model was developed through regression analysis to predict the final Sa. The model's accuracy demonstrates its ability to predict Sa.

Table 4. 6 The CCD Experimental Runs and Resulting Sa of CH-MR Finishing of Ti64 Alloy

Run Order	pH Value (pH)	Working Gap (WG)	Rotational Speed (RS)	Current (C)	Sa (nm)
1	7	0.5	250	2.5	70.24
2	5	0.5	350	3.5	50.02
3	5	0.5	350	1.5	57.03
4	9	0.5	150	3.5	62.20
5	9	0.5	350	3.5	59.60
6	9	1.5	150	1.5	85.20
7	5	1.5	350	3.5	78.08
8	5	1.5	350	1.5	89.80

9	5	1.5	150	3.5	46.30
10	7	1.0	250	1.5	70.70
11	5	1.5	150	1.5	52.33
12	7	1.0	250	2.5	65.52
13	9	1.0	250	2.5	73.43
14	9	1.5	350	3.5	67.00
15	7	1.0	250	2.5	65.52
16	5	0.5	150	3.5	38.20
17	7	1.5	250	2.5	80.92
18	9	0.5	350	1.5	71.55
19	9	1.5	150	3.5	60.52
20	7	1.0	150	2.5	59.92
21	9	1.5	350	1.5	80.50
22	9	0.5	150	1.5	75.30
23	7	1.0	250	3.5	69.20
24	7	1.0	350	2.5	71.90
25	5	0.5	150	1.5	44.67
26	5	1.0	250	2.5	55.20
27	5	0.5	150	3.5	38.40
28	9	1.5	350	3.5	74.80

4.4.3 Machining Process

The experiment utilized a finishing tool setup attached to a 3-axis CNC machine; this setup consisted of an electromagnetic coil connected to the MR finishing on the tool's tip (Fig. 4.5 a). MR is a flexible polishing material made from (CIPs) and abrasive particles (CeO_2), which functions like a Newtonian fluid without a magnet. It changes its viscosity to a semisolid state when exposed to a magnetic field, resisting deformation and enhancing its strength. The magnetic field influences the MR fluid and the relative motion between the workpieces, thereby inducing motion between them. This motion, affected by the magnetic

field, impacts the behavior of magnetic particles, abrasives, carrier fluid, and stabilizers (Fig. 5.14b). A permanent magnet was placed beneath the workpiece to enhance the magnetic flux density and the finishing process.

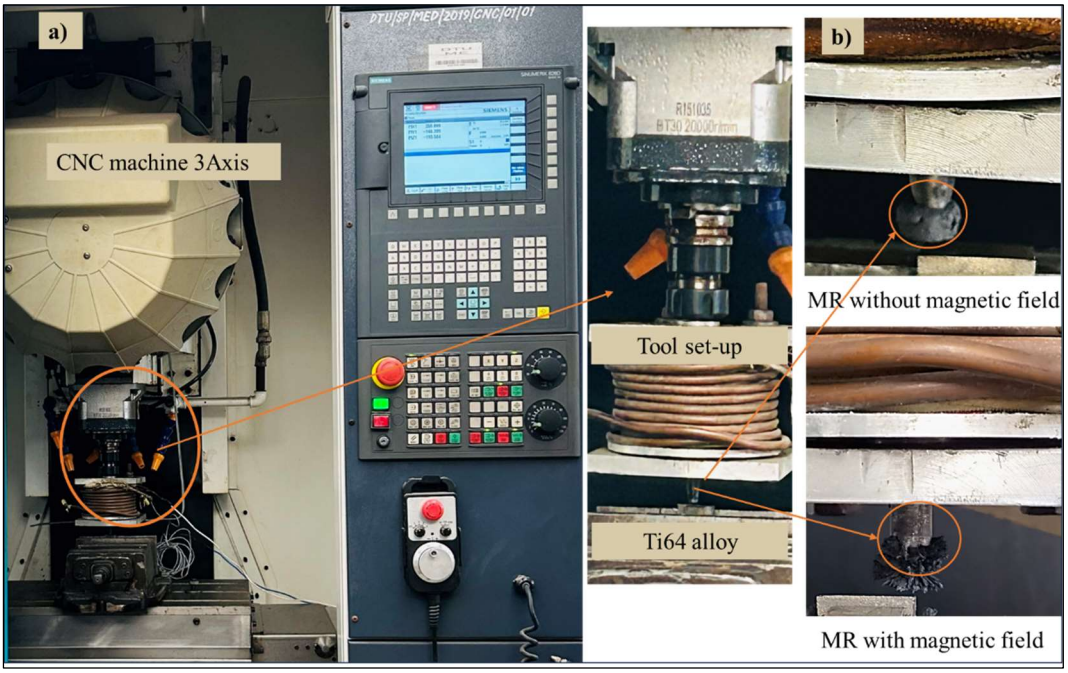

Fig. 4. 5 CNC machine with Setup tool (a), MR finishing under the effect of the magnetic field, and without the influence of the magnetic field (b)

4.4.3.1 Specifications of CNC Machine

The machine features a 650 × 400 mm worktable with a 300 kg capacity and X/Y/Z travel of 500/400/330 mm. The spindle operates at 150–20,000 rpm with a No. 30 (7:24) taper and supports a 16-tool changer (BT30-45°), handling tools with a diameter of up to 150 mm and a length of 200 mm, weighing up to 2 kg. Tool change times range from 1.5 to 1.8 seconds. Cutting speeds reach 20,000 mm/min, with rapid feed rates of 48 mm/min. Precision is ensured with 0.010 mm positioning and 0.006 mm repeatability. The machine requires an air pressure of 0.5–0.7 MPa, with dimensions of 2146 × 1600 × 2280 mm, and a weight of 2750 kg.

4.5 The Characterizations

4.5.1 Surface Morphology

The study employed field-emission scanning electron microscopy (FESEM) to capture images of sample surfaces and analyze surface morphology, homogeneity, and texture. EDS was used for elemental analysis, while Fourier transform infrared (FTIR) spectroscopy was used to analyze surface chemistry and functional groups of the samples, recording chemical bond characteristics in the 500-4000 cm^{-1} range.

Fig. 4. 6 Scanning Electron Microscope attached with an EDS detector.

4.5.2 Mechanical Properties

The microhardness, tribological tests, surface roughness, adhesion, and wettability were analyzed to determine the mechanical properties of the Ti46 alloy.

4.5.2.1 The Microhardness

The surface microhardness of the samples was measured using a Vickers microhardness tester (Struers, DURAMINTM, Denmark, Model No. Duramin-40

M1), which can apply loads of 1-1000 g. The experimental sample (Group A) was subjected to a 10-second test, during which a force of 0.5 kg was applied with indentation. The results were obtained by averaging ten indented samples, in accordance with ASTM E384 for conducting microhardness tests. Then, we calculated the variation in microhardness as the difference between the initial and final microhardness values after treatment.

Change in microhardness = Final microhardness − Initial microhardness **(8)**

We used the formula above to calculate the percentage improvement in microhardness. To determine the percentage, the difference in microhardness is divided by the initial microhardness value and then multiplied by 100%.

Percentage improvement = Change in Microhardness/Initial Microhardness) × 100 **(9)**

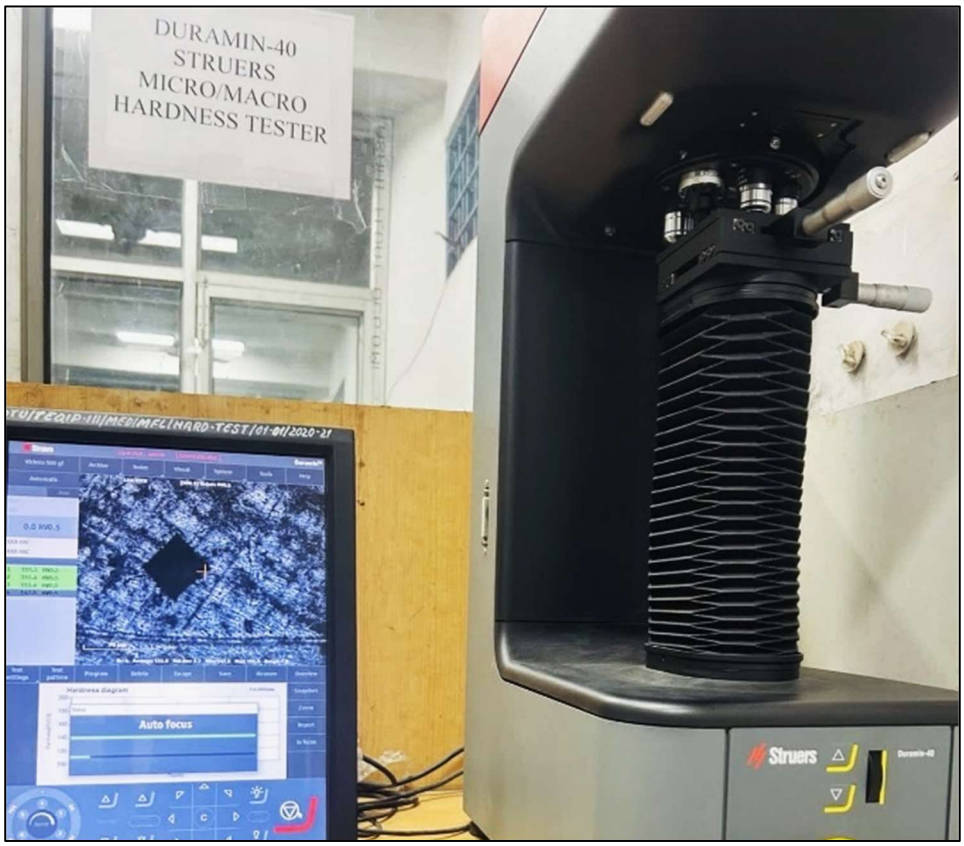

Fig. 4. 7 Vickers Hardness Machine (Duramin-40 M1 (ASTM E384)

4.5.2.2. Tribological

The tribological analysis was performed according to ASTM G133, using a reciprocating tribometer equipped with a liner. The load range employed consists of three magnitudes: 10 N, 15 N, and 20 N. The frequency is 5 Hz, the stroke range is 5 mm, and the temperature is maintained at 37 °C. A sheet of EN31 steel was accurately divided into squares with dimensions of (30*30* 5) mm, and the pins were perfectly shaped to have a diameter of 6 mm and a length of 15 mm using a WEDM machine to guarantee excellent dimensional precision. The prepared pins were the treated sample (group A).

The coefficient of friction (COF) was measured using a linear reciprocating tribometer in accordance with ASTM-G133, while the wear rate (Wr) was determined using the weight-loss method. The Wr was determined as:

$$\mathbf{(Wr) = V / (N * D)} \qquad \mathbf{(10)}$$

Wr is measured in mm^3/N-m and is calculated using the volume of wear loss (V) in (mm^3), the applied load (N) in Newtons, and the sliding distance (D) in meters (m) .

Where,

$$\mathbf{Volume\ loss\ (mm^3) = Mass\ loss\ (gm)/\ Density\ (gm/cm^3)\ *1000} \qquad \mathbf{(11)}$$

Fig. 4. 8 Linear Reciprocating tribometer (ASTM-G133)

38

4.5.2.3.1 Surface Roughness

The samples were cleaned with deionized water, and the surface area (Sa) was measured before and after the modification. Sa was evaluated using a roughness measuring tool manufactured by Taylor-Hobson. A random selection of five locations was made to obtain average values before and after the treatment.

Fig. 4. 9 Surface roughness tester (Taylor-Hobson)

4.5.3 Corrosion Characterization

The electrochemical analysis test was performed using a PAR Model 2273 workstation from Princeton, USA. The system used a three-electrode configuration, with a platinum wire as the counter electrode, a saturated calomel electrode (SCE) as the reference electrode, and a working electrode with a sample surface area of 2.05 cm^2. The experiment was conducted at 37 °C in a glass container (30 mL of HBSS). Initially, the open-circuit potential (Eocp) of each sample was assessed. Potentiodynamic polarization was performed at a scan rate of 0.5 mV/s from -0.3 V SEC to -1.5 V SEC. Each experiment was performed three times to ensure precise, reliable outcomes. The Tafel extrapolation was used to study the potentiodynamic curves and determine the electrochemical parameters, including the corrosion potential (E_{corr}, V), current density (I_{corr}, A/cm^2), and Tafel slopes, anodic Tafel coefficient (βa), and cathodic Tafel coefficient (βc) ($V\ dec^{-1}$) data. The corrosion rate (V_{corr}) can be measured using Faraday's law as :

$$(V_{corr}) = 0.00327 \times I_{corr} \times E_{qw} / D \quad (12)$$

Where the I_{corr} is the corrosion current density in ($\mu A/cm^2$), E_{qw} is the equivalent weight of the sample, calculated according to ASTM Standard 1999 [267], and D is the sample density in (g/cm^3).

Fig. 4. 10 Potentiostat/Galvanostat Device

4.5.4 The Biocompatibility

The hemolysis test was conducted to assess the cytotoxicity and biocompatibility of the Ti64 alloy in vitro, according to ISO 10993-4:2009 and ASTM F756-00 [268,269]. Healthy blood was collected from adult volunteers and stored in heparin-containing tubes. Phosphate-buffered saline (PBS) was prepared, and samples measuring 20 × 10 × 5 mm were submerged in a centrifuge tube containing 10 mL of PBS. The ratio of sample surface area to PBS volume was kept at 3:1 cm^2/mL. The centrifuge tubes were placed in a shaking bath and incubated at 37°C for 30 minutes. Then, 0.2 mL of diluted blood (prepared by mixing 2 mL of whole blood with 2.5 mL of PBS) was added to the tubes. The mixtures were then incubated at 37°C for 1 hour. A negative control was 10 mL of PBS, while a positive control was 10 mL of distilled water. We centrifuged the tubes for 15 minutes at 1500 rpm. The supernatant, the liquid above the sediment, was carefully collected and transported to cuvettes for spectroscopic analysis using a Shimadzu UV-1800 UV/Visible Scanning Spectrophotometer after centrifugation. The measurements were taken at a wavelength of 545 nm [270]. The hemolysis ratio (Hr) is measured as a percentage using the following formula

[269]:

$$\mathbf{Hr\ (\%) = (\ D_{test} - D_{(-)}\ ) / (\ D_{(+)} - D_{(-)}\ ) \times 100} \quad \mathbf{(13)}$$

D_{test} is the sample absorbance, $D_{(-)}$ is the negative control, and $D_{(+)}$ is the positive control.

CHAPTER 5: RESULTS AND DISCUSSION

This chapter discusses a novel thermochemical surface modification process for Ti64 alloy, aiming to improve its mechanical properties, biocompatibility, and bioactivity for biomedical applications (Part 1). It also discusses an integrated chemical treatment with magneto-rheological finishing, utilizing a CCD to assess the effects of CH-MR process parameters on (Sa), with optimized parameters to minimize Sa (Part 2).

Part 1

5.1 Surface Modification by THCP

The primary objective of this study is to develop a novel thermochemical process using environmental chemicals with varying pH values (5, 7, and 9) to enhance the mechanical properties, biocompatibility, bioactivity, and biodegradability of Ti64 alloy for long-term biomedical applications. This novel process involves two stages: an intermediate thermochemical stage and immersion in HBSS to achieve simulated mineralization. Aside from the primary goal, the secondary objective is to investigate the impact of different pH values on surface characterization using Fourier transform infrared spectroscopy (FTIR), field-emission scanning electron microscopy (FESEM), and energy-dispersive X-ray analysis (EDS) to evaluate biocompatibility and bioactivity for biomedical implant applications.

5.1.1 Surface Morphology

The surface structure and chemical element composition of the metal are key parameters that affect cell activity on metal modification and ultimately direct the process of tissue integration. The interface is the primary site for communication with implant constituents and the physiological surroundings [271]. EDS and FESEM were used to assess the surface morphology of the Ti64 alloy after the thermochemical process.

The samples (group A) had modified surface morphology, as shown in Fig. 5.1(A). In addition, Fig. 5.1(B) shows the particle size distribution and descriptive data of Ti64 alloy surface particles after thermochemical treatment with ($C_6H_8O_7$) and H_2O_2 at pH 5, 7, and 9. The figures illustrate how pH affects the surface particle size of the alloy during treatment.

Fig. 5.1(A.a) shows the Ti64 alloy before treatment, serving as a baseline for comparing treated samples and assessing the effects of thermochemical treatment. An untreated sample has a smooth surface with fewer visible scratches. After surface modification (with pH 5), the surface appeared to be coated with homogeneous spherical tiny particles, averaging a diameter of 0.398 ± 0.16 µm (Fig. 5.1 A.b); this may be because treating with a slightly acidic pH level can promote the precipitation of spherical particles due to certain chemical equilibria. After surface modification (with pH7), the FESEM demonstrated a denser layer with a more heterogeneous morphology with spherical particles of greater size (Fig. 5.1A.c). There was a significant variation in the size of aggregates, with an average size of 0.624 ± 0.23 µm. The variability in particle size can enhance the surface roughness, potentially enhancing cell adhesion and growth. After surface modification (with pH9), the surface has a homogeneous layer composed of nearly spherical particles and less uniform particles than at pH 5 and 7 (Fig. 5.1A.d), where the particles have an average diameter of around 0.59 ± 0.15 µm. Under a neutral pH value (7), reactions occur slowly, allowing a thicker layer to be deposited on the surface than in acidic or alkaline environments. The ImageJ analysis tool (64-bit Java 1.8.0) was utilized to ascertain the particle size, and a FESEM micrograph was used to acquire descriptive statistics (Fig. 5.1B). We have recognized that chemical reactions at different pH values change the surface morphology, highlighting the significant influence of pH on the thermochemical process.

119

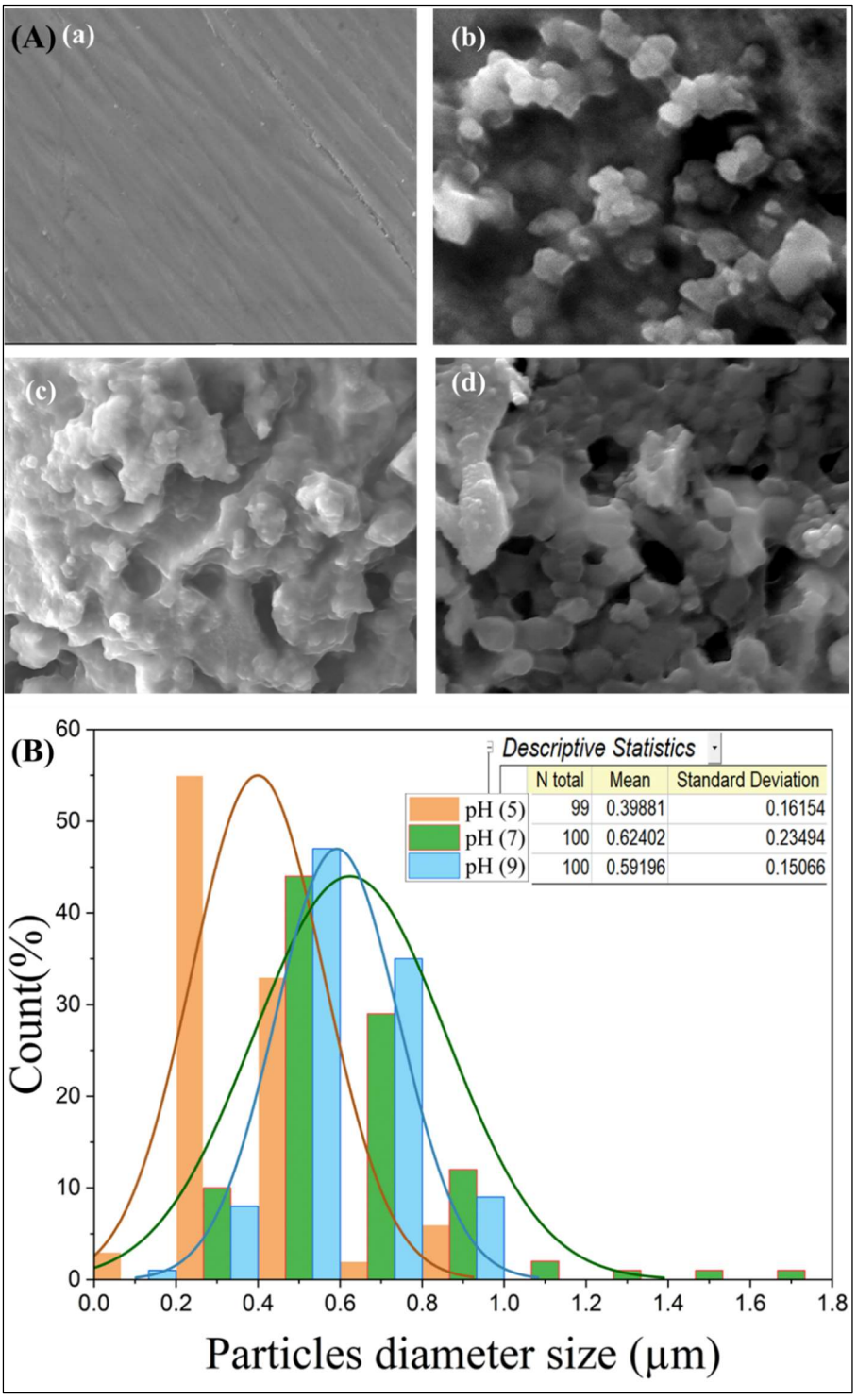

Fig. 5. 1A) FESEM image of surface morphology of Samples A.a) without modification, A.b) (with pH5), A.c) (with pH7), A.d) (with pH9), and (B) the average particle size diameter for the surface modification (group A)

EDS spectra (Fig. 5.2) indicate the element composition in wt.% for samples (group A). The untreated sample reveals a high (Ti) concentration of 79.0 %, with the presence of oxygen (O), aluminum (Al), and vanadium (V). This mixture provides the baseline alloy without any surface modification. The element composition differs significantly before and after the novel processes with different pH values (5,7 and 9). After modification with (pH 5), the Ti content declines to 58.2 %, while the oxygen content rises significantly to 24.3 %; this suggests the formation of a surface oxide layer (TiO_2), probably due to the oxidative nature of H_2O_2 (Fig. 5.2a). The presence of other elements on the surface, such as sodium (Na), potassium (K), (Ca), and chlorine (Cl), indicates that the eco-friendly chemicals have absorbed these elements. Fig. 5.2 (c) illustrates surface modification (with pH 7). There is a reduction in the Ti content to 51.2 %, with an oxygen content of 27.4 %, indicating a more extensive oxide layer development than at pH 5. Increased surface element diversity may improve corrosion resistance and bioactivity of the alloy. In the same way, Fig. 5.2 (d) illustrates surface modification (with pH 9). Ti is the lowest at 46.8 %, and oxygen is the highest at 28.3 %, indicating the most extensive oxide layer. Ti and oxygen show that the samples have been effectively deposited with TiO_2 nanoparticles. The substantial surface modification suggests surface reconfiguration and improved characteristics.

Notable variations in Al and V composition on the surface indicate that reducing the V and Al concentration on surfaces can enhance mechanical properties, increase biocompatibility, and improve corrosion resistance. The lack of Al and V ions in the layer suggests that no metallic ions were released throughout the thickening of the oxide layer; this means the native layer may have a shielding effect, preventing the release of harmful ions when exposed to a biological environment [272].

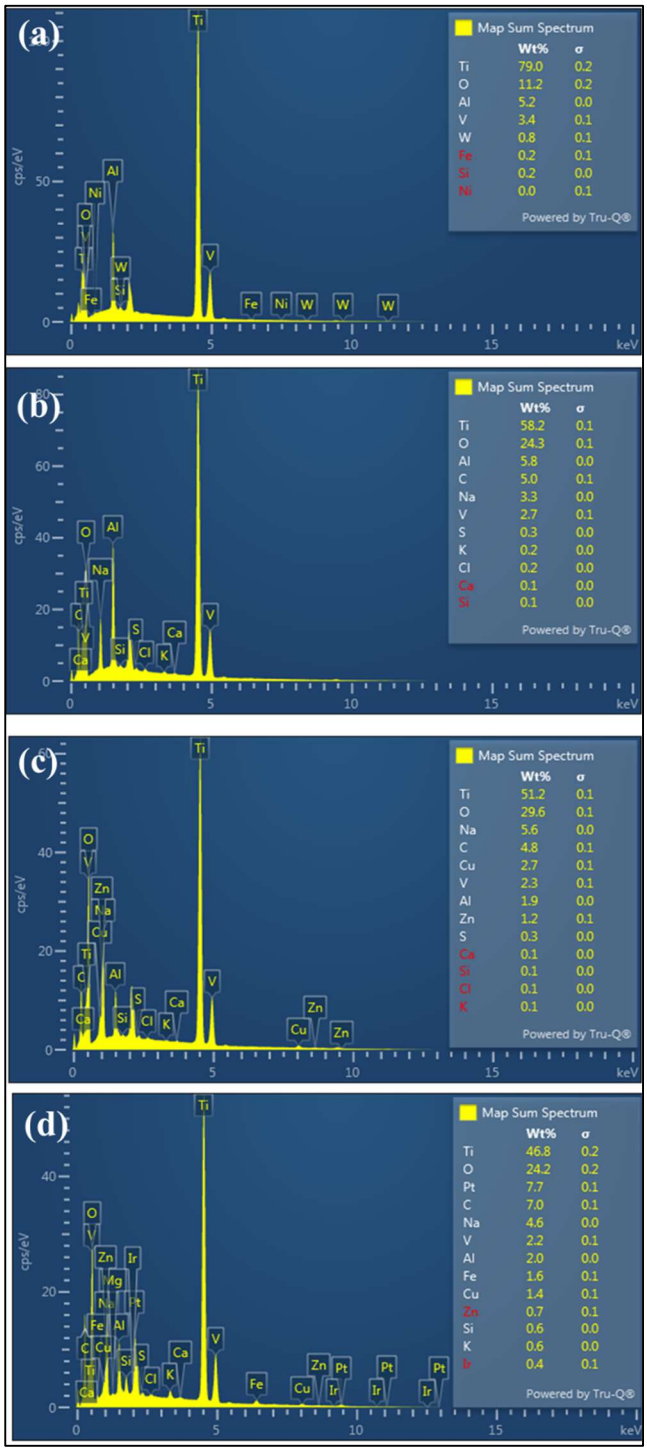

Fig. 5. 2 EDS spectra with the composition (W%) of Ti64 alloy (group A), a) before processing, b) after processing (with pH 5), c) after processing (with pH 7), and d) after processing (with pH 9)

In addition, the graphic representation of the changed surface in cross-section can be found in Fig. 5.3. The Ti64 alloy substrate was entirely covered by the modified layer, which did not include any pores or fractures in its structure. The coating layer may offer significant advantages in preventing the deterioration of the Ti64 alloy. As shown in Fig. 5.3 (a), the bright zone of the coating has a measured thickness of approximately 20.5 µm. However, this does not imply that the layer's entire thickness must be the same size [273,274].

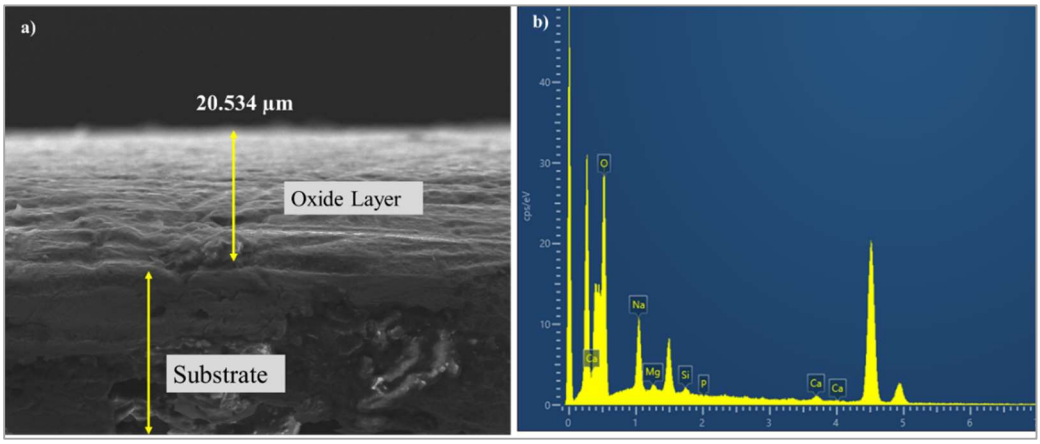

Fig. 5. 3 Cross-sectional morphology of the deposited layer on the Ti64 alloy (a), b) EDS analysis of the layer on the surface

Fig. 5.4 illustrates FTIR spectra (taken in the range) that offer vital information regarding the chemical bonding and functional groups found on the surface of the Ti64 alloy following the thermochemical process with ($C_6H_8O_7$) and H_2O_2 at various pH levels.

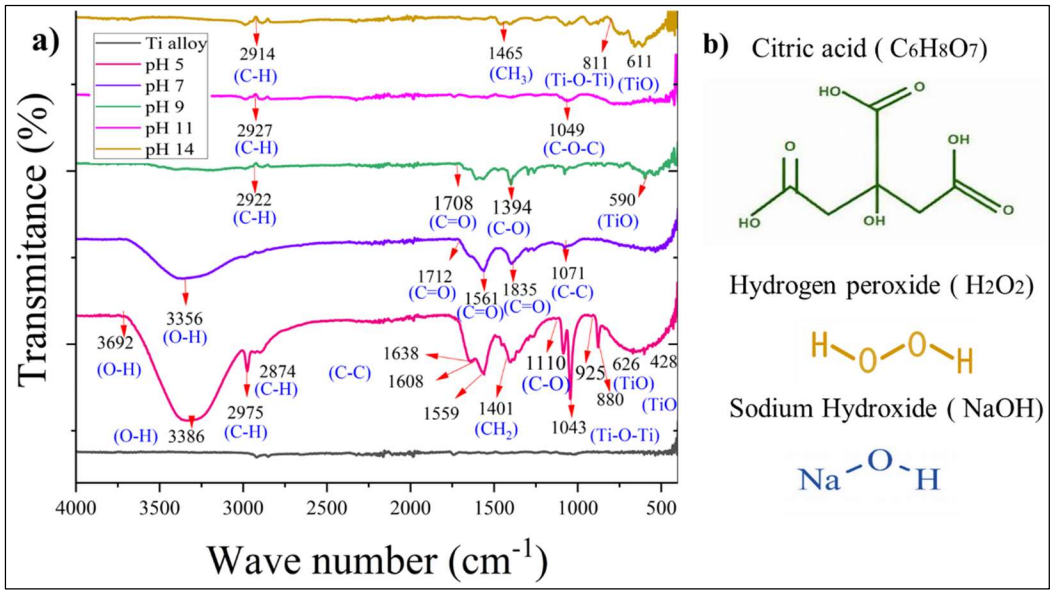

Fig. 5. 4 FTIR spectrum for samples Group (A) (a), and b) the formula of the chemical solution used in the process

Fig. 5.4 (a) displays the spectrum of the Ti64 alloy after modification with pH values of 5, 7, and 9. The most prominent peaks in the frequency range of 500−1500 cm^{-1} correspond to (Ti-O) and (Ti-O-Ti) bonds. In contrast, the spectrum of the untreated alloy does not exhibit any significant peaks. After modification (with pH 5), the spectrum exhibits peaks at 2874 cm^{-1} (C-H stretching) and 1401 cm^{-1} (C-H bending), showing the presence of organic groups from ($C_6H_8O_7$) and a prominent peak at 1600 cm^{-1}, indicating H-O-H bending, indicating water molecule adsorption. Additionally, the appearance of bands in the spectrum at 880 cm^{-1}, caused by the Ti-O-Ti bond, is proof of the presence of the oxide layer on the surface of the alloy that has been functionalized. Also, a significantly elongated band at 554 cm^{-1} is observed, which can be ascribed to the presence of the Ti-O bond [275]. Following the surface modification (with pH 7), the presence of peaks at 2922 cm^{-1} (which signifies C-H stretching) and 1618 cm^{-1} (which signifies H-O-H bending) suggests the existence of similar organic molecules and water adsorption as in pH 5. In the same way, after processing (with pH 9), the sample spectra reveal a peak at 3685 cm^{-1} (Ti-OH), which indicates the presence of (-OH) that can be generated through ($C_6H_8O_7$) hydrolysis, hydration,

or the reaction of hydroxide compounds. Hydroxyl groups modify Ti64 alloy surface chemistry, wettability, adhesion, and chemical reactivity [276]. Peaks at 554 cm^{-1} and 428 cm^{-1} indicate Ti-O bonds, while peaks at 1043 cm^{-1} imply Ti-O-Ti bonds, indicating an oxide layer composition modified by alkaline treatment.

The presence of carbonyl-containing compounds and hydroxyl groups on the surface of the Ti alloy suggests that the treatment has caused substantial changes to the surface [275,277]. These modifications can improve corrosion resistance and enhance bioactivity and biocompatibility in medical implants.

5.1.2. Mechanical Properties

5.1.2.1The Microhardness

The microhardness test was performed using a Vickers microhardness tester (Fig. 5.5a) according to ASTM E384. Samples (group A) were measured to investigate the effects of the novel process on surface microhardness under different pH levels. Three samples were selected after the thermochemical process at pH 5, 7, and 9, respectively, representing acidic, neutral, and alkaline environments.

Fig. 5.5(b) shows a significant increase in the microhardness of the samples. After modification (with pH 5), the microhardness increased from an initial average value of 341.69 HV to 403.39 HV. These findings demonstrate that acidic conditions remove surface impurities and form a more durable surface layer, thereby increasing material hardness. The material's hardness significantly increased after processing (with pH 7). The average microhardness increased by 71%. This enhancement suggests that the material's hardness increased in a neutral pH environment, possibly due to surface oxidation, phase transitions, or the formation of protective surface layers. Additionally, the average microhardness following thermochemical treatment (at pH 9) is 442.1 HV, indicating a slight improvement of 0.29 %.

Compared to other studies, the enhanced hardness resulting from the

thermochemical process is attributed to the increased volume percentage and thickness of the oxide layer on the surface. The novel process enhances the surface hardness, potentially attributed to the rutile phase, which exhibits a higher microhardness value than the anatase phase [278].

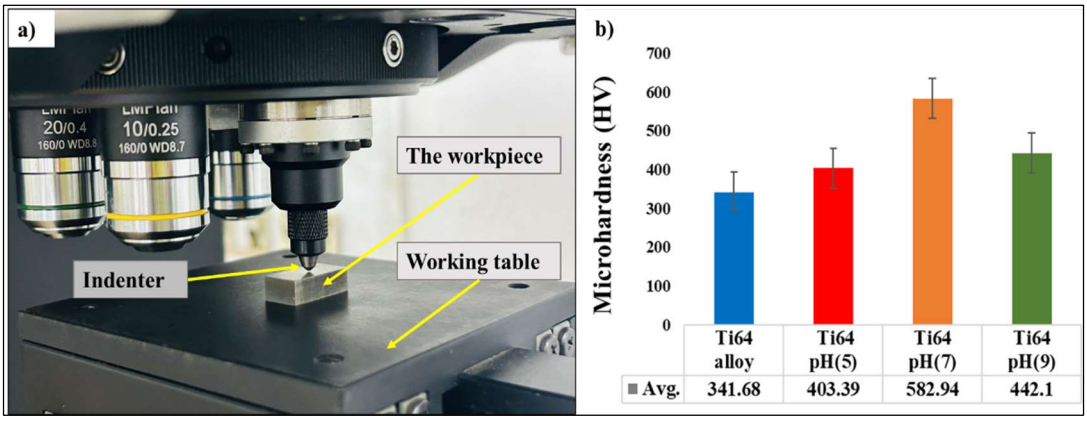

Fig. 5. 5 The microhardness tester of sample group (A): a) the microhardness tester, b) the microhardness of sample group A

5.1.2.2 The Surface Roughness

Surface roughness (Sa) is considered the most important characteristic of osseointegration. Research has shown that roughness promotes the growth of bone cells and the formation of bone minerals. As shown in Fig.7 (a), the new process increases the surface roughness of the Ti64 alloy samples (group A). It has been observed that there is a clear correlation between the pH value and the increase in Sa. According to ASTM C1624-05, ceramic thin films with a thickness of less than 30 µm must have a roughness parameter Sa < 0.5 µm for proper adhesion to substrates. The (Sa) after the process modification with pH values 5, 7, and 9 was measured as 0.28, 0.26, and 0.30 µm, respectively (Fig. 5.6 7c). These measurements meet ASTM standards, ensuring adequate adhesion of the film to the substrate. The sample values comply with the standard, as the film thickness for all substrates in this study was approximately 20.5 µm (Fig. 5.3 (a)). 5.3(a)) [279].

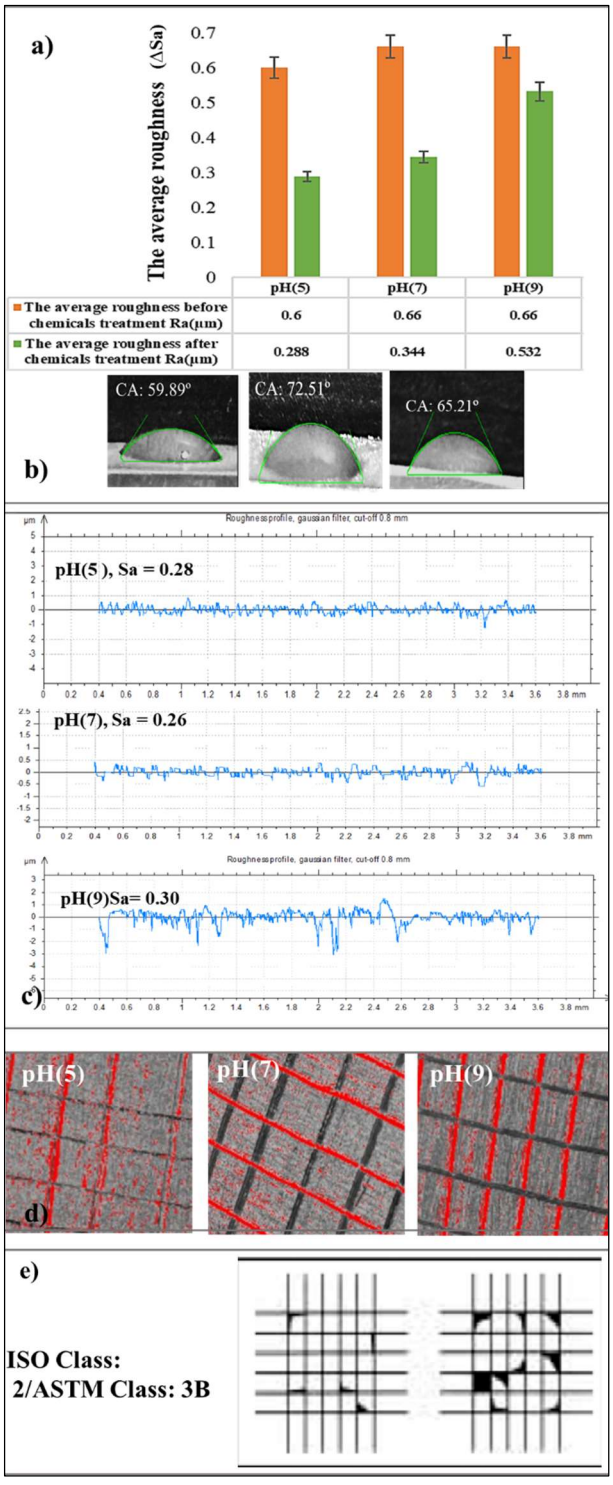

Fig. 5. 6 Surface characterization of Samples (Group A), a) the average surface roughness, b) contact angle, c) roughness profile, d) the adhesion test, and e) the ISO Class: 2/ASTM Class: 3 B.

The water contact angle is commonly used to assess surface wettability and hydrophilicity, which are crucial for biomedical applications [280]. Decreasing the contact angle increases the wettability and enhances the possibility of cell adhesion, which is essential for implants. Hydrophobicity depends on the contact angle between a liquid droplet and a solid surface. The hydrophilic surfaces' contact angles range from 0° to 90° [281]. Fig.5.6 (b) illustrates the measurements of contact angle derived from droplet photographs using the optical system of the goniometer. The contact angle was determined from the images using the ImageJ Software tool. The Ti64 alloy, after surface modification by pH levels (5, 7, and 9), shows a contact angle below 90°, indicating a hydrophilic surface. Surface modification at a pH of 7 results in the lowest contact angle, and a decrease in the contact angle increases hydrophilicity, thereby enhancing the initial attachment of cells to the biomaterial surface. Reducing the contact angle and thus increasing surface hydrophilicity improves the ability of cells, particularly osteoblasts, to attach, spread, and proliferate on the biomaterial. Hydrophilic surfaces promote protein adsorption, facilitating integrin-mediated cell adhesion. This leads to improved osseointegration and a favorable microenvironment for osteoblast attachment and spreading on implant surfaces. Lower contact angles also support higher cell proliferation rates, especially in bone regeneration and tissue engineering applications [282]. The wettability of a material significantly influences its surface energy, which is influenced by its hydrophilic properties, which affect its chemical interaction with liquids [282]. Two factors influence the adhesion strength of a thin film to various substrates: the surface energy and the adhesion strength. Both of these factors depend on the surface's wettability.

According to ASTM (D 3359–B) [283], a tape adhesive test was performed on three samples with pH values of 5, 7, and 9. Upon removal of the tape, the samples were examined using an optical microscope (Fig. 5.6(d)). The edges and joints of the cuts were exhibiting material degradation. A segment of the mesh, between 5% and 15%, was reportedly delaminated (Fig. 5.6 (e)).

5.1.2.3 Tribology

Tribological analysis was done using an ASTM G133 reciprocating tribometer setup (Fig. 5.7a). Fig. 5.7(b) illustrates the bar graph of the wear rate of samples (group A) subjected to three different loads (10, 15, and 20 N), a frequency of 5 Hz, a stroke range of 5 mm, and a temperature of 37°C. The wear rate results indicate that the primary improvement in wear rate is attributed to low material loss. Consistent findings were observed during modification, where the wear factor was reduced [284]. In addition, there was a maximum reduction of 64.29 % in wear rate at load (10 N) after surface modification (with a pH 7) compared to the untreated Ti64 alloy.

Fig. 5.7.c illustrates the line graphs of the coefficients of friction (COF) of the samples (group A), the COF curve of Ti64 alloy that has been exposed to thermochemical process with varied pH values (5, 7, and 9), and subjected to varying loads (10, 15, and 20). During the early wear stage, the COF increases rapidly due to the facile wearing of the oxide scale on the Ti64 alloy. The COF exhibits significant variation when a force of 10 N is applied to the sample, but these fluctuations diminish as the applied load increases. Under loads of 10 N, 15 N, and 20 N, the COF values were lower at pH 7 than for the untreated Ti64 alloy, which had the highest COF. Moreover, an increase in load decreases the COF. The wear rate of Ti64 alloy is positively correlated with the applied load, yielding the same result as previously reported [285]. Additionally, Liu (2018) [274] reported that increasing the applied load enhanced the surface roughness of the sample and expanded the contact area, thereby increasing the shearing stress in the contact region. Therefore, plastic deformation is more likely to occur as the temperature of the contact region increases, demonstrating that the COF decreases with increasing load [286].

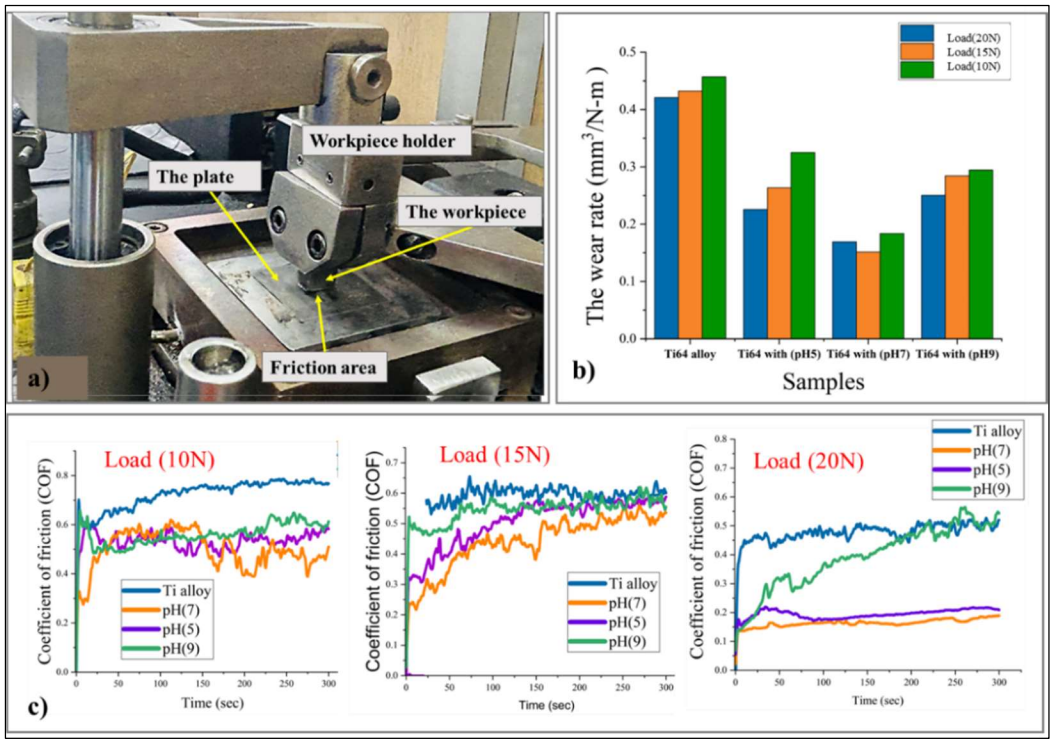

Fig. 5. 7 (a) Schematic of linear tribometer with sample, b) the wear rate of samples (group A), c) the friction coefficient (COF) of samples (group A)

The novel process modifies the surface of Ti64 alloy, resulting in enhanced mechanical properties, including reduced friction and wear, which ultimately improves the implant's longevity and biocompatibility.

5.1.3 In Vitro Hemocompatibility

The hemolysis ratio is crucial to biomaterial blood compatibility, with lower values suggesting higher compatibility. According to ASTM F756-00 standard, biomaterials must have a hemolysis ratio (Hr) < 5 % [287]. This work investigated the hemolysis ratios of the Ti64 alloy in different pH values (sample group A) using a Scanning Spectrophotometer. Fig. 5.8 (a) shows absorbance spectra of hemolysis tests on samples from group A with different pH treatments, corresponding to the absorbance of hemoglobin at 545 nm. The hemolysis ratio of Ti64 alloy after modification (at pH 5) decreased by 0.034 %. After modification (at pH 7), the sample had the lowest hemolysis ratio of 0.027 %, indicating the

highest blood compatibility and minimizing RBC lysis. After modification (pH 9), the sample had a hemolysis ratio of 0.039 % (Fig. 5.8 b).

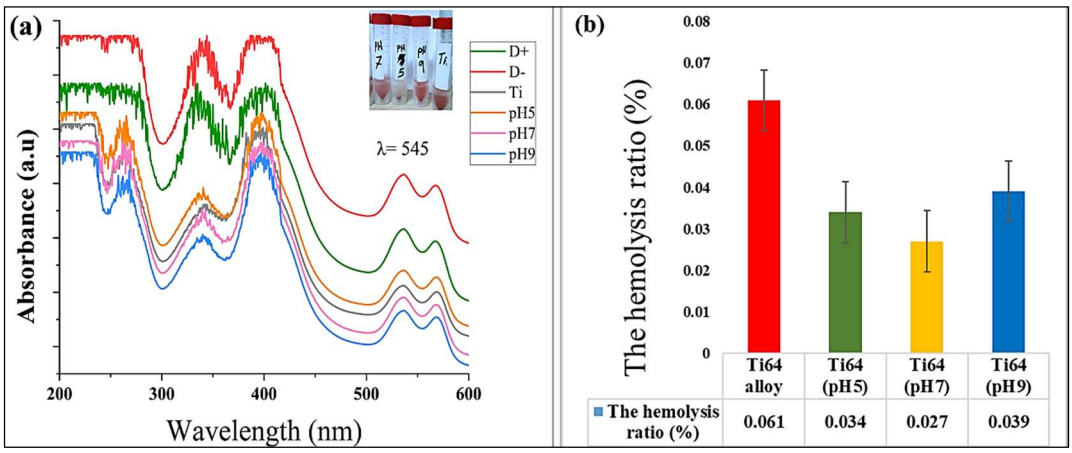

Fig. 5. 8 The hemolysis test on the samples (group A) (a), b) the result of the hemolysis ratio (%) for samples (group A)

5.1.4 The Corrosion Behavior

The electrochemical analysis test shown in Fig. 5.9 (a) shows the optical microscopic images of the surface morphology of Ti64 alloy (sample group B). The unmodified alloys reveal a rough, uneven surface, indicating considerable surface deterioration and corrosion. The corrosion rate is also much lower than that of the unmodified alloy, exhibiting considerable corrosion resistance.

Fig. 5.9 (b) displays the potentiodynamic polarization curves and provides detailed information about the electrochemical behavior of samples (group B). The corrosion potential (E_{corr}) is a critical parameter representative of the tendency of an alloy to rust in a specific environment. The polarization curves indicate that the modified Ti64 alloy displays a lower current density (I_{corr}), indicating decreased corrosion rates and enhanced corrosion resistance compared to the primary alloy. The electrochemical parameters obtained using Tafel extrapolation are listed in Table 5.1. The material's exceptional corrosion resistance is demonstrated by its high E_{corr}, low I_{corr}, and high Rp values [288]. The corrosion potential (E_{corr}) of the modified Ti64 alloy with pH values 5,7 and 9 were -0.575 V, -0.552 V, and -0.598 V, respectively. These changes were consistent with the observed decrease in

current density. Lower I_{corr} values in modified samples, especially with pH 7 having the lowest value of 5.18E-7 A.cm^{-2}, indicating a faster anodic reaction rate, and lower βa and βc values, indicating a slower reaction rate and highest polarization resistance (Rp) (7.514E+4 Ω.cm^2), suggesting increased corrosion resistance. The V_{corr} in mm/year quantifies material degradation in a simulated biological environment. The high V_{corr} suggests material degradation and poor corrosion resistance in biological environments. The V_{corr} has improved after applying a novel process with pH levels of 5.7 and 9, resulting in approximately 1.975 × 10^-2, 1.078 × 10^-2, and 1.615 × 10^-2 mm/year, respectively. This improvement is attributed to the formation of a stable and protective oxide layer on the alloy surface, further demonstrating the success of the novel process. The data indicate that applying the novel process on the Ti64 alloy with eco-friendly chemicals (pH 7) is the most effective for preventing corrosion. Electrochemical corrosion forms an oxide layer on the surface, which acts as a barrier against further corrosion [289]. Also, corrosion resistance is enhanced by the formation of an apatite layer, which acts as an additional barrier to ionic diffusion [174]. High corrosion resistance in physiological environments prevents metal ions from entering the bloodstream, making Ti64 alloy suitable for biostability and biocompatibility [290].

Table 5. 1 Electrochemical parameters of Ti64 alloy samples (group B)

Type	**E_{corr} (V/SCE)**	**I_{corr} (A.cm^{-2})**	**βa (V.dec^{-1})**	**βc (V.dec^{-1})**	**Rp (Ω.cm^2)**	**V_{corr} (mm/ year)**
Ti64 alloy	- 0.639	1.665E-6	2.685	0.118	2.931E+4	5.299 E-2
Ti64 (pH 5)	- 0.575	5.641E-7	0.911	0.197	6.539 E+4	1.795 E-2
Ti64 (pH 7)	- 0.552	5.18E-7	0.234	0.098	7.514 E+4	1.078 E-2
Ti64 (pH 9)	- 0.598	5.075E-7	0.67	0.106	7.539 E+4	1.615 E-2

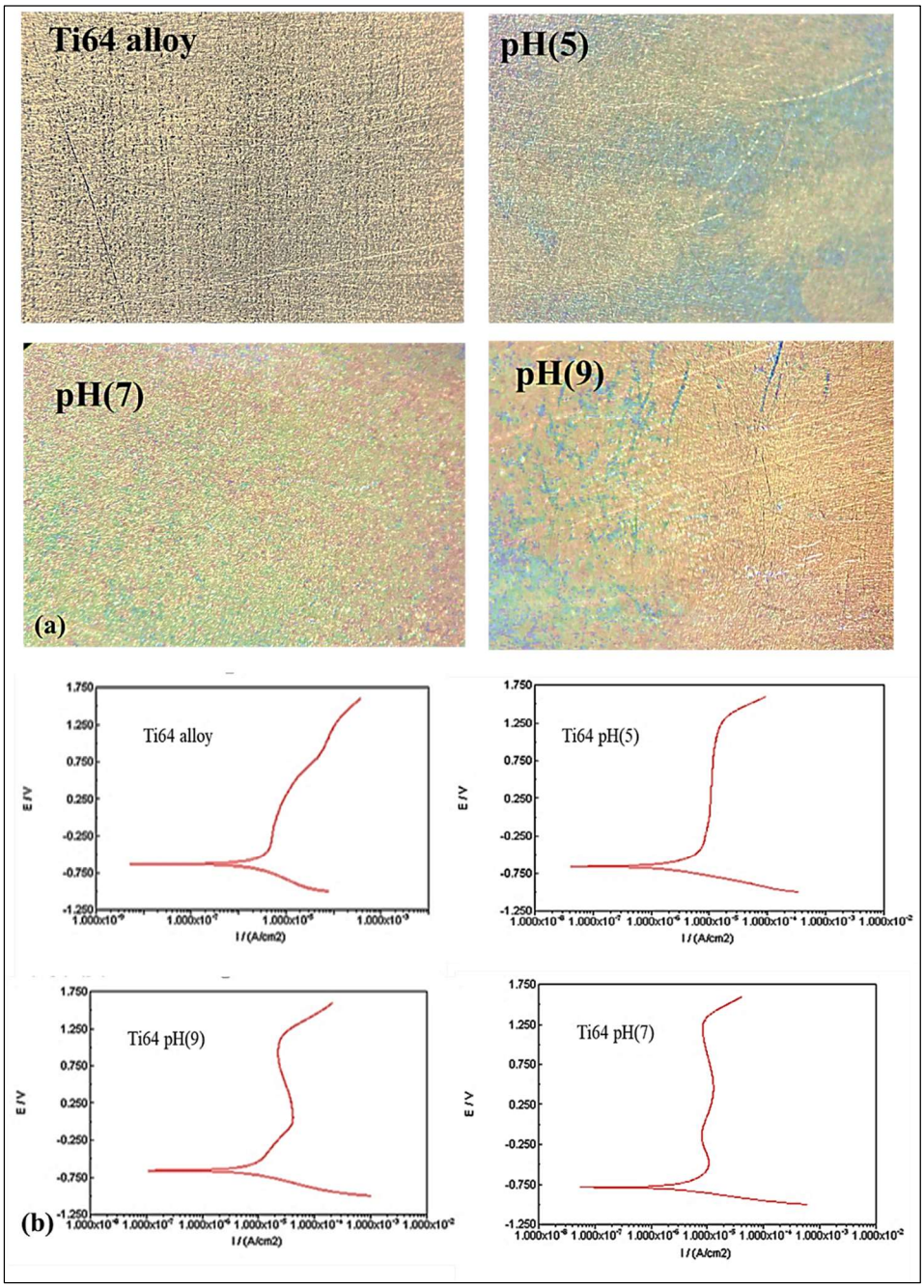

Fig. 5. 9 Surface Morphology of Ti64 alloy samples (group B) by optical microscopic images at 1000× magnification (a); (b) Potentiodynamic polarization curves for samples group B

5.1.5 The Bioactivity

99

Bioactivity refers to a biomaterial's ability to interact with the biological environment by forming a thin apatite layer with specific calcium and phosphorus concentrations. This apatite interacts with bone tissue and the implanted material, creating chemical bonds that promote osseointegration and reduce biomaterial rejection. Generally, apatite exhibits variations in chemical composition, which can be identified by using the calcium-to-phosphorus (Ca/P) atomic ratio for the most commonly encountered species [291]. One of the forming apatites is hydroxyapatite, which is present in bones and can support bone growth and stimulate bone formation in regions where it is implanted, constituting 30-70% of bone composition. This mineral is the least soluble and most stable among the apatites. The atomic ratio of calcium to phosphorus (Ca/P) is around 1.67 to ensure biocompatibility and bioactivity [292].

Fig. 5.10 displays the EDS spectra and FESEM micrographs of Ti64 alloy (sample group B), illustrating its microstructure and elemental composition. The EDS spectra show no significant peaks for the Ti64 alloy before surface modification, indicating that the alloy substrate dominates. The micrograph displays a relatively smooth surface with minimal hydroxyapatite formation (Fig. 5 .10a). Examination using EDS for selected points in the images showed no peaks for (Ca) or phosphorus (P), indicating a low level of element homogeneity in the investigated region [293]. After modification (at pH 5), there is an increase in O, Ca, and P; the micrograph displays the initial formation of hydroxyapatite in the form of spherical layers on the surface, providing a rougher surface compared to the primary Ti64 alloy (Fig. 5.10.b). After modification (at pH 7), EDS Spectra show more substantial peaks for Ca and P, confirming extensive hydroxyapatite deposition, and the micrograph demonstrates a dense and uniform layer of hydroxyapatite crystal growth, suggesting optimal conditions for hydroxyapatite formation. In the same way, after surface modification (at pH 9), the EDS Spectra show Ca and P peaks, and the micrograph displays extensive hydroxyapatite crystal formation, though slightly less uniform than the pH 7 sample (Fig. 5.10.c).

Table 5.2 illustrates Ca and P atomic percentages (at %) and the Ca/P ratio. Ca/P ratios of Ti64 alloy after modification at pH 5, 7, and 9 were 1.63, 1.67, and 2.01, respectively. These pH variations among surface modification samples (group B) can affect hydroxyapatite precipitation and the Ca/P ratio of the deposited layer. With an atomic ratio of 1.67, hydroxyapatite is a stable, biocompatible mineral that makes up 30 –70 % of bone and is advantageous for osteoconductive bone growth [292]. Ergun 2008 [294] also found that greater Ca/P ratios (up to 2.5) may improve osteoblast adhesion to calcium phosphate and BMSC-Ca-P interactions.

Table 5. 2 Ca/P atomic ratio (at%) of Ti64 alloy (group B) after soaking in the HBSS for 15 days

	Surface modification with different pH values		
Atomic ratio (at% %)	pH (5)	pH (7)	pH (9)
Ca (at% %)	1.67	1.84	1.55
P (at% %)	1.02	1.10	0.77
Ca/P	1.63	1.67	2.01

22

The novel process's bioactivity is confirmed by the Ca/P ratio of 1.67, which is comparable to human bone hydroxyapatite [295]. Higher pH levels may increase the Ca/P ratio due to chemical reactions and ion concentrations during the thermochemical process. A higher pH may enhance the deposition of calcium phosphate compounds, thereby increasing the layer's Ca/P ratio. Therefore, pH must be regulated during surface modification for biomedical applications to change composition and properties.

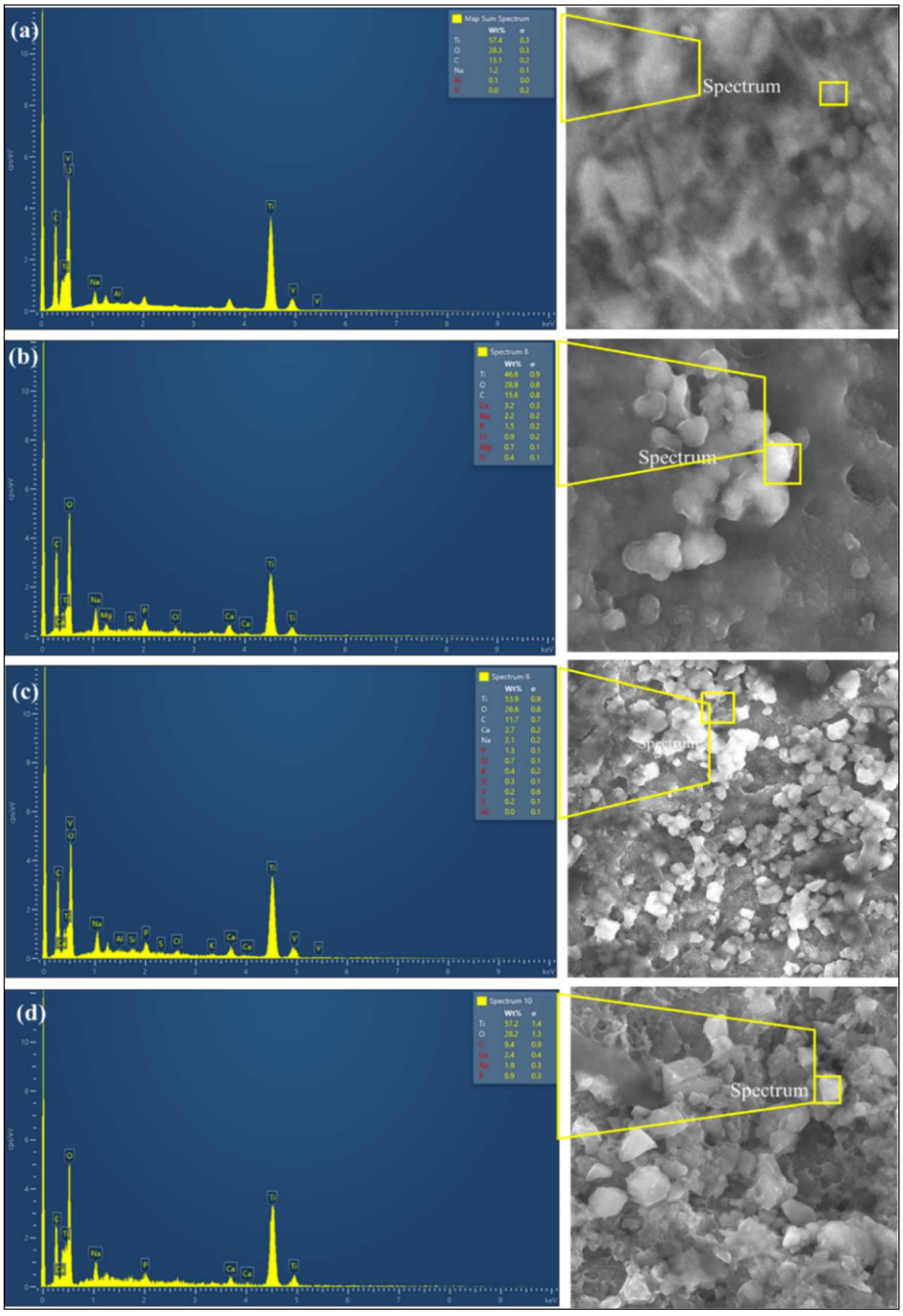

Fig. 5. 10 EDS spectra of samples (group B) with FESEM micrographs showing the hydroxyapatite grown on the surface, a) before processing, b) after processing (with pH5), c) after processing (with pH7), d) after processing (with pH9)

Fig. 5.11 illustrates FTIR spectra of the Ti64 alloy subjected to a thermochemical process with pH 5,7, 9, and then immersed in (HBSS) for 15 days, along with the surface-modified layer cross-sectional SEM image. The cross-sectional SEM image reveals a distinct coating layer of approximately 20.38 µm on the Ti64 alloy surface, likely associated with the thermochemical process and subsequent submersion in HBSS (Fig. 5.11a). The uniform thickness of this layer indicates effective surface modification, which is essential for improving biocompatibility and corrosion resistance.

The FTIR spectra (Fig. 5.11b) of the Ti64 alloy, obtained following the thermochemical process at different pH values (5, 7, and 9) and immersion in HBSS, reveal the presence of distinctive bonds, specifically Ti-O and PO_4^{3-}. The bands at 632 cm^{-1}, 3024 cm^{-1}, and 1643 cm^{-1} verify that the peaks are caused by the stretching of (OH) [174,296]. The presence of PO_4^{3-} groups can be detected in the bands located at 1197, 1080, and 610 cm^{-1}, which correspond to the vibration of the asymmetric phosphate bond [297].

The presence of these phosphate groups suggests the formation of a calcium phosphate layer, such as hydroxyapatite, which is vital for bioactivity and bone integration. The prominent peak observed at approximately 1408-1405 cm^{-1} can be attributed to carbonate groups CO_3^{2-}. These carbonate groups may have been incorporated into the hydroxyapatite structure, enhancing its resemblance to natural bone minerals. The Ti64 alloy (with pH7) reveals a high peak, indicating higher Ti-O and PO_4^{3-} groups, suggesting that a neutral pH condition is more effective during surface modification. In addition, the Na^+ ions exchanged with H_3O^+ or H^+ ions formed a Ti-OH layer promoted by Ca^{2+} or high OH^- concentration, creating apatite. Ca^{2+} ions nucleated carbonate-hydroxyapatite by interacting with PO_4^{3-} and CO_3^{2-} ions to form a Ca-P surface layer. This layer formed carbonate hydroxyapatite, like bone apatite [298].

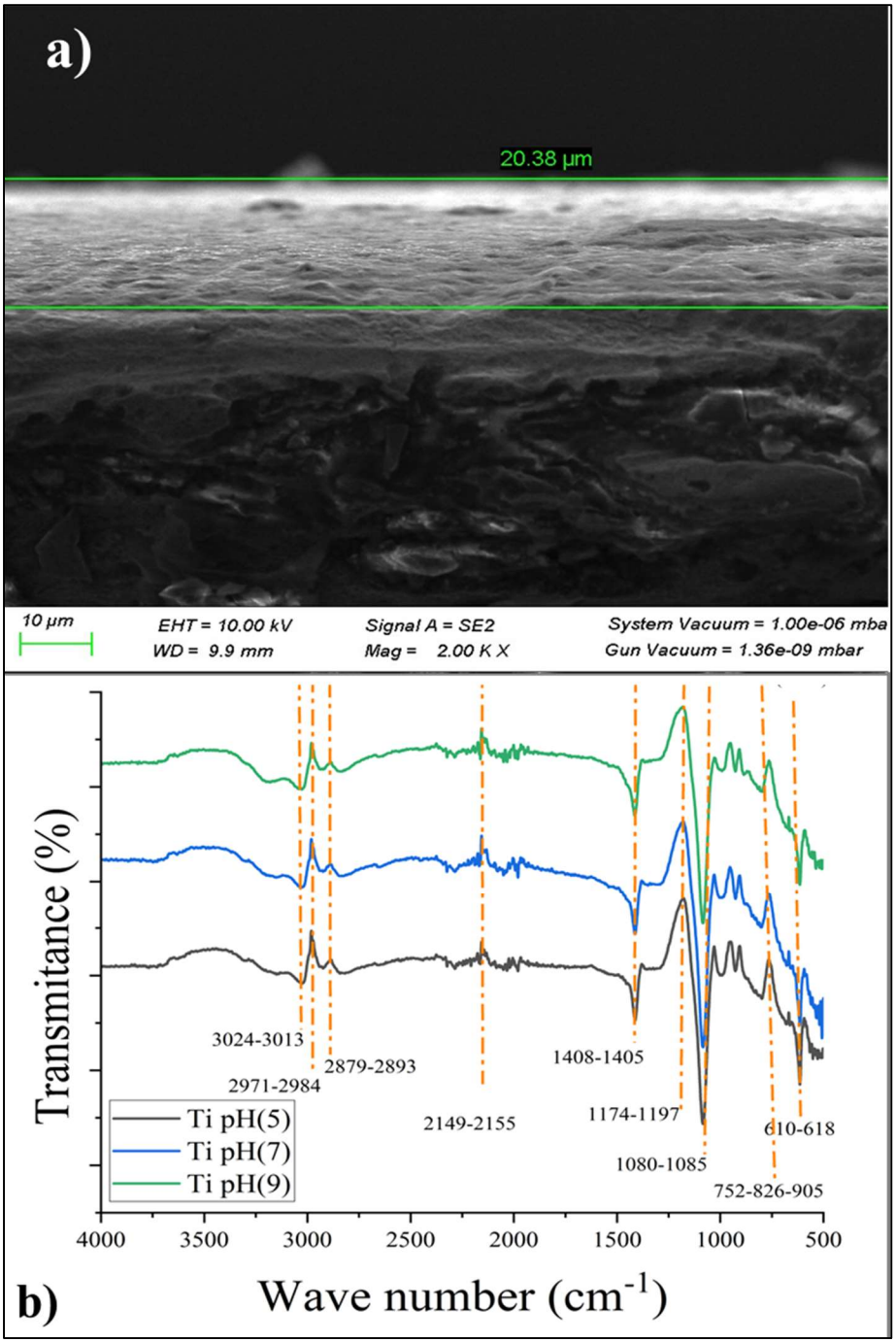

Fig. 5. 11 The cross-section of the Ti64 alloy surface modification (a); FTIR spectra of samples after chemical modification and immersion in HBSS for 15 days with pH values (5,7, and 9)

5.1.6 Summary

A novel thermochemical process, THCP, is developed using $C_6H_8O_7$ and H_2O_2 at pH levels of 5, 7, and 9 for the surface modification of Ti64 alloy. The process significantly enhanced mechanical properties, biocompatibility, and bioactivity, confirming the effectiveness of eco-friendly chemical treatment for biomedical implants.

The eco-friendly chemicals provide a strong foundation for chemical surface modification of Ti64 alloy, enabling bio-implants without environmental hazards; however, further refinement is necessary to achieve the ultra-smooth surfaces required for advanced biomedical applications. To address this, the next stage of the research focuses on developing a sustainable chemical-assisted magneto-rheological CH-MR finishing process, building upon the modifications achieved through THCP.

Part 2

5.2 Surface Finishing by CH-MR Process

5.2.1 Experimentation

The CH-MR process combines chemical treatment with magnetorheological (MR) finishing.

5.2.1.1 The Chemical Mechanism of the CH-MR Process

The chemical process created a soft layer on the Ti64 alloy surface by using environmentally friendly H2O2 and C6H8O7, while regulating pH with NaOH at 5, 7, and 9. The oxide layer on the Ti64 alloy may enhance the efficiency and effectiveness of the mechanical finishing process. The pH of the chemical solution plays a crucial role in determining surface roughness, as it directly affects the alloy's polishing response.

Fig. 5 .12 displays optical microscopy and FESEM images of the Ti64 alloy surface after treatment with environmentally friendly chemicals at different pH levels (5, 7, and 9), revealing significant differences in oxide layer formation and surface morphology. The chemical treatment of the Ti64 alloy surface at an acidic pH (5) produces rapid oxidation due to the increased concentration of H^+ ions in the solution. Excessive dissolution can lead to rapid oxide formation, enhancing material removal and polishing. Moreover, H_2O_2 and $C_6H_8O_7$ react to generate peracids in acidic environments. These peracids are effective oxidizers that boost oxidative capacity and efficiency. This procedure yields a thinner, more uniform oxide layer, resulting in softer interference colors (Fig. 5.12a).

In Fig. 5.12b, where the treatment is conducted at a neutral pH (7), the oxide layer is less uniform compared to pH 5, possibly due to reduced chemical reactivity and a less effective oxidation process. In Figure 4c, the chemical treatment of the Ti64 alloy at an alkaline pH (9) produces thicker layers and a darker coloration. This observation is consistent with the demonstration that excessive oxidation of Ti alloys at higher pH values forms thicker oxide layers. In

an alkaline environment, H_2O_2 and OH^- can enhance the efficiency of the Ti64 alloy and promote corrosion through oxidation and complexation processes.

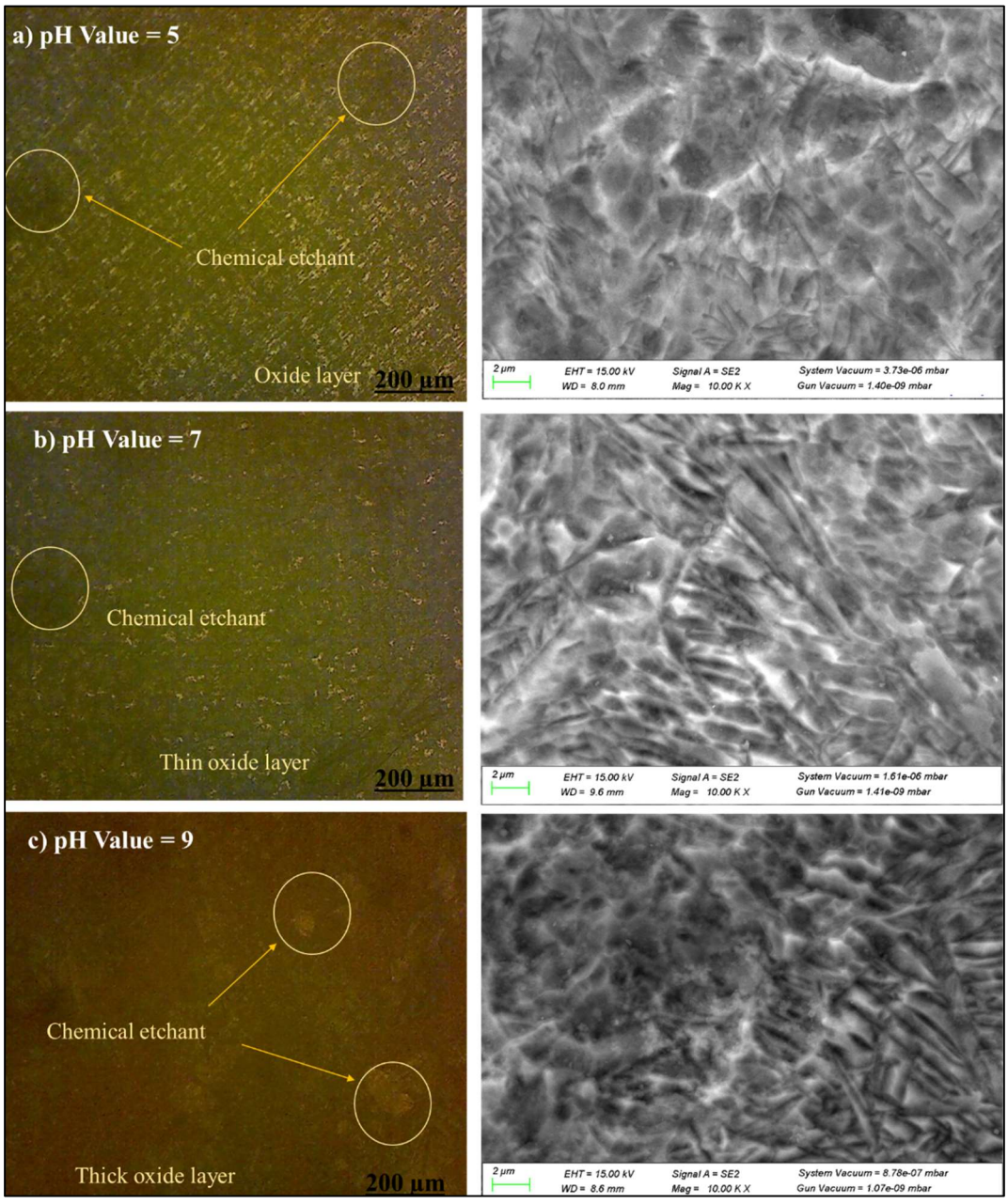

Fig. 5. 12 Optical microscopy along with FESEM for the formation of the oxide layer by chemical treatment with eco-friendly chemicals on Ti64 alloy, a) with (pH 5), b) with (pH 7), and c) with (pH 9)

$C_6H_8O_7$ may react with H_2O_2 to produce peracids (peroxyacids), more

efficient oxidizing agents. These peracids can significantly enhance the oxidative capacity [299]. NaOH affects this reaction by shifting the balance toward the production of peracids and enhancing oxidation [263].

The dissociation of citric acid involves its breakdown into protons (H^+) and the citrate anion ($C_6H_5O_7^{3-}$) :

$$C_6H_8O_7 \rightleftharpoons 3H^+ + C_6H_5O_7^{3-}$$

The oxidation of Ti64 alloy by H_2O_2 promotes the formation of a layer on the surface; the reaction occurs as follows:

$$2Al + 3H_2O_2 \rightarrow Al_2O_3 + 3H_2O$$

$$V + 2H_2O_2 \rightarrow VO_2 + 2H_2O$$

$$Ti + 2\,H_2O_2 \rightarrow TiO_2 + 2H_2O$$

Subsequent reactions of these oxides with protons include:

$$Al_2O_3 + 6H^+ \rightarrow 2Al^{3+} + 3H_2O$$

$$VO_2 + 2H^+ + 4H_2O \rightarrow [VO(H_2O)_5]^{2+}$$

Furthermore, H_2O_2 may react with Ti in the presence of citric acid [262].

$$Ti + 2H_2O_2 + 2H^+ \rightarrow TiO^{2+} + 3H_2O$$

$$TiO^{2+} + H_2O_2 \rightarrow [TiO(H_2O_2)]^{2+}$$

Due to its reactivity and stabilizing properties, the $[TiO(H_2O_2)]^{2+}$ complex is essential in catalysis and environmental chemistry.

Fig. 5.13 illustrates the effect of chemical treatment on the formation of an oxide layer on the Ti64 alloy. The cross-sectional morphology verifies the formation of oxides on the surface. Surface characterization reveals a coating film on the surface. At the same time, the underlying substrate remains intact without any damage (Fig. 5.13a). EDS analysis shows that the oxide layer's composition varies with pH, with higher oxygen content at higher pH, indicating thicker oxide layers. The layer exhibits distinct growth characteristics across different pH levels:

it remains thin at pH 5, demonstrates moderate growth at pH 7, and achieves maximum intensity at pH 9 (Fig. 5.13 b-c-d). The result, as discussed by Deng et al. [300], showed that TiO_2 and $TiO_2 \times H_2O$ are the primary components of the outer surface oxide layer. Also, Chen et al. [301] demonstrated that the oxidation of Ti alloy intensifies at higher pH levels.

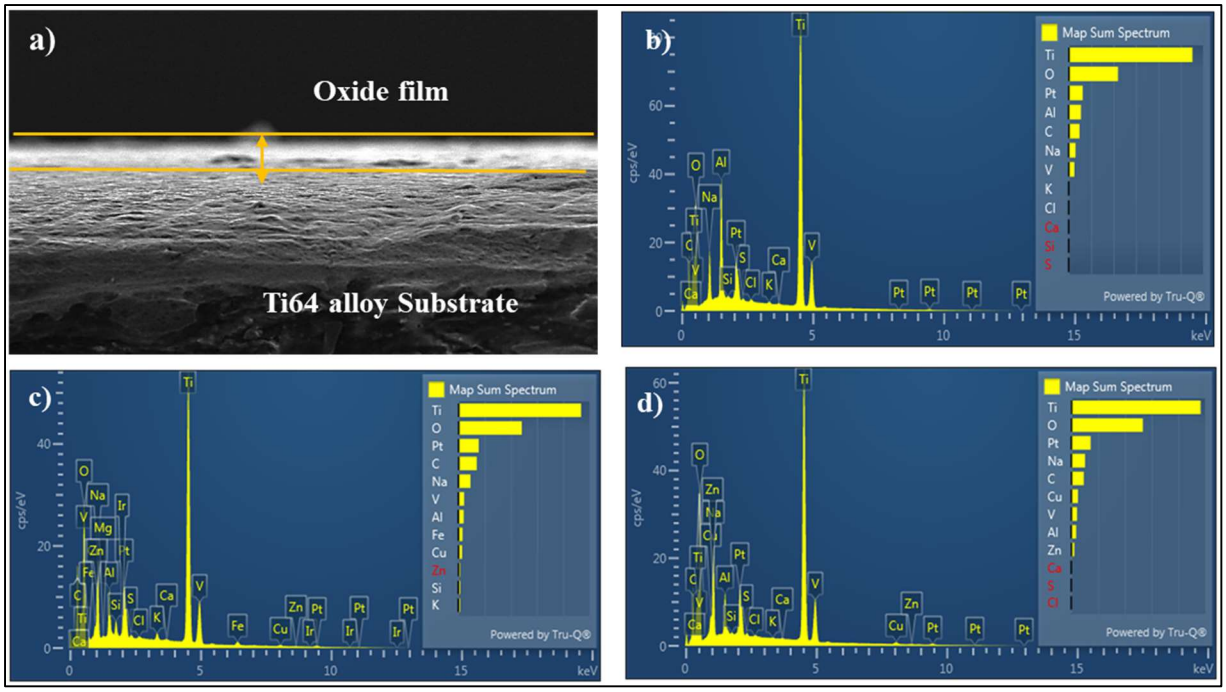

Fig. 5. 13 a) Cross-section for the oxide layer on the Ti64 alloy, b) EDS images for the growth of the oxide layer with (pH5), c) with (pH 7), and d) with (pH9).

The sustainable CH-MR finishing process forms an oxide film on Ti64 alloy, which may enhance material removal and reduce Sa, demonstrating its effectiveness at the nanoscale.

5.2.1.2 Regression Model

51 Regression analysis is a mathematical framework for characterizing the relationship between one or more input predictors and a response variable, and for predicting new observations. The predictive mathematical models have been developed using Minitab.

41 The mathematical model has been developed based on the design of

experiments for surface roughness Sa. The fitted mathematical equations for all the selected responses are presented in the following equations:

$$Sa = -118.1 + 36.44\,PH - 23.8\,WG + 0.386\,RS + 2.9\,C - 1.461\,PH*PH + 21.7\,WG*WG - 0.000425\,RS*RS - 0.21\,C*C - 2.93\,PH*WG - 0.02900\,PH*RS - 0.919\,PH*C + 0.0730\,WG*RS - 1.85\,WG*C + 0.0054\,RS*C$$

The results analysis is illustrated in Table 5.3, which presents the Analysis of Variance (ANOVA) for the most significant terms on the final Sa.

The pH value, working gap, tool spindle rotational speed, and current are represented by pH, WG, RS, and C, respectively. The ANOVA analysis confirms that the developed model, with an adjusted R^2 of 94.89%, is adequate and reliable, as validated by comparing the obtained Fisher's value (Fstd) with the standard Fisher's value (Freg) at a 95% confidence interval (Freg > Fstd). Additionally, the data suggest that the experimental model has a significant impact on Sa in all linear terms. The quadratic and two-factor interaction effects are crucial in the model's ability to capture non-linear relationships. However, the main effect terms have a stronger influence than the interaction effects. The normal probability plot in Fig.5.15 a confirms that the model's assumptions are consistent with the generated regression equation, as evidenced by the high R^2 (coefficient of determination) of 94.08%. Moreover, the Pareto chart in Fig. 5.15b highlights the most significant terms influencing the regression model, further validating its accuracy and reliability.

Table 5. 3 Analysis of variance (ANOVA) for Sa

Source	DF	Adj SS	Adj MS	F-Value	P-Value	Remarks
Model	14	4695.94	335.424	17.26	0.0000	$F^{reg}_{model} > F^{std}$ The regression
Linear	4	3230.97	807.743	41.56	0.0000	
PH	1	947.39	947.392	48.75	0.0000	
WG	1	778.19	778.188	40.04	0.0000	

RS	1	635.78	635.777	32.71	0.0000	model is
C	1	491.49	491.494	25.29	0.0000	statistically
Square	4	250.67	62.667	3.22	0.048	significant
pH*Ph	1	87.6	87.602	4.51	0.054	
WG*WG	1	75.31	75.312	3.88	0.071	
RS*RS	1	46.32	46.317	2.38	0.147	
C*C	1	0.11	0.113	0.01	0.94	
2-Way Interaction	6	1009.89	168.316	8.66	0.001	
pH*WG	1	148.5	148.503	7.64	0.016	
pH*R	1	583.48	583.475	30.02	0.0000	
pH*C	1	58.29	58.291	3	0.107	
WG*RS	1	231.15	231.15	11.89	0.004	
WG*C	1	14.77	14.772	0.76	0.399	
RS*C	1	5.1	5.103	0.26	0.617	
Error	13	252.66	19.435			
Lack-of-Fit	10	222.22	22.222	2.19	0.281	Insignificant
Pure Error	3	30.44	10.147			
Total	27	4948.6				
			R^2 (adj) =	94.89%		
			R^2 (pred) =	89.40%		

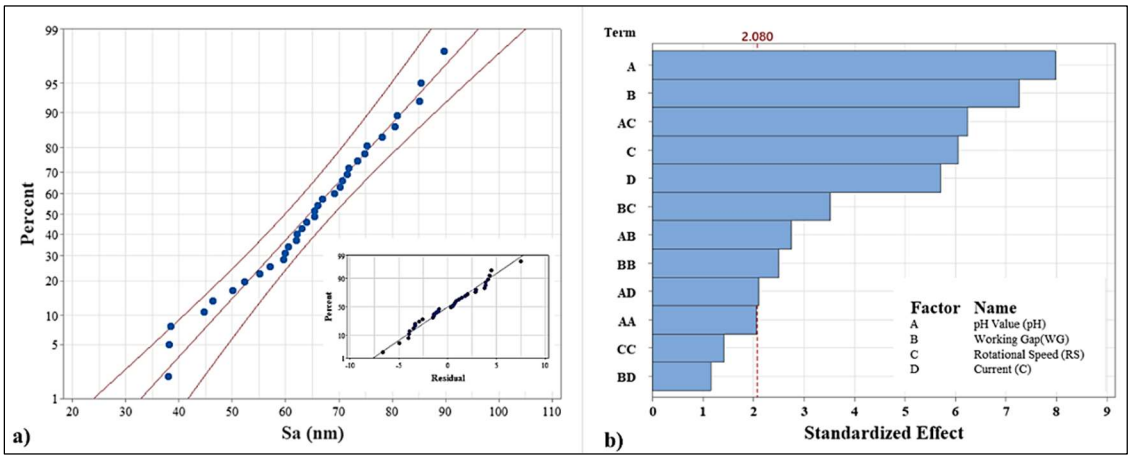

Fig. 5. 14 Graphs for response surface regression analysis: Normal probability plot (a), Pareto chart for standardized effect (α = 0.05) (b)

5.2.3 Influence of the Process Parameters on the Sa

Fig. 5 .16a illustrates the individual effects of pH, WG, RS, and C on the mean Sa of Ti64 alloy during the CH-MR process. Indicating that lower pH, smaller WG, lower RS, and higher C are favorable for achieving smoother surfaces. The pie chart depicts the percentage contribution of each factor and its interactions. The pH value is the most critical factor, contributing 19.14%, followed by WG, RS, and C, which contribute 15.73%, 12.85%, and 9.93%, respectively (Fig. 5.16b). These findings underscore the crucial importance of optimizing primary process parameters, specifically pH and WG, to achieve nano-level surface finishes in advanced CH-MR finishing of Ti64 alloy.

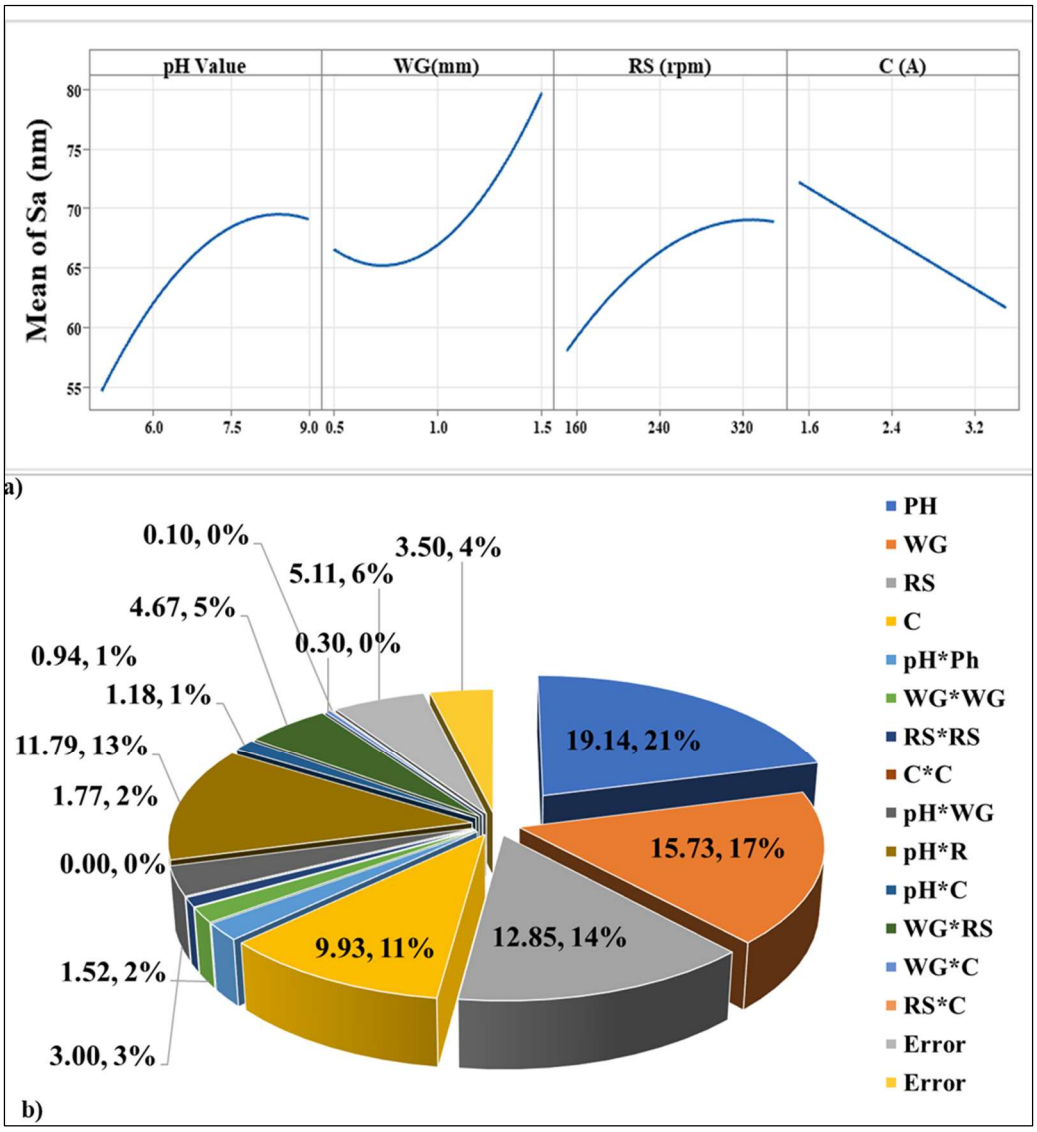

Fig. 5. 15 The main effect plot for CH-MR process parameters on the Sa (a) and the pie chart for the percentage contribution of various significant factors (b).

The individual impact of process factors on Sa was discussed further in subsequent sections.

5.2.3.1 The Effect of pH Value

Fig. 5.17 demonstrates the interactions among pH, WG, and RS on the Sa of Ti64 alloy. The least Sa was found at the lowest pH and the smallest WG (0.5 mm). In addition, the contour plot shows that low WG and low pH yield smoother

surfaces, whereas higher WG and higher pH yield rougher surfaces. At an acidic pH (5), the formation of peracids from C_6H_8O and H_2O_2 affects the oxidation layer on the surface, leading to a higher material removal rate. Conversely, the alkaline pH (9) increases roughness due to the presence of more Na^+ and OH^- ions on the Ti64 alloy surface; these ions adsorb onto the surface, potentially forming a stable oxide layer that is resistant to further degradation and material removal. Similar findings by Deng (2022) [300] demonstrate that Sa increases with higher pH values, aligning with the observed trend in this study. Additionally, previous studies show that pH levels between 7 and 10 affect material removal rates and improve surface roughness [302].

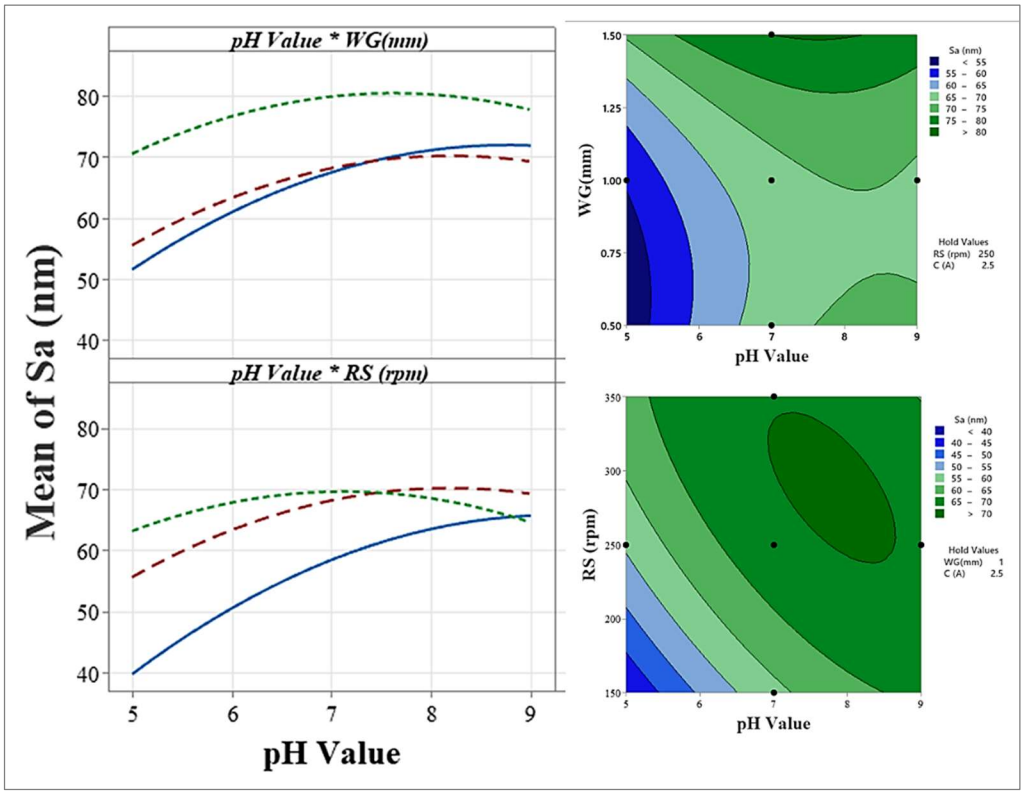

Fig. 5. 16 Interaction effects of Sa vs. pH value, RS, and WG with the contour plot.

5.2.3.2. The Effect of the Working Gap (WG)

Fig. 5.18 illustrates the interaction effect of Sa and WG, with further analysis of 3D surface plots and contour plots to provide a comprehensive understanding of the parameter interaction. A smaller WG increases the effectiveness of the MR fluid in removing material. At the same time, a lower RS maintains abrasive particle engagement, preventing them from being displaced by centrifugal forces. The Sa decreases with a smaller WG between the tool core tip and the workpiece, as the magnetic flux density is inversely proportional to the working gap. As the gap decreases, the magnetic field intensity increases, leading to higher normal and shear forces [303].

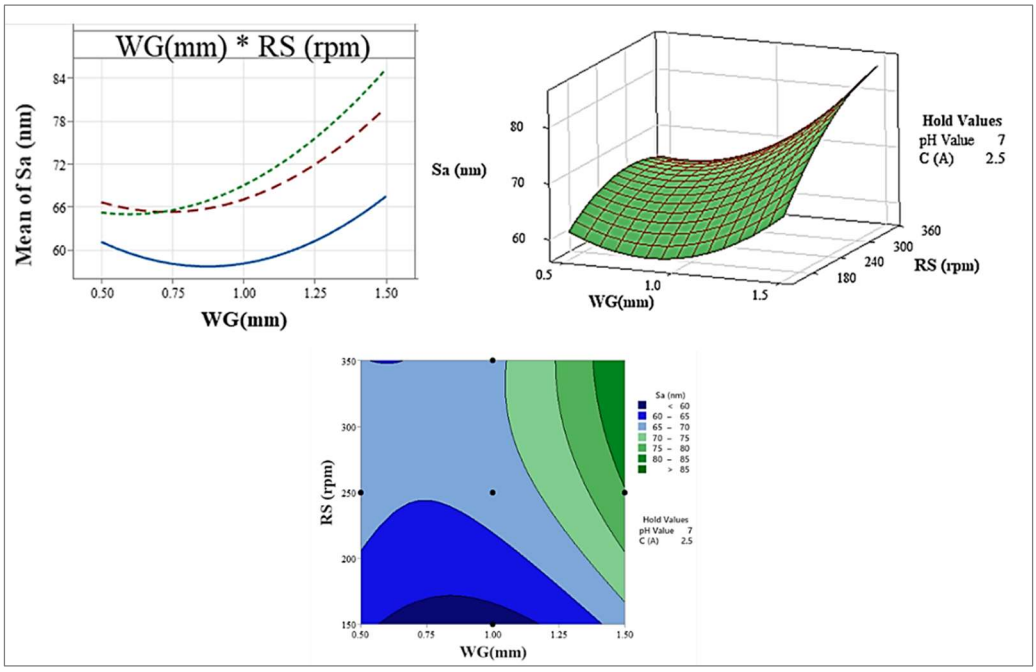

Fig. 5. 17 Interaction effects of Sa vs. WG and RS with 3D plot surface and contour plot.

5.2.3.3 The Effect of Tool Rotational Speed (RS)

The interaction plot shows a significant decrease in Sa association with lower RS (150 rpm), especially with less WG (Fig. 5.18). At higher rotational speeds, centrifugal forces can displace abrasive particles from the working gap, diminishing the finishing process's effectiveness. Since centrifugal force increases

with the square of the rotational speed, increasing speed can negatively impact the reduction in Sa. To maintain effective finishing, the magnetic normal force must be stronger than the centrifugal force to securely hold the abrasive particles at higher speeds [304]

5.2.3.4 The Effect of Current (C)

Fig. 5.19 illustrates a 3D surface plot and the corresponding contour map, showing the combined effects of WG and RS on the Sa of Ti64 alloy, with pH and C maintained at 7 and 2.5 A, respectively. A noticeable drop in Sa occurs as C increases from 1.5 A to 3.5 A, particularly with a smaller WG, indicating that higher C enhances finishing by boosting the magnetic flux density at the MR finishing at the tool tip. Consequently, the abrasives are trapped in CIPs chains with greater gripping power, which improves the finishing action. Additionally, the contour plot indicates that higher C and smaller WG are associated with lower Sa values. The regions with the lowest brightness on the contour plot, indicating the smoothest surfaces, are found at the highest C of 3.5 (A) and the smallest WG (0.5 mm). Overall, the interaction between a higher current and a smaller working gap is favorable for minimizing surface roughness. Furthermore, the ANOVA analysis (Table 7) reveals that C significantly reduces Sa by 9.93%.

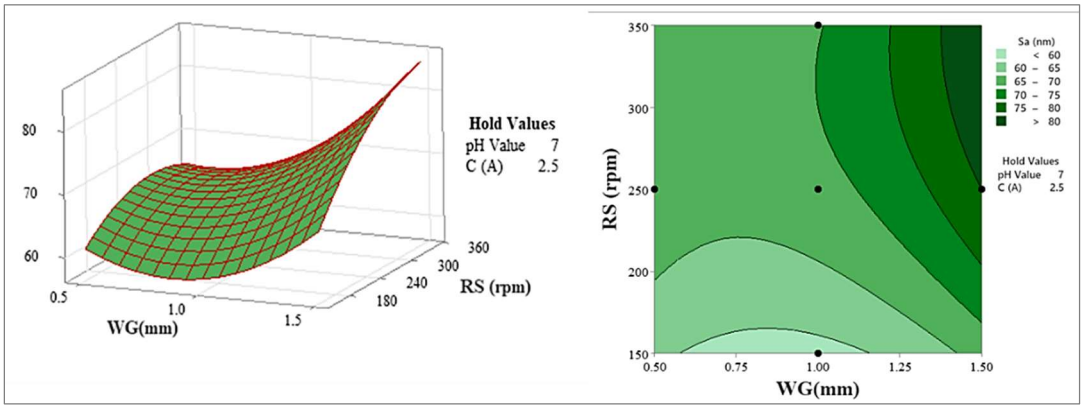

Fig. 5. 18 The interaction plot of Sa vs. C and WG with the contour plot

5.2.4 Process Parameters Optimization

The response surface model for Sa (Equation 9) was systematically optimized to identify interactions among the CH-MR process parameters. As shown in Fig. 5.20, Sa is significantly influenced by pH, WG, RS, and C. The analysis indicates that Sa decreases with lower pH values, higher magnetizing currents, smaller working gaps, and lower rotational speeds. Optimal conditions were achieved at pH 5, WG 0.5 mm, RS 150 rpm, and C 3.5 A, yielding a minimum Sa value of 35.35.

Table 5.4 presents the validation of predictive model accuracy. The experimental Sa value of 38.20 nm closely matches the predicted value of 35.36 nm, yielding a minimal prediction error of 2.85%. This small discrepancy underscores the computational model's high predictive accuracy, confirming its reliability and robustness in forecasting surface finish outcomes under optimized CH-MR process conditions. The slight margin of error in the experimental design validates the efficacy of the parameter optimization. Furthermore, the consistency between the theoretical and empirical results underscores the effectiveness of the computational algorithm in identifying near-optimal parameters, thereby ensuring precise control over surface quality.

The mean error was 4.62%, indicating strong agreement between the model predictions and the experimental results. The validated model thus serves as a reliable predictive process control framework, enabling the achievement of target surface finishes with minimal experimentation. This not only enhances production efficiency but also reduces resource consumption and ensures consistent quality in critical applications, such as biomedical implants.

Table 5. 4 The experimental and predicted Sa values for CH-MR optimal Sa

	Parameters				**Surface Roughness (Sa) (nm)**		
No.	pH value	C (A)	WG (mm)	RS (rpm)	Experimental value	Predicted value	% Predicted errors
1	5	3.5	0.5	150	38.20	35.35	7.46
2	5	3.5	0.5	150	36.80	35.35	3.94
3	5	3.5	0.5	150	34.50	35.35	2.46
						Average	4.62

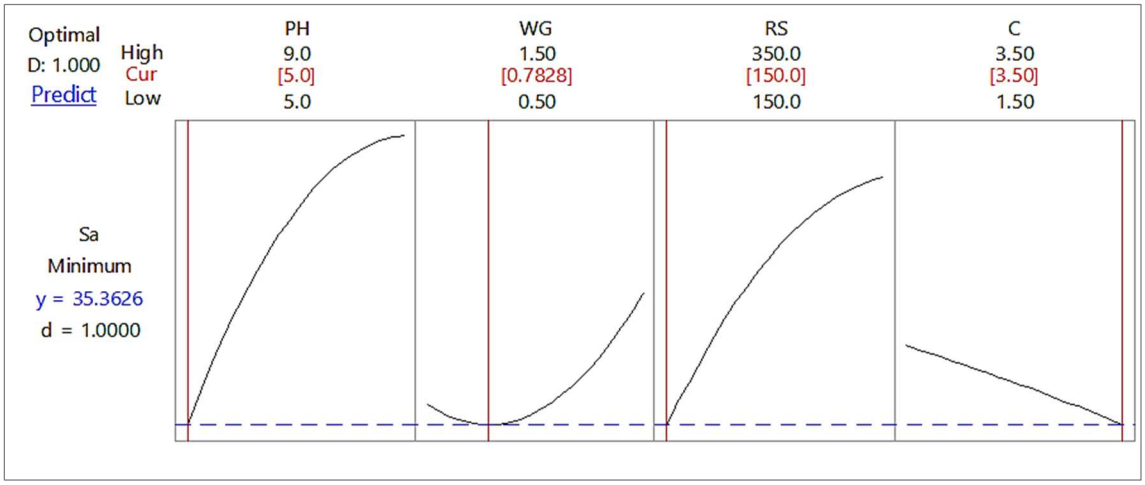

Fig. 5. 19 Plot optimization for Sa with CH-MR process parameters

5.2.5 Surface Roughness (Sa) Analysis

The roughness of Ti64 alloy was measured before and after CH-MR finishing using a roughness measuring tool manufactured by Taylor-Hobson Surtronic. Five surface roughness measurements are taken at the same spot during an experiment to exclude false effects. Fig. 5.21 illustrates the reduction in Sa from 500 nm to 38.20 with the optimum parameters in a 30-minute finishing time. Roughness profiles reveal that higher-magnitude roughness peaks are present in the initial sample and are reduced after CH-MR finishing.

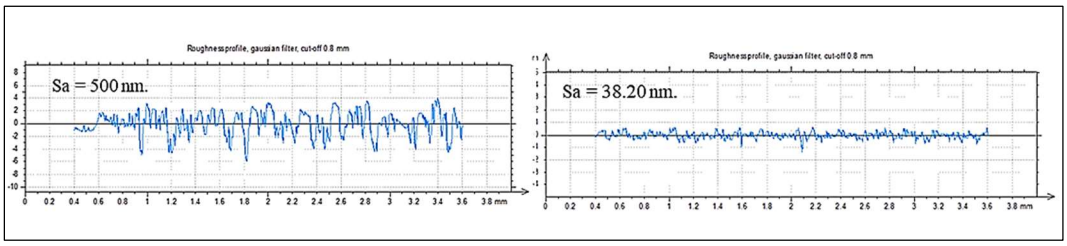

Fig. 5. 20 Roughness profile for Ti64 alloy before and after the CH-MR process

109

Fig. 5.22 shows the surface morphology of Ti64 alloy, as analyzed using AFM and SEM, before and after the CH-MR process with optimal parameters. Figure 14a shows the SEM image of the Ti64 alloy before the CH-MR process, which displays more scratches, machining marks, and grooves. Following the CH-MR process with optimal parameters, a significant improvement in surface roughness was observed, indicating the effective minimization of surface irregularities and defects, thereby ensuring surface integrity and precision (Fig. 5.22b). The AFM topographical analysis reveals the irregular peaks and valleys of Ti64 alloy before processing (Fig. 5.22 c). The CH-MR process, with optimal parameters, effectively removes irregular peaks and valleys in Ti64 alloy, resulting in a smoother, more uniform surface topography on the nanometer scale, which indicates efficient material removal and improved surface quality (Fig. 5.22d).

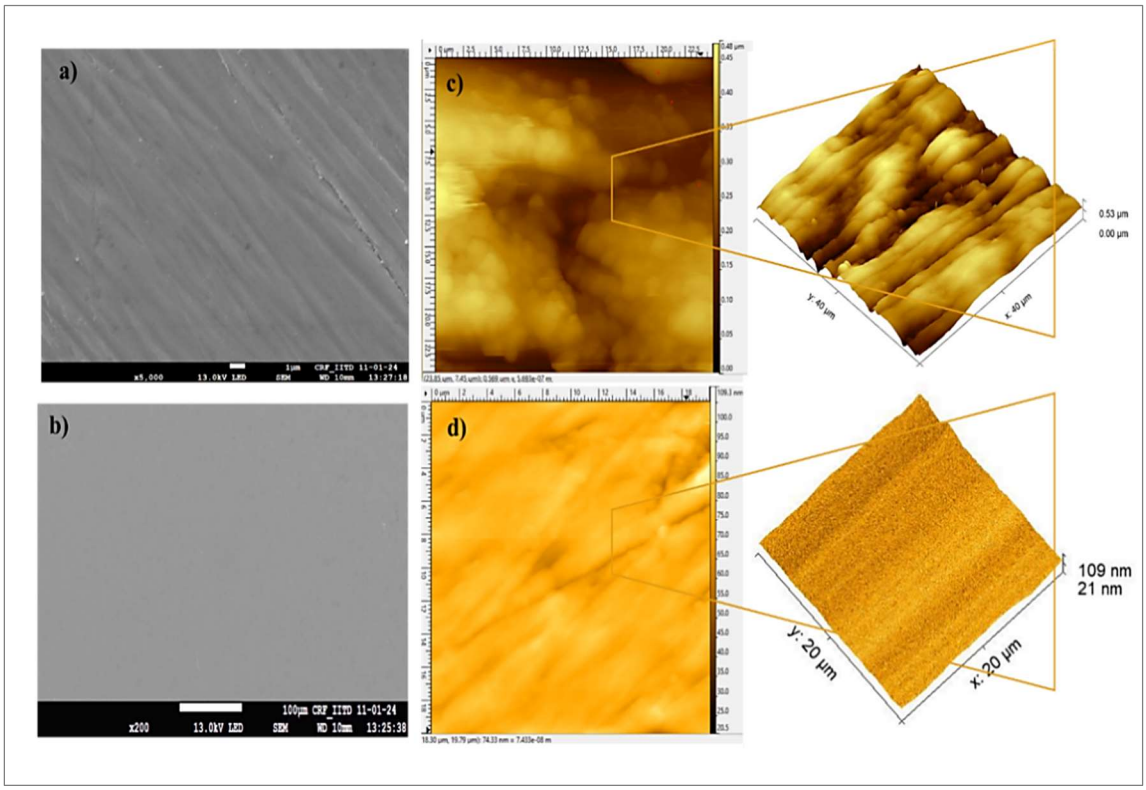

Fig. 5. 21 SEM images of Ti64 alloy before the CH-MR process (a), and after CH-MR with optimal parameters (b), AFM image for Ti64 alloy before the CH-MR process (c), and after CH-MR with optimal parameters (d)

The XPS analysis reveals the mechanisms of the chemical reaction of the Ti64 alloy surface with the eco-friendly reagent and the subsequent CH-MR processing (Fig. 5.23). Fig. 5.23 a reveals significant changes in surface and binding energy after the chemical treatment of a Ti64 alloy, which leads to enhanced peak intensities for oxygen and carbon; based on the result, the binding energies of higher peaks for elements observed include Ti 2p, O 1s, V 2p, and C 1s at 456.5 eV, 527.5 eV, and 282 eV, respectively, confirming the surface oxidation and potential organic contamination. Following the CH-MR process, a notable reduction in peak intensities is observed, suggesting the effective removal of surface contaminants and oxide layers while preserving the underlying surface. A C 1s peak indicates the remaining organic species from the citric acid treatment. Also, the Al 2p binding energy was detected at 72.1 eV and 72.2 eV, further

supporting the formation of the aluminum oxides. These measurements align with the Al-O binding energies reported by Li et al. (2009) [305].

The high-resolution analysis of Ti 2p (Fig. 5.23 b) reveals that the most prominent element in the Ti64 alloy has three peaks at 457.5 eV, 458.5 eV, and 464 eV, corresponding to Ti^0 $2p_{3/2}$, Ti^{4+} $2p_{3/2}$, and Ti^{4+} $2p_{1/2}$, respectively. These peaks confirm the presence of the Ti^{4+} oxidation state [306,307]. The ions of Ti^{4+} ions reacted with O^{2-} ions, consequently forming TiO_2; this is also confirmed by the existence of (528.6 – 529.7 eV) in O1s. Additionally, the high-resolution analysis of O 1s (Fig. 5.23c) reveals that O 1s spectra at 530 eV show surface oxide TiO_2 formation during chemical treatment. A slight increase in binding energy after chemical treatment suggests the formation of more oxidized on the surface, possibly due to reactions between hydrogen peroxide and citric acid, which generate peroxyacids that are more capable of oxidation. The decrease in the O 1s peak after the CH-MR process confirms the removal of oxidation from the surface without affecting subsurface integrity.

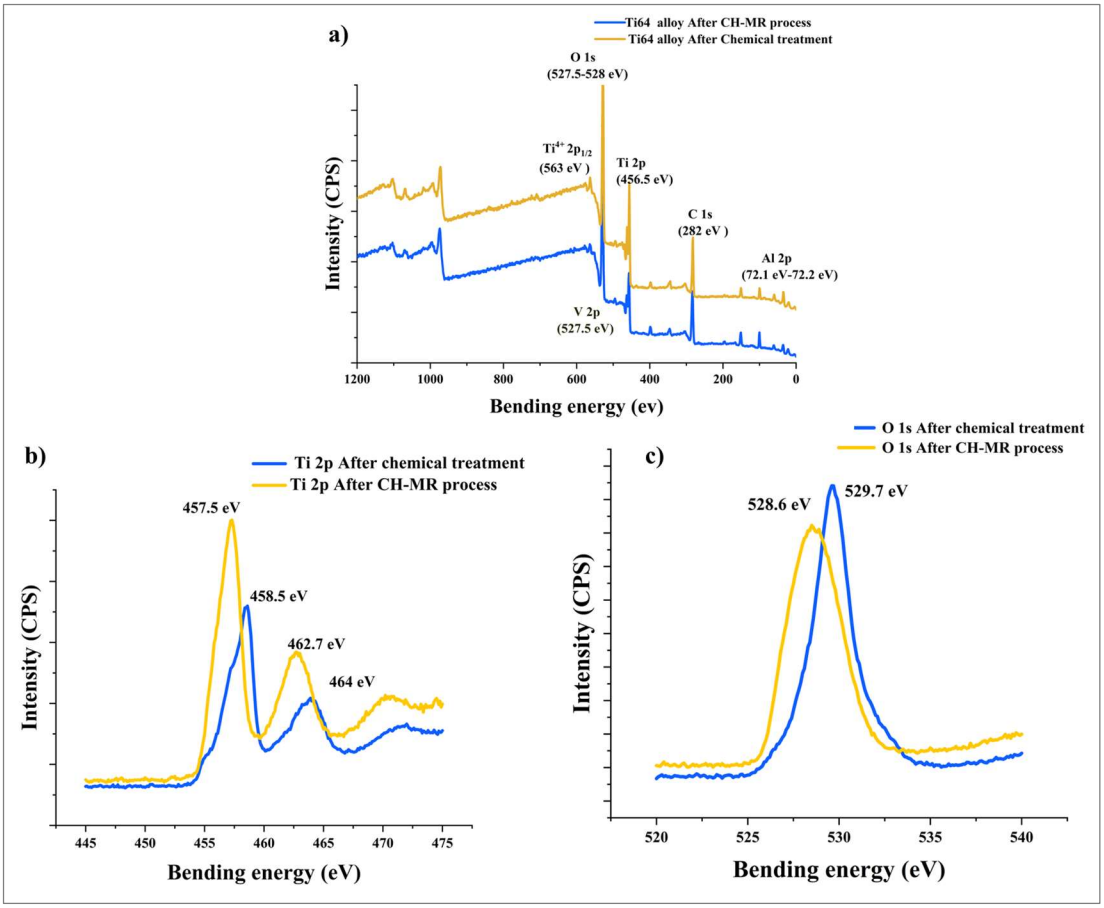

Fig. 5. 22 XPS spectra of Ti64 alloy surface sequence elements (a) after eco-friendly treatment, and after the CH-MR process (b) high-resolution spectrum Ti 2p, and (c) O 1s

In a nutshell, the advanced CH-MR process significantly improves Sa compared to conventional finishing processes. For instance, the AFM process reduced Sa from 230 nm to 95.8 nm after 5 hours of finishing [80]. Similarly, the MAF process reduced the roughness from 1.195 μm to 0.073 μm with optimal process parameters within 90 min. [150]. Furthermore, the MFAF process achieved a Sa of 11.32 nm in a finishing time of 4.30 hours with optimal process parameters [93]. In contrast, the CH-MR process for finishing the Ti64 alloy achieves a Sa of $\leq$ 40 nm in just 30 min., while also enhancing surface integrity by reducing surface grooves and peaks. Moreover, traditional chemical polishing methods often rely on corrosive acids such as HNO_3, HF [308], (H_2SO_4) [120], or

HCl [309]. While these acids are effective for polishing, they produce hazardous byproducts that pose risks to human health and the environment. A sustainable CH-MR process has been developed to overcome hazards, reduce time, and enhance finishing quality.

5.2.6 Summary

The study developed a sustainable CH-MR process to achieve a nanoscale surface finish on Ti64 alloy using eco-friendly chemicals. RSM was used via CCD to evaluate the effects of CH-MR parameters on the alloy's surface area (Sa). The research found that citric acid reacts with hydrogen peroxide to form peroxyacids, which enhance mechanical polishing efficiency. pH regulation with NaOH also influenced surface behavior during finishing. ANOVA revealed pH as the most influential parameter, followed by WG, RS, and C as secondary factors. The CH-MR process effectively reduced the Sa of Ti64 alloy from 500 nm to 38.20 nm, achieving a minimum Sa of 38.20 nm within 30 minutes under optimal conditions. Post-process characterization confirmed exceptional surface integrity and minimal defects, and XPS elucidated the finishing mechanism by correlating surface oxidation states to enhance chemical-mechanical synergy. The CH-MR process could be applied to other Ti alloys and hard-to-machine materials for high-precision finishing and sustainable manufacturing in the aerospace and medical sectors.

CHAPTER 6: CONCLUSIONS AND FUTURE SCOPE

This chapter presents the conclusions of the investigation into the thermochemical process TCHP for surface modification of Ti64 alloy and the finishing surface by the CH-MR process, followed by a discussion of the future scope of the present work.

6.1 Conclusions

Titanium and its alloys are widely employed in biomedical applications due to their exceptional biocompatibility, excellent mechanical properties, corrosion resistance, surface hardness, and high strength, which surpass those of other metals used in medical implants. These alloys are widely used in the fabrication of artificial implants, including hip and knee joints. The performance of these implants depends on surface characterization, which affects the life and functionality of replacement components. Therefore, it is necessary to achieve a superior surface quality that closely matches the required features and dimensional accuracy.

This study develops novel eco-friendly processes for chemomechanical magnetorheological (CH-MR) and Thermomechanical surface modification (THCP) of Ti64 alloy to enhance both surface quality and bioactivity. The CH-MR process primarily focuses on nano-finishing Ti alloys and surface modification to achieve higher surface quality, durability, and functionality for replacement implant parts, overcoming the limitations of hazardous chemicals, reducing finishing time, and enhancing surface quality. The CH-MR process involves the synergistic integration of chemical pretreatment, which selectively oxidizes and softens the Ti64 alloy surface, thereby facilitating MR finishing to achieve nano-level roughness with reduced time and improved surface quality. Experiments were designed using a Central Composite Design (CCD) to evaluate the effect of process parameters on the surface roughness (Sa). After that, the process parameters were optimized to achieve the minimum surface area Sa.

Surface characterization of the Ti64 alloy post-finishing properties was performed using Atomic Force Microscopy (AFM), Field Emission Scanning Electron Microscopy (FESEM), and X-ray Photoelectron Spectroscopy (XPS). AFM analyzed nanoscale topography, FESEM revealed microscale morphological changes, and XPS identified surface chemical states and oxide layer composition. These characterizations validated the CH-MR process's ability to enhance surface roughness and confirmed the absence of contamination or subsurface damage, which is crucial for biomedical and aerospace applications.

The THCP surface modification of Ti64 alloy was performed using environmental chemicals with varying pH values (5, 7, and 9). The process improves mechanical properties, biocompatibility, bioactivity, and biodegradability for long-term biomedical applications. The process involves an intermediate thermochemical stage and immersion in HBSS for simulated mineralization. Then, to investigate the impact of different pH values on surface characterization using Fourier transform infrared spectroscopy (FTIR), field-emission scanning electron microscopy (FESEM), and energy-dispersive X-ray analysis (EDS) to evaluate biocompatibility and bioactivity for biomedical implant applications.

The investigation into these areas is expected to make significant contributions to the fields of implants, materials science, and engineering, particularly by enhancing the durability and performance of finishing materials across industries such as aerospace, automotive, and biomedical implants. The research work has led to the following conclusions.

- The CH-MR process is a sustainable, advanced manufacturing method that uses eco-friendly chemicals for surface softening, opening new possibilities for a green approach to advanced manufacturing.
- Citric acid reacts with hydrogen peroxide to form peroxy acids, powerful oxidizing agents that enhance mechanical polishing efficiency.
- In the CH-MR process, regulating pH with NaOH influences surface

behavior during finishing, as an alkaline pH creates thicker oxide layers and reduces material removal. In contrast, an acidic pH enhances the finishing rate and efficiency.

- In the CH-MR process, ANOVA revealed pH as the most influential parameter (19.14% contribution), followed by WG (15.73%), RS (12.55%), and C (9.93%) as secondary factors. The remaining variation is attributed to parameter interactions.
- The CH-MR process effectively reduced the Sa of Ti64 alloy from 500 nm to 38.20 nm, within 30 minutes under optimal conditions.
- In the CH-MR process, post-process characterization using FESEM and AFM confirms exceptional surface integrity and minimal defects. XPS elucidates the finishing mechanism by correlating surface oxidation states to enhance chemical-mechanical synergy.
- THCP significantly enhances the mechanical properties of Ti64, increasing the average microhardness by 71% due to the formation of a protective surface layer. Additionally, the modified alloy (at pH 7) exhibits a substantially lower wear rate compared to the unmodified alloy, with a maximum reduction of 64.29 %.
- The surface modification by the THCP at different pH levels (5, 7, and 9) produces a contact angle below 90°, indicating a hydrophilic surface that promotes improved initial cell adhesion to the biomaterial surface.
- The novel THCP shows enhanced bioactivity at a Ca/P ratio of approximately 1.67, indicating the presence of hydroxyapatite (HA), which is essential for its biological functionality. This ratio correlates excellently with crystallinity.
- The novel THCP significantly improves biocompatibility, especially at pH (7) , showing a lower hemolysis ratio of 0.027 %, indicating the highest effectiveness in minimizing RBC lysis.

- The corrosion potential (E_{corr}) of the modified Ti64 alloy by THCP at pH values 5,7 and 9 were - 0.575 V, -0.552, and -0.598 V, respectively. Corrosion resistance improved with the decrease in current density (I_{corr}).
- A bioactive Titana (TiO_2) layer with an anatase structure can be created with the use of H_2O_2 treatment, which promotes the development of apatite and, as a result, improves the integration of bone implants.
- The utilization of hydrogen peroxide and citric acid in manufacturing aligns with the increasing need for environmentally friendly and non-hazardous surface modification techniques in the field of biomedical engineering.
- Citric acid enhances the thickness and uniformity of the oxide layer, improving corrosion resistance, hydrophilicity, and possibly antibacterial properties, all crucial for implant longevity and reducing infection risk.
- The research directly addresses the need for sustainable materials and non-hazardous, high-performance finishing for industrial applications, thereby bridging the gap between academic research and practical application.

6.2 Future Scope of Work

This thesis investigates experimental methods to enhance the surface modification of Ti alloys for biomedical applications, highlighting the potential for further advancement through hybrid and advanced finishing techniques while optimizing process parameters. Moreover, various surface modification techniques can be explored to enhance the mechanical, chemical, and biological properties of Ti alloys for biomedical implant applications. Additional evaluations, including cytocompatibility testing and in vitro cell culture experiments, can reveal the material's physiological behavior and long-term biocompatibility. There are several new areas for future work:

- Investigating the potential application of the CH-MR process to ceramics and composite materials could significantly enhance its industrial applicability and effectiveness.
- AI-driven parameter optimization utilizes machine learning algorithms to predict the optimal process parameters for various implant geometries, thereby reducing the need for trial-and-error experimentation.
- Applying the CH-MR process for additive manufacturing 3D-printed Ti64 alloy lattices, ensuring surface uniformity in complex porous structures critical for bone ingrowth.
- The CH-MR process, primarily used for Ti64 alloy, can also be applied to other alloys and hard-to-machine materials for high-precision finishing and sustainable manufacturing in the aerospace and medical sectors.
- Most previous studies focused on nano-finishing the regular shape of Ti alloys. However, further investigation is needed to complete the irregular parts required for medical applications. Finite element modeling is necessary for optimizing predictive process parameters.
- In future studies, it will be possible to conduct systematic investigations into the

effects of varying H_2O_2 and citric acid concentrations, treatment durations, and temperatures to optimize surface quality for specific biomedical applications.

REFERENCES

[1] Hashmi AW, Mali HS, Meena A, Saxena KK, Ahmad S, Agrawal MK, et al. A comprehensive review on surface post-treatments for freeform surfaces of bio-implants. J Mater Res Technol 2023;23:4866–908. https://doi.org/10.1016/j.jmrt.2023.02.007.

[2] Niinomi M. Mechanical biocompatibilities of titanium alloys for biomedical applications. J Mech Behav Biomed Mater 2008;1:30–42. https://doi.org/10.1016/J.JMBBM.2007.07.001.

[3] Sarraf M, Rezvani Ghomi E, Alipour S, Ramakrishna S, Liana Sukiman N. A state-of-the-art review of the fabrication and characteristics of titanium and its alloys for biomedical applications. Bio-Design Manuf 2022;5:371–95. https://doi.org/10.1007/s42242-021-00170-3.

[4] Balazic M, Kopac J, Jackson MJ, Ahmed W. Review: titanium and titanium alloy applications in medicine. vol. 1. 2007. https://doi.org/10.1504/IJNBM.2007.016517.

[5] Kang LM, Yang C. A Review on High-Strength Titanium Alloys: Microstructure, Strengthening, and Properties. Adv Eng Mater 2019;21. https://doi.org/10.1002/adem.201801359.

[6] Zhang S, Yu Y, Wang H, Ren L, Yang K. Study on mechanical behavior of Cu-bearing antibacterial titanium alloy implant. J Mech Behav Biomed Mater 2022;125:104926. https://doi.org/10.1016/J.JMBBM.2021.104926.

[7] Brunski JB. No Title 2004;In B.D. Ra.

[8] Manjaiah M, Laubscher RF. A review of the surface modifications of titanium alloys for biomedical applications. Mater Tehnol 2017;51:181–93. https://doi.org/10.17222/mit.2015.348.

[9] Tsai CH, Hung CH, Kuo CN, Chen CY, Peng YN, Shie MY. Improved Bioactivity of 3D Printed Porous Titanium Alloy Scaffold with Chitosan/Magnesium-Calcium Silicate Composite for Orthopaedic Applications. Mater 2019, Vol 12, Page 203

2019;12:203. https://doi.org/10.3390/MA12020203.

[10] Zhang H, Cooper LF, Zhang X, Zhang Y, Deng F, Song J, et al. Titanium nanotubes induce osteogenic differentiation through the FAK/RhoA/YAP cascade. RSC Adv 2016;6:44062–9. https://doi.org/10.1039/C6RA04002K.

[11] Costa TNQ, Dotta TC, Galo R, Soares ME da C, Pedrazzi V. Effect of tribocorrosion on surface-treated titanium alloy implants: A systematic review with meta-analysis. J Mech Behav Biomed Mater 2023;145:106008. https://doi.org/10.1016/J.JMBBM.2023.106008.

[12] Leyens C PM. Titanium and Titanium Alloys: Fundamentals and Applications - Google Books 2006. https://books.google.co.in/books?hl=en&lr=&id=okSA1N1xAxgC&oi=fnd&pg=PR5&dq=Leyens+C,+Peters+M.+Titanium+and+titanium+alloys:+fundamentals+and+applications.+Wiley+Online+Library%3B+2006&ots=WjN6AQAi7K&sig=EdEjlFLrlW_NDYWCkZmOmWjSTyY&redir_esc=y#v=onepage&q&f=false (accessed May 24, 2023).

[13] S. Kalpakjian. Manufacturing Engineering and Technology (Addison-Wesley Publishing Company, Inc. USA 1995). Manuf Process Eng Mater 5th Ed Pearson, 2014 2006;1999:1–6.

[14] Gautam S, Bhatnagar D, Bansal D, Batra H, Goyal N. Recent advancements in nanomaterials for biomedical implants. Biomed Eng Adv 2022;3:100029. https://doi.org/10.1016/j.bea.2022.100029.

[15] Moghadasi K, Mohd Isa MS, Ariffin MA, Mohd jamil MZ, Raja S, Wu B, et al. A review on biomedical implant materials and the effect of friction stir based techniques on their mechanical and tribological properties. J Mater Res Technol 2022;17:1054–121. https://doi.org/10.1016/j.jmrt.2022.01.050.

[16] Costa TB da, Pereira RBD, Lauro CH, Brandão LC, Davim JP. Statistical learning and optimization of the helical milling of the biocompatible titanium Ti-6Al-7Nb alloy. Int J Adv Manuf Technol 2023;125:1789–813.

https://doi.org/10.1007/s00170-022-10686-2.

[17] Nakai M, Iwasaki T, Ueki K. Differences in the effect of surface texturing on the wear loss of β-type Ti–Nb–Ta–Zr and (α+β)-type Ti–6Al–4V ELI alloys in contact with zirconia in physiological saline solution. J Mech Behav Biomed Mater 2021;124:104808. https://doi.org/10.1016/J.JMBBM.2021.104808.

[18] Lütjering G (Gerd), Williams JC (James C. Titanium 2003:379.

[19] Boyer RR. An overview on the use of titanium in the aerospace industry. Mater Sci Eng A 1996;213:103–14. https://doi.org/10.1016/0921-5093(96)10233-1.

[20] C. Leyens MP. Titanium and Titanium Alloys | Wiley Online Books. 2003.

[21] Zhang LC, Chen LY, Wang L. Surface Modification of Titanium and Titanium Alloys: Technologies, Developments, and Future Interests. Adv Eng Mater 2020;22:1–37. https://doi.org/10.1002/adem.201901258.

[22] Khanna N, Davim JP. Design-of-experiments application in machining titanium alloys for aerospace structural components. Measurement 2015;61:280–90. https://doi.org/10.1016/J.MEASUREMENT.2014.10.059.

[23] Cui C, Hu BM, Zhao L, Liu S. Titanium alloy production technology, market prospects and industry development. Mater Des 2011;32:1684–91. https://doi.org/10.1016/J.MATDES.2010.09.011.

[24] Golaz B, Michaud V, Lavanchy S, Månson JAE. Design and durability of titanium adhesive joints for marine applications. Int J Adhes Adhes 2013;45:150–7. https://doi.org/10.1016/J.IJADHADH.2013.04.003.

[25] Festas A, Ramos A, Davim JP. Machining of titanium alloys for medical application - a review. Https://DoiOrg/101177/09544054211028531 2021;236:309–18. https://doi.org/10.1177/09544054211028531.

[26] Geetha M, Singh AK, Asokamani R, Gogia AK. Ti based biomaterials, the ultimate choice for orthopaedic implants – A review. Prog Mater Sci 2009;54:397–425. https://doi.org/10.1016/J.PMATSCI.2008.06.004.

[27] Pałka K, Pokrowiecki R. Porous Titanium Implants: A Review. Adv Eng Mater 2018;20:1700648. https://doi.org/10.1002/ADEM.201700648.

[28] Lazoglu I, Ehsan Layegh Khavidaki S, Mamedov A. Mechanics of Titanium Machining 2014:57–78. https://doi.org/10.1007/978-3-662-43902-9_3.

[29] T. BR. Reaction of bone to multiple metallic implants. Surg Gynecol Obs 1940;71:59–602.

[30] Witt F, Bosker BH, Bishop NE, Ettema HB, Verheyen CCPM, Morlock MM. The relation between titanium taper corrosion and cobalt-chromium bearing wear in large-head metal-on-metal total hip prostheses: A Retrieval Study. J Bone Jt Surg - Am Vol 2014;96:e157(1). https://doi.org/10.2106/JBJS.M.01199.

[31] Xue L, Koul AK, Bibby M, Wallace W, Islam M. A Survey Of Surface Treatments To Improve The FrettingFatigue Resistance Of Ti-6Al-4V. WIT Trans Eng Sci 1970;8:310. https://doi.org/10.2495/SURF950311.

[32] Stadlinger B, Ferguson SJ, Eckelt U, Mai R, Lode AT, Loukota R, et al. Biomechanical evaluation of a titanium implant surface conditioned by a hydroxide ion solution. Br J Oral Maxillofac Surg 2012;50:74–9. https://doi.org/10.1016/J.BJOMS.2010.11.013.

[33] Mutalib NA, Ismail I, Soffie SM, Aqida SN. Magnetorheological finishing on metal surface: A review. IOP Conf. Ser. Mater. Sci. Eng., vol. 469, Institute of Physics Publishing; 2019. https://doi.org/10.1088/1757-899X/469/1/012092.

[34] Bahl S, Das S, Suwas S, Chatterjee K. Engineering the next-generation tin containing β titanium alloys with high strength and low modulus for orthopedic applications. J Mech Behav Biomed Mater 2018;78:124–33. https://doi.org/10.1016/J.JMBBM.2017.11.014.

[35] Liu X, Chu PK, Ding C. Surface modification of titanium, titanium alloys, and related materials for biomedical applications. Mater Sci Eng R Reports 2004;47:49–121. https://doi.org/10.1016/J.MSER.2004.11.001.

[36] Faria ACL, Rodrigues RCS, Claro APRA, de Mattos M da GC, Ribeiro RF. Wear resistance of experimental titanium alloys for dental applications. J Mech Behav Biomed Mater 2011;4:1873–9. https://doi.org/10.1016/J.JMBBM.2011.06.004.

[37] Niinomi M. Recent research and development in titanium alloys for biomedical applications and healthcare goods. Sci Technol Adv Mater 2003;4:445–54. https://doi.org/10.1016/J.STAM.2003.09.002/XML.

[38] Matsuda Y, Nakamura T, Ido K, Oka M, Okumura H, Matsushita T. Femoral component made of Ti-15MO-5Zr-3Al alloy in total hip arthroplasty. J Orthop Sci 1997;2:166–70. https://doi.org/10.1007/BF02492973/METRICS.

[39] Koizumi H, Ishii T, Okazaki T, Kaketani M, Matsumura H, Yoneyama T. Castability and mechanical properties of Ti-15Mo-5Zr-3Al alloy in dental casting. J Oral Sci 2018;60:285–92. https://doi.org/10.2334/josnusd.17-0280.

[40] Hussein MA, Kumar AM, Azeem MA, Sorour AA, Saravanan S. Ti–30Nb–3Ag alloy with improved corrosion resistance and antibacterial properties for orthopedic and dental applications produced by mechanical alloying. J Mech Behav Biomed Mater 2023;142:105851. https://doi.org/10.1016/j.jmbbm.2023.105851.

[41] Zhao T, Li Y, Liu Y, Zhao X. Nano-hardness, wear resistance and pseudoelasticity of hafnium implanted NiTi shape memory alloy. J Mech Behav Biomed Mater 2012;13:174–84. https://doi.org/10.1016/J.JMBBM.2012.04.004.

[42] Cheng Y-L, Lee C-Y, Huang Y-L, Buckner CA, Lafrenie RM, Dénommée JA, et al. Titanium and Titanium Alloys as Biomaterials Chapter. Intech 2016;11:13.

[43] Arifin A, Sulong AB, Muhamad N, Syarif J, Ramli MI. Material processing of hydroxyapatite and titanium alloy (HA/Ti) composite as implant materials using powder metallurgy: A review. Mater Des 2014;55:165–75. https://doi.org/10.1016/j.matdes.2013.09.045.

[44] Müeller WD, Gross U, Fritz T, Voigt C, Franklin KB, Fischer P, et al. Evaluation of the interface between bone and titanium surfaces being blasted by aluminium oxide

or bioceramic particles. Clin Oral Implants Res 2003;14:349–56. https://doi.org/10.1034/J.1600-0501.2003.00791.X.

[45] Fousova M, Vojtech D, Jablonska E, Fojt J, Lipov J. Novel Approach in the Use of Plasma Spray: Preparation of Bulk Titanium for Bone Augmentations. Mater 2017, Vol 10, Page 987 2017;10:987. https://doi.org/10.3390/MA10090987.

[46] Watari F, Yokoyama A, Omori M, Hirai T, Kondo H, Uo M, et al. Biocompatibility of materials and development to functionally graded implant for bio-medical application. Compos Sci Technol 2004;64:893–908. https://doi.org/10.1016/J.COMPSCITECH.2003.09.005.

[47] Paulo Davim J. Mechanical Behavior of Biomaterials. Mech Behav Biomater 2019:1–133. https://doi.org/10.1016/C2016-0-04173-6.

[48] Rafieerad AR, Bushroa AR, Zalnezhad E, Sarraf M, Basirun WJ, Baradaran S, et al. Microstructural development and corrosion behavior of self-organized TiO2 nanotubes coated on Ti–6Al–7Nb. Ceram Int 2015;41:10844–55. https://doi.org/10.1016/J.CERAMINT.2015.05.025.

[49] Civantos A, Domínguez C, Pino RJ, Setti G, Pavón JJ, Martínez-Campos E, et al. Designing bioactive porous titanium interfaces to balance mechanical properties and in vitro cells behavior towards increased osseointegration. Surf Coatings Technol 2019;368:162–74. https://doi.org/10.1016/J.SURFCOAT.2019.03.001.

[50] Wang Q, Zhou P, Liu S, Attarilar S, Ma RLW, Zhong Y, et al. Multi-scale surface treatments of titanium implants for rapid osseointegration: A review. Nanomaterials 2020;10:1–27. https://doi.org/10.3390/nano10061244.

[51] Heimke. Clinical application of ceramic osseo – or soft tissue - inte-grated implant. Orthop Ceram Implant 1984;4 1-19 1948.

[52] Wang J, Chen W, Han F. Study on the magnetorheological finishing method for the WEDMed pierced die cavity. Int J Adv Manuf Technol 2015;76:1969–75. https://doi.org/10.1007/S00170-014-6402-6/METRICS.

[53] Shaw MC (Milton C. Principles of abrasive processing 1996:574.

[54] Jain VK. Abrasive-based nano-finishing techniques: An overview. Mach Sci Technol 2008;12:257–94. https://doi.org/10.1080/10910340802278133.

[55] Sirwal SA, Singh AK, Paswan SK. Experimental analysis of magnetorheological finishing of blind hole surfaces using permanent magnet designed tools. J Brazilian Soc Mech Sci Eng 2020;42:1–23. https://doi.org/10.1007/S40430-020-2225-6/TABLES/13.

[56] Davim JP. Nontraditional machining processes: Research advances. Nontradit Mach Process Res Adv 2013;9781447151791:1–232. https://doi.org/10.1007/978-1-4471-5179-1/COVER.

[57] Davim JP. Surface integrity in machining. Surf Integr Mach 2010:1–215. https://doi.org/10.1007/978-1-84882-874-2/COVER.

[58] Rajput AS, Singh A, Kapil S, Das M. Investigations on the trochoidal toolpath for processing the biomaterial through magnetorheological fluid assisted finishing process. J Manuf Process 2022;76:812–27. https://doi.org/10.1016/j.jmapro.2022.02.055.

[59] Sihag N, Kala P, Pandey PM. Analysis of Surface Finish Improvement during Ultrasonic Assisted Magnetic Abrasive Finishing on Chemically treated Tungsten Substrate. Procedia Manuf 2017;10:136–46. https://doi.org/10.1016/j.promfg.2017.07.040.

[60] Rajput AS, Das M, Kapil S. Investigations on a hybrid chemo-magnetorheological finishing process for freeform surface quality enhancement. J Manuf Process 2022;81:522–36. https://doi.org/10.1016/j.jmapro.2022.07.015.

[61] Rajput AS, Das M, Kapil S. A comprehensive review of magnetorheological fluid assisted finishing processes. Mach Sci Technol 2022;26:339–76. https://doi.org/10.1080/10910344.2022.2129982.

[62] Sidpara AM, Jain VK. Nanofinishing of freeform surfaces of prosthetic knee joint

implant. Proc Inst Mech Eng Part B J Eng Manuf 2012;226:1833–46. https://doi.org/10.1177/0954405412460452.

[63] Harris DC. History of magnetorheological finishing. Https://DoiOrg/101117/12882557 2011;8016:206–27. https://doi.org/10.1117/12.882557.

[64] Kordonski WI, Jacobs SD. MAGNETORHEOLOGICAL FINISHING. Https://DoiOrg/101142/S0217979296001288 2012;10:2837–48. https://doi.org/10.1142/S0217979296001288.

[65] Kordonski WI, Golini D. Fundamentals of Magnetorheological Fluid Utilization in High Precision Finishing. Http://DxDoiOrg/101106/011M-CJ25-64QC-F3A6 1999;10:683–9. https://doi.org/10.1106/011M-CJ25-64QC-F3A6.

[66] Singh RK, Singh DK, Gangwar S. Advances in Magnetic Abrasive Finishing for Futuristic Requirements - A Review. Mater Today Proc 2018;5:20455–63. https://doi.org/10.1016/J.MATPR.2018.06.422.

[67] Qian C, Fan Z, Tian Y, Liu Y, Han J, Wang J. A review on magnetic abrasive finishing. Int J Adv Manuf Technol 2021;112:619–34. https://doi.org/10.1007/s00170-020-06363-x.

[68] Barman A, Das M, Pathak VK. Optimization of magnetic field assisted finishing process during nanofinishing of titanium alloy (grade-5) implant using soft computing approaches. Int J Model Simul 2022;42:920–35. https://doi.org/10.1080/02286203.2021.2001720.

[69] Alam Z, Jha S. Modeling of surface roughness in ball end magnetorheological finishing (BEMRF) process. Wear 2017;374–375:54–62. https://doi.org/10.1016/J.WEAR.2016.11.039.

[70] Ma F, Wang Z, Liu Y, Sha Z, Zhang S. Machining Performance for Ultrasonic-Assisted Magnetic Abrasive Finishing of a Titanium Alloy: A Comparison with Magnetic Abrasive Finishing. Machines 2022;10.

https://doi.org/10.3390/machines10100902.

[71] Kumari C, Chak SK. Study on influential parameters of hybrid AFM processes: a review. Manuf Rev 2019;6:23. https://doi.org/10.1051/MFREVIEW/2019022.

[72] Amir M, Mishra V, Sharma R, Iqbal F, Ali SW, Kumar S, et al. Development of magnetic nanoparticle based nanoabrasives for magnetorheological finishing process and all their variants. Ceram Int 2023;49:6254–61. https://doi.org/10.1016/j.ceramint.2022.11.033.

[73] Fletcher AJ, Hull JB, Mackie J, Trengove SA. Computer Modelling of the Abrasive Flow Machining Process. Surf Eng 1990:592–601. https://doi.org/10.1007/978-94-009-0773-7_59.

[74] Dixit N, Sharma V, Kumar P. Research trends in abrasive flow machining: A systematic review. J Manuf Process 2021;64:1434–61. https://doi.org/10.1016/j.jmapro.2021.03.009.

[75] Rhoades L. Abrasive flow machining: a case study. J Mater Process Technol 1991;28:107–16. https://doi.org/10.1016/0924-0136(91)90210-6.

[76] Jackson MJ, Davim JP. Machining with abrasives. Mach with Abrasives 2011:1–423. https://doi.org/10.1007/978-1-4419-7302-3/COVER.

[77] Jain RK, Jain VK, Dixit PM. Modeling of material removal and surface roughness in abrasive flow machining process. Int J Mach Tools Manuf 1999;39:1903–23. https://doi.org/10.1016/S0890-6955(99)00038-3.

[78] Hiremath S. A Review on Abrasive Flow Machining (AFM). Procedia Technol 2016;25:1297–304. https://doi.org/10.1016/J.PROTCY.2016.08.224.

[79] Basha SM, Basha MM, Venkaiah N, Sankar MR. A review on abrasive flow finishing of metal matrix composites. Mater Today Proc 2021;44:579–86. https://doi.org/10.1016/J.MATPR.2020.10.353.

[80] Zhang L, Huang Y, Chen G, Xu M, Xia W, Fu Y. Experimental study of coverage constraint abrasive flow machining of titanium alloy artificial joint surface. Proc Inst

Mech Eng Part B J Eng Manuf 2019;233:2399–409. https://doi.org/10.1177/0954405419840553.

[81] Kumar M, Kumar A, Yadav HNS, Alok A, Das M. Abrasive based finishing method applied on biomedical implants: A review. Mater Today Proc 2021;47:3985–92. https://doi.org/10.1016/j.matpr.2021.04.137.

[82] Kumar M, Alok A, Kumar V, Das M. Advanced abrasive-based nano-finishing processes: challenges, principles and recent applications. Mater Manuf Process 2022;37:372–92. https://doi.org/10.1080/10426914.2021.2001509.

[83] Sambharia J, Mali HS. Recent developments in abrasive flow finishing process: A review of current research and future prospects. Https://DoiOrg/101177/0954405417731466 2017;233:388–99. https://doi.org/10.1177/0954405417731466.

[84] Subramanian KT, Balashanmugam N, Shashi Kumar PV. Nanometric Finishing on Biomedical Implants by Abrasive Flow Finishing. J Inst Eng Ser C 2016;97:55–61. https://doi.org/10.1007/S40032-015-0190-0/FIGURES/7.

[85] Leng Y, Yang D, Ming P, - al, Cunningham N, Guay D, et al. Effect of surface roughness and surface topography on wettability of machined biomaterials using flexible viscoelastic polymer abrasive media. Surf Topogr Metrol Prop 2019;7:015004. https://doi.org/10.1088/2051-672X/AAF6F6.

[86] Sankar MR, Jain VK, Ramkumar J. Experimental investigations into rotating workpiece abrasive flow finishing. Wear 2009;267:43–51. https://doi.org/10.1016/J.WEAR.2008.11.007.

[87] Chang GW, Yan BH, Hsu RT. Study on cylindrical magnetic abrasive finishing using unbonded magnetic abrasives. Int J Mach Tools Manuf 2002;42:575–83. https://doi.org/10.1016/S0890-6955(01)00153-5.

[88] Yan BH, Lin YC, Huang FY. Development of magneto abrasive flow machining process. Int J Mach Tools Manuf 2002;42:953–9. https://doi.org/10.1016/S0890-

6955(02)00021-4.

[89] Yamaguchi H, Shinmura T, Ikeda R. Study of Internal Finishing of Austenitic Stainless Steel Capillary Tubes by Magnetic Abrasive Finishing. J Manuf Sci Eng 2007;129:885–92. https://doi.org/10.1115/1.2738957.

[90] Kang J, Yamaguchi H. Internal finishing of capillary tubes by magnetic abrasive finishing using a multiple pole-tip system. Precis Eng 2012;36:510–6. https://doi.org/10.1016/J.PRECISIONENG.2012.01.006.

[91] Barman A, Das M. Magnetic field assisted finishing process for super-finished Ti alloy implant and its 3D surface characterization. J Micromanufacturing 2018;1:154–69. https://doi.org/10.1177/2516598418785506.

[92] Kishore K, Sinha MK, Chauhan SR. A comprehensive investigation of surface morphology during grinding of Inconel 625 using conventional grinding wheels. J Manuf Process 2023;97:87–99. https://doi.org/10.1016/j.jmapro.2023.04.053.

[93] Barman A, Das M. Toolpath generation and finishing of bio-titanium alloy using novel polishing tool in MFAF process. Int J Adv Manuf Technol 2019;100:1123–35. https://doi.org/10.1007/s00170-017-1050-2.

[94] 7207-2:2011(en) I. ISO 7207-2:2011(en). Implants for surgery — components for partial and total knee joint prostheses — Part 2: articulating surfaces made of metal. Ceram Plast Mater 2017, n.d. n.d.

[95] Yamaguchi H, Srivastava AK, Tan MA, Riveros RE, Hashimoto F. Magnetic abrasive finishing of cutting tools for machining of titanium alloys. CIRP Ann 2012;61:311–4. https://doi.org/10.1016/J.CIRP.2012.03.066.

[96] Jha S, Jain VK. Design and development of the magnetorheological abrasive flow finishing (MRAFF) process. Int J Mach Tools Manuf 2004;44:1019–29. https://doi.org/10.1016/J.IJMACHTOOLS.2004.03.007.

[97] Choi YT, Cho JU, Choi SB, Wereley NM. Constitutive models of electrorheological and magnetorheological fluids usingviscometers. Smart Mater Struct 2005;14:1025.

https://doi.org/10.1088/0964-1726/14/5/041.

[98] Ahmad S, Singari RM, Mishra RS. Development of Al2O3-SiO2 based magnetic abrasive by sintering method and its performance on Ti-6Al-4V during magnetic abrasive finishing. Trans Inst Met Finish 2021;99:94–101. https://doi.org/10.1080/00202967.2021.1865644.

[99] Rabinow J. The magnetic fluid clutch. Electr Eng 2013;67:1167–1167. https://doi.org/10.1109/ee.1948.6444497.

[100] Sidpara AM, Jain VK. Nanofinishing of freeform surfaces of prosthetic knee joint implant. Http://DxDoiOrg/101177/0954405412460452 2012;226:1833–46. https://doi.org/10.1177/0954405412460452.

[101] Hou N, Wang M, Wang B, Zheng Y, Zhou S, Song C. Fundamental functions of physical and chemical principles in the polishing of titanium alloys: mechanisms and problems. Int J Adv Manuf Technol 2022;118:2079–97. https://doi.org/10.1007/s00170-021-08100-4.

[102] Prakash C, Singh S, Pramanik A, Basak A, Królczyk G, Bogdan-Chudy M, et al. Experimental investigation into nano-finishing of β-TNTZ alloy using magnetorheological fluid magnetic abrasive finishing process for orthopedic applications. J Mater Res Technol 2021;11:600–17. https://doi.org/10.1016/j.jmrt.2021.01.046.

[103] Sidpara A, Jain VK. Rheological properties and their correlation with surface finish quality in MR fluid-based finishing process. Mach Sci Technol 2014;18:367–85. https://doi.org/10.1080/10910344.2014.925372.

[104] Singh S, Prakash C, Pramanik A, Basak A, Shabadi R, Królczyk G, et al. Magneto-rheological fluid assisted abrasive nanofinishing of β-phase ti-nb-ta-zr alloy: Parametric appraisal and corrosion analysis. Materials (Basel) 2020;13:1–15. https://doi.org/10.3390/ma13225156.

[105] Baghel P, Singh S, Nagdeve L, Jain VK, Sharma ND. Preliminary investigations

into finishing of artificial dental crown. Int J Precis Technol 2015;5:229. https://doi.org/10.1504/ijptech.2015.073827.

[106] Sylwia S. SURFACE MODIFICATIONS OF Ti AND ITS ALLOYS 2010. https://doi.org/10.2478/v10077-010-0003-3.

[107] Das M, Jain VK, Ghoshdastidar PS. Computational fluid dynamics simulation and experimental investigations into the magnetic-field-assisted nano-finishing process. Http://DxDoiOrg/101177/0954405412440230 2012;226:1143–58. https://doi.org/10.1177/0954405412440230.

[108] Nagdeve L, Jain VK, Ramkumar J. Differential finishing of freeform surfaces (knee joint) using R-MRAFF process and negative replica of workpiece as a fixture. Mach Sci Technol 2018;22:671–95. https://doi.org/10.1080/10910344.2017.1402929.

[109] Kumar S, Jain VK, Sidpara A. Nanofinishing of freeform surfaces (knee joint implant) by rotational-magnetorheological abrasive flow finishing (R-MRAFF) process. Precis Eng 2015;42:165–78. https://doi.org/10.1016/j.precisioneng.2015.04.014.

[110] Nagdeve L, Jain VK, Ramkumar J. Experimental Investigations into Nano-finishing of Freeform Surfaces Using Negative Replica of the Knee Joint. Procedia CIRP 2016;42:793–8. https://doi.org/10.1016/J.PROCIR.2016.02.321.

[111] Nagdeve L, Jain VK, Ramkumar J. Preliminary investigations into nano-finishing of freeform surface (femoral) using inverse replica fixture. Int J Adv Manuf Technol 2019;100:1081–92. https://doi.org/10.1007/s00170-017-1459-7.

[112] Alam Z, Khan DA, Jha S. MR fluid-based novel finishing process for nonplanar copper mirrors. Int J Adv Manuf Technol 2019;101:995–1006. https://doi.org/10.1007/s00170-018-2998-2.

[113] Jha S, Jain VK. Rheological characterization of magnetorheological polishing fluid for MRAFF. Int J Adv Manuf Technol 2009;42:656–68. https://doi.org/10.1007/S00170-008-1637-8/METRICS.

[114] Khan DA, Jha S. Synthesis of polishing fluid and novel approach for nanofinishing of copper using ball-end magnetorheological finishing process. Https://DoiOrg/101080/1042691420171328112 2017;33:1150–9. https://doi.org/10.1080/10426914.2017.1328112.

[115] Beier M, Scheiding S, Gebhardt A, Loose R, Risse S, Eberhardt R, et al. Fabrication of high precision metallic freeform mirrors with magnetorheological finishing (MRF). Https://DoiOrg/101117/122035986 2013;8884:139–52. https://doi.org/10.1117/12.2035986.

[116] Bhavsar P, Unune DR. Magnetorheological Polishing Tool for Nano-Finishing of Biomaterials. Proceeding 10th Int Conf Precesion, Meso, Micro Nano Eng 2018:6–10.

[117] Liu X, Chu PK, Ding C. Surface nano-functionalization of biomaterials. Mater Sci Eng R Reports 2010;70:275–302. https://doi.org/10.1016/j.mser.2010.06.013.

[118] Zhang Y, Li J, Che S, Yang Z, Tian Y. Chemical leveling mechanism and oxide film properties of additively manufactured Ti–6Al–4V alloy. J Mater Sci 2019;54:13753–66. https://doi.org/10.1007/s10853-019-03855-4.

[119] Biswas A, Srikant PVS, Manna I, Chatterjee UK, Dutta Majumdar J. Chemical oxidation of Ti-6Al-4v for improved wear and corrosion resistance. Surf Eng 2008;24:442–6. https://doi.org/10.1179/174329408X286097.

[120] Ban S, Iwaya Y, Kono H, Sato H. Surface modification of titanium by etching in concentrated sulfuric acid. Dent Mater 2006;22:1115–20. https://doi.org/10.1016/J.DENTAL.2005.09.007.

[121] Lamolle SF, Monjo M, Rubert M, Haugen HJ, Lyngstadaas SP, Ellingsen JE. The effect of hydrofluoric acid treatment of titanium surface on nanostructural and chemical changes and the growth of MC3T3-E1 cells. Biomaterials 2009;30:736–42. https://doi.org/10.1016/J.BIOMATERIALS.2008.10.052.

[122] Cho SA, Park KT. The removal torque of titanium screw inserted in rabbit tibia

treated by dual acid etching. Biomaterials 2003;24:3611–7. https://doi.org/10.1016/S0142-9612(03)00218-7.

[123] Attar H, Bönisch M, Calin M, Zhang LC, Zhuravleva K, Funk A, et al. Comparative study of microstructures and mechanical properties of in situ Ti-TiB composites produced by selective laser melting, powder metallurgy, and casting technologies. J Mater Res 2014;29:1941–50. https://doi.org/10.1557/JMR.2014.122/METRICS.

[124] Martin JY, Schwartz Z, Hummert TW, Schraub DM, Simpson J, Lankford J, et al. Effect of titanium surface roughness on proliferation, differentiation, and protein synthesis of human osteoblast-like cells (MG63). J Biomed Mater Res 1995;29:389–401. https://doi.org/10.1002/JBM.820290314.

[125] Variola F, Yi J-H, Richert L, Wuest JD, Rosei F, Nanci A. Tailoring the surface properties of Ti6Al4V by controlled chemical oxidation 2007. https://doi.org/10.1016/j.biomaterials.2007.11.040.

[126] Shi G sheng, Ren L fei, Wang L zhi, Lin H sheng, Wang S bin, Tong Y qing. H2O2/HCl and heat-treated Ti-6Al-4V stimulates pre-osteoblast proliferation and differentiation. Oral Surgery, Oral Med Oral Pathol Oral Radiol Endodontology 2009;108:368–75. https://doi.org/10.1016/J.TRIPLEO.2009.05.033.

[127] Lee MH, Park IS, Min KS, Ahn SG, Park JM, Song KY, et al. Evaluation of in vitro and in vivo tests for Surface-modified Titanium by H2so4 and H2O2 Treatment. Met Mater Int 2007;13:109–15. https://doi.org/10.1007/BF03027560/METRICS.

[128] Guo J, Padilla RJ, Ambrose W, De Kok IJ, Cooper LF. The effect of hydrofluoric acid treatment of TiO 2 grit blasted titanium implants on adherent osteoblast gene expression in vitro and in vivo. Biomaterials 2007;28:5418–25. https://doi.org/10.1016/j.biomaterials.2007.08.032.

[129] Zheng G, Jiao Q, Li C, Ding Y, He J, Jiang Y, et al. Influence of nitridation on the microstructure and corrosion behavior of reactive plasma sprayed TiCN coatings. Surf Coatings Technol 2020;396:125954. https://doi.org/10.1016/J.SURFCOAT.2020.125954.

[130] Din SH. Biomedical Applications of Titanium and Its Alloys. Proc Eng Sci 2021;3:41–52. https://doi.org/10.24874/PES03.01.005.

[131] Zhang Z, Shi Z, Du Y, Yu Z, Guo L, Guo D. A novel approach of chemical mechanical polishing for a titanium alloy using an environment-friendly slurry. Appl Surf Sci 2018;427:409–15. https://doi.org/10.1016/J.APSUSC.2017.08.064.

[132] Khodaei M, Hossein Kelishadi S. The effect of different oxidizing ions on hydrogen peroxide treatment of titanium dental implant. Surf Coatings Technol 2018;353:158–62. https://doi.org/10.1016/J.SURFCOAT.2018.08.037.

[133] Teixeira A. Development of an Electropolishing Method for Titanium Materials 2011.

[134] Ashikur Rahman Khan M, Rahman MM. Surface finish characteristics of titanium alloy in a non conventional technique. Mater Today Proc 2017;4:9352–5. https://doi.org/10.1016/J.MATPR.2017.06.183.

[135] Ozdemir Z, Ozdemir A, Basim GB. Application of chemical mechanical polishing process on titanium based implants. Mater Sci Eng C 2016;68:383–96. https://doi.org/10.1016/j.msec.2016.06.002.

[136] Kaushik RM, Bhandakkar AB, Patro TU. Solution of emulsifiable oil and hydrogen peroxide for chemical-mechanical polishing of Ti alloy - A green approach. Mater Lett 2014;122:252–5. https://doi.org/10.1016/j.matlet.2014.02.059.

[137] Liang C, Liu W, Li S, Kong H, Zhang Z, Song Z. A nano-scale mirror-like surface of Ti-6Al-4V attained by chemical mechanical polishing. Chinese Phys B 2016;25. https://doi.org/10.1088/1674-1056/25/5/058301.

[138] Liu J, Wang Z, Xu Z. Electrochemical Polishing of Ti6Al4V Alloy Assisted by High-Speed Flow of Micro-Abrasive Particles in NaNO3 Electrolyte. Materials (Basel) 2022;15:1–18. https://doi.org/10.3390/ma15228148.

[139] De Nardo L, Altomare L, Del Curto B, Cigada A, Draghi L. Electrochemical surface modifications of titanium and titanium alloys for biomedical applications. Coatings

Biomed Appl 2012:106–42. https://doi.org/10.1533/9780857093677.1.106.

[140] Simka W, Mosiałek M, Nawrat G, Nowak P, Zak J, Szade J, et al. Electrochemical polishing of Ti–13Nb–13Zr alloy. Surf Coatings Technol 2012;213:239–46. https://doi.org/10.1016/J.SURFCOAT.2012.10.055.

[141] Wang Y, Zhao W, Wu Y, - al, Jie W, Yang F, et al. Study on electrochemical polishing of TC4 alloy. Mater Res Express 2021;8:106520. https://doi.org/10.1088/2053-1591/AC1F4C.

[142] Mulik RS, Pandey PM. Mechanism of Surface Finishing in Ultrasonic-Assisted Magnetic Abrasive Finishing Process. Https://DoiOrg/101080/104269142010499580 2010;25:1418–27. https://doi.org/10.1080/10426914.2010.499580.

[143] Mulik RS, Pandey PM. Ultrasonic assisted magnetic abrasive finishing of hardened AISI 52100 steel using unbonded SiC abrasives. Int J Refract Met Hard Mater 2011;29:68–77. https://doi.org/10.1016/J.IJRMHM.2010.08.002.

[144] Chen Y. Z, 2019. Parameter Optimization Design and Analysis of Ultrasonic Composite Magnetic Abrasive Finishing. Surf Technol 2019, 48, 268–274 n.d.

[145] Zhou K, Chen Y, Du ZW, Niu FL. Surface integrity of titanium part by ultrasonic magnetic abrasive finishing. Int J Adv Manuf Technol 2015;80:997–1005. https://doi.org/10.1007/S00170-015-7028-Z/METRICS.

[146] Çelik M, Gürün H, Çaydaş U. Surface modification of wire-EDMed Ti6Al4V alloy by ultrasonic assisted magnetic abrasive finishing technique. Surf Topogr Metrol Prop 2022;10. https://doi.org/10.1088/2051-672X/ac68fe.

[147] Davim JP. Nonconventional Machining. Nonconv Mach 2022:1–195. https://doi.org/10.1515/9783110584479/EPUB.

[148] Sihag N, Kala P, Pandey PM. Experimental investigations of chemo-ultrasonic assisted magnetic abrasive finishing process. Int J Precis Technol 2015;5:246. https://doi.org/10.1504/ijptech.2015.073822.

[149] Khan DA, Alam Z, Jha S. IMECE2016-65974 2017:1–5.

[150] Tian Y, Shi C, Fan Z, Zhou Q. Experimental investigations on magnetic abrasive finishing of Ti-6Al-4V using a multiple pole-tip finishing tool. Int J Adv Manuf Technol 2020;106:3071–80. https://doi.org/10.1007/s00170-019-04871-z.

[151] Singh S, Prakash C. Effect of cryogenic treatment on the microstructure, mechanical properties and finishability of β-TNTZ alloy for orthopedic applications. Mater Lett 2020;278:128461. https://doi.org/10.1016/j.matlet.2020.128461.

[152] Amalia Yunia Rahmawati. Mechanical Behaviour of Biomaterials. 2020.

[153] Sibum H. Titanium and Titanium Alloys—From Raw Material to Semi-finished Products. Adv Eng Mater 2003;5:393–8. https://doi.org/10.1002/ADEM.200310092.

[154] Abdullah Naji FA, Murtaza Q, Niranjan MS. Challenges and opportunities in nano finishing of titanium alloys for biomedical applications: A review. Precis Eng 2024;88:81–99. https://doi.org/10.1016/j.precisioneng.2024.01.019.

[155] Sandrini E, Giordano C, Busini V, Signorelli E, Cigada A. Apatite formation and cellular response of a novel bioactive titanium. J Mater Sci Mater Med 2007;18:1225–37. https://doi.org/10.1007/s10856-007-0122-5.

[156] Graves SE, Davidson D, Ingerson L, Ryan P, Griffith EC, McDermott BFJ, et al. The Australian Orthopaedic Association National Joint Replacement Registry. Med J Aust 2004;180. https://doi.org/10.5694/J.1326-5377.2004.TB05911.X.

[157] Damiati L, Eales MG, Nobbs AH, Su B, Tsimbouri PM, Salmeron-Sanchez M, et al. Impact of surface topography and coating on osteogenesis and bacterial attachment on titanium implants. J Tissue Eng 2018;9:2041731418790694–2041731418790694. https://doi.org/10.1177/2041731418790694.

[158] Sul YT, Johansson CB, Jeong Y, Albrektsson T. The electrochemical oxide growth behaviour on titanium in acid and alkaline electrolytes. Med Eng Phys 2001;23:329–46. https://doi.org/10.1016/S1350-4533(01)00050-9.

[159] Zieliński A, Sobieszczyk S. Corrosion of titanium biomaterials, mechanisms, effects and modelisation. Corros Rev 2008;26:1–22. https://doi.org/10.1515/CORRREV.2008.1/MACHINEREADABLECITATION/RIS.

[160] Arenas MA, Pérez-Jorge C, Conde A, Matykina E, Hernández-López JM, Pérez-Tanoira R, et al. Doped TiO2 anodic layers of enhanced antibacterial properties. Colloids Surfaces B Biointerfaces 2013;105:106–12. https://doi.org/10.1016/J.COLSURFB.2012.12.051.

[161] Prando D, Brenna A, Diamanti MV, Beretta S, Bolzoni F, Ormellese M, et al. Corrosion of titanium: Part 1: Aggressive environments and main forms of degradation. J Appl Biomater Funct Mater 2017;15:e291–302. https://doi.org/10.5301/jabfm.5000387.

[162] Fazel M, Salimijazi HR, Golozar MA, Garsivaz Jazi MR. A comparison of corrosion, tribocorrosion and electrochemical impedance properties of pure Ti and Ti6Al4V alloy treated by micro-arc oxidation process. Appl Surf Sci 2015;324:751–6. https://doi.org/10.1016/J.APSUSC.2014.11.030.

[163] Liu J, Alfantazi A, Asselin E. A new method to improve the corrosion resistance of titanium for hydrometallurgical applications. Appl Surf Sci 2015;332:480–7. https://doi.org/10.1016/j.apsusc.2015.01.140.

[164] Williamson RS, Disegi J, Janorkar A V., Griggs JA, Roach MD. Effect of duty cycle on the crystallinity, pore size, surface roughness and corrosion resistance of the anodized surface on titanium. Surf Coatings Technol 2015;277:278–88. https://doi.org/10.1016/j.surfcoat.2015.07.020.

[165] Variola F, Zalzal SF, Leduc A, Barbeau J, Nanci A. Oxidative nanopatterning of titanium generates mesoporous surfaces with antimicrobial properties. Int J Nanomedicine 2014;9:2319–25. https://doi.org/10.2147/IJN.S61333.

[166] Verdeguer P, Gil J, Punset M, Manero JM, Nart J, Vilarrasa J, et al. Citric Acid in the Passivation of Titanium Dental Implants: Corrosion Resistance and Bactericide

Behavior. Materials (Basel) 2022;15. https://doi.org/10.3390/ma15020545.

[167] Gupta A, Dhanraj M, Sivagami G. Status of surface treatment in endosseous implant: A literary overview. Indian J Dent Res 2010;21:433–8. https://doi.org/10.4103/0970-9290.70805.

[168] Izman S, Rafiq M, Anwar M, Nazim EM, Rosliza R, Shah A, et al. Surface Modification Techniques for Biomedical Grade of Titanium Alloys: Oxidation, Carburization and Ion Implantation Processes. Titan Alloy - Towar Achiev Enhanc Prop Divers Appl 2012. https://doi.org/10.5772/36318.

[169] Zhao X, Ren X, Wang C, Huang B, Ma J, Ge B, et al. Enhancement of hydroxyapatite formation on titanium surface by alkali heat treatment combined with induction heating and acid etching. Surf Coatings Technol 2020;399. https://doi.org/10.1016/j.surfcoat.2020.126173.

[170] Yao Y tong, Liu S, Swain M V., Zhang X ping, Zhao K, Jian Y tao. Effects of acid-alkali treatment on bioactivity and osteoinduction of porous titanium: An in vitro study. Mater Sci Eng C 2019;94:200–10. https://doi.org/10.1016/j.msec.2018.08.056.

[171] Kokubo T, Yamaguchi S. Novel bioactive titanate layers formed on ti metal and its alloys by chemical treatments. Materials (Basel) 2010;3:48–63. https://doi.org/10.3390/ma3010048.

[172] Gostin PF, Helth A, Voss A, Sueptitz R, Calin M, Eckert J, et al. Surface treatment, corrosion behavior, and apatite-forming ability of ti-45Nb implant alloy. J Biomed Mater Res - Part B Appl Biomater 2013;101 B:269–78. https://doi.org/10.1002/jbm.b.32836.

[173] Zablotsky M, Meffert R, Mills O, Burgess A, Lancaster D. The macroscopic, microscopic and spectrometric effects of various chemotherapeutic agents on the plasma-sprayed hydroxyapatite-coated implant surface. Clin Oral Implants Res 1992;3:189–98. https://doi.org/10.1034/j.1600-0501.1992.030406.x.

[174] Panda S, Kazama M, Kawai T, Biswas CK, Paul S. Controlled surface modification of Ti6Al4V using biomimetic mineralization via thermo-chemical route improves bioactivity. Ceram Int 2022;48:11286–97. https://doi.org/10.1016/j.ceramint.2021.12.351.

[175] Mirdamadi SH, Khodaei M, Valanezhad A, Watanabe I, Nejatidanesh F, Savabi O. Effect of post heat treatment on surface properties of hydrogen peroxide (H2O2) treated titanium. J Mater Res Technol 2022;18:584–90. https://doi.org/10.1016/J.JMRT.2022.02.095.

[176] Al. C et. J of Periodontal Research - 2021 - Cordeiro - Optimizing citric acid protocol to control implant-related infections An in.pdf 2021.

[177] Wheelis SE, Gindri IM, Valderrama P, Wilson TG, Huang J, Rodrigues DC. Effects of decontamination solutions on the surface of titanium: Investigation of surface morphology, composition, and roughness. Clin Oral Implants Res 2016;27:329–40. https://doi.org/10.1111/clr.12545.

[178] Nagdeve L, Jain VK, Ramkumar J. Nanofinishing of freeform/sculptured surfaces: State-of-the-art. Manuf Rev 2018;5:1–20. https://doi.org/10.1051/mfreview/2018005.

[179] Katti KS. Biomaterials in total joint replacement. Colloids Surfaces B Biointerfaces 2004;39:133–42. https://doi.org/10.1016/J.COLSURFB.2003.12.002.

[180] Surya MS, Prasanthi G, Kumar AK, Sridhar VK, Gugulothu SK. Optimization of cutting parameters while turning Ti-6Al-4 V using response surface methodology and machine learning technique. Int J Interact Des Manuf 2021;15:453–62. https://doi.org/10.1007/S12008-021-00774-0.

[181] Davim JP. Machining of Titanium Alloys 2014. https://doi.org/10.1007/978-3-662-43902-9.

[182] Parameswari G, Jain VK, Ramkumar J, Nagdeve L. Experimental investigations into nanofinishing of Ti6Al4V flat disc using magnetorheological finishing process. Int

J Adv Manuf Technol 2019;100:1055–65. https://doi.org/10.1007/s00170-017-1191-3.

[183] Fan Z, Tian Y, Zhou Q, Shi C. Enhanced magnetic abrasive finishing of Ti–6Al–4V using shear thickening fluids additives. Precis Eng 2020;64:300–6. https://doi.org/10.1016/j.precisioneng.2020.05.001.

[184] Fan Z, Tian Y, Liu Z, Shi C, Zhao Y. Investigation of a novel finishing tool in magnetic field assisted finishing for titanium alloy Ti-6Al-4V. J Manuf Process 2019;43:74–82. https://doi.org/10.1016/j.jmapro.2019.05.007.

[185] Tien DH, Duy TN, Thoa PTT. Applying GPR-FGRA hybrid algorithm for prediction and optimization of eco-friendly magnetorheological finishing Ti–6Al–4V alloy. Int J Interact Des Manuf 2022. https://doi.org/10.1007/s12008-022-00995-x.

[186] GOLINI D, SCHNEIDER G, FLUG P, DeMARCO M. The Ultimate Flexible optics manufacturing technology: Magnetorheological Finishing. Opt Photonics News 2001;12:20. https://doi.org/10.1364/OPN.12.10.000020.

[187] McKee RL. Machining with abrasives. 1982. https://doi.org/10.1016/0141-6359(83)90040-5.

[188] Petare AC, Jain NK. A critical review of past research and advances in abrasive flow finishing process. Int J Adv Manuf Technol 2018;97:741–82. https://doi.org/10.1007/S00170-018-1928-7/METRICS.

[189] Niranjan MS, Jha S. Optimum selection of machining parameters in ball end magnetorheological finishing process. Int J Precis Technol 2015;5:217. https://doi.org/10.1504/IJPTECH.2015.073826.

[190] Ranjan P, Balasubramaniam R, Jain VK. Analysis of magnetorheological fluid behavior in chemo-mechanical magnetorheological finishing (CMMRF) process. Precis Eng 2017;49:122–35. https://doi.org/10.1016/j.precisioneng.2017.02.001.

[191] Sadiq A, Shunmugam MS. Investigation into magnetorheological abrasive honing

(MRAH). Int J Mach Tools Manuf 2009;49:554–60. https://doi.org/10.1016/J.IJMACHTOOLS.2009.02.009.

[192] Saraswathamma K, Jha S, Rao PV. Rheological characterization of MR polishing fluid used for silicon polishing in BEMRF process. Mater Manuf Process 2015;30:661–8. https://doi.org/10.1080/10426914.2014.994767.

[193] Zantye PB, Kumar A, Sikder AK. Chemical mechanical planarization for microelectronics applications. Mater Sci Eng R Reports 2004;45:89–220. https://doi.org/10.1016/J.MSER.2004.06.002.

[194] Denkena B, Köhler J, Van der Meer M. A roughness model for the machining of biomedical ceramics by toric grinding pins. CIRP J Manuf Sci Technol 2013;6:22–33. https://doi.org/10.1016/j.cirpj.2012.07.002.

[195] Kanish TC, Narayanan S, Kuppan P, Denis Ashok S. Investigations on wear behavior of Magnetic Field Assisted Abrasive Finished SS316L material. Mater Today Proc 2018;5:12734–43. https://doi.org/10.1016/J.MATPR.2018.02.257.

[196] Jain VK, Sidpara A, Sankar MR, Das M. Nano-finishing techniques: A review. Proc Inst Mech Eng Part C J Mech Eng Sci 2012;226:327–46. https://doi.org/10.1177/0954406211426948.

[197] Pandey K. Silicon Wafers ; Its Manufacturing Processes and Finishing Techniques : an Overview 2022.

[198] Jain VK, Ranjan P, Suri VK, Komanduri R. Chemo-mechanical magneto-rheological finishing (CMMRF) of silicon for microelectronics applications. CIRP Ann - Manuf Technol 2010;59:323–8. https://doi.org/10.1016/j.cirp.2010.03.106.

[199] Ranjan P, Balasubramaniam R, Suri VK. Development of chemo-mechanical magnetorheological finishing process for super finishing of copper alloy. Int J Manuf Technol Manag 2013;27:130–41. https://doi.org/10.1504/IJMTM.2013.058909.

[200] Han X, Ma J, Tian A, Wang Y, Li Y, Dong B, et al. Colloids and Surfaces B :

Biointerfaces Surface modification techniques of titanium and titanium alloys for biomedical orthopaedics applications : A review. Colloids Surfaces B Biointerfaces 2023;227:113339. https://doi.org/10.1016/j.colsurfb.2023.113339.

[201] Takeuchi M, Abe Y, Yoshida Y, Nakayama Y, Okazaki M, Akagawa Y. Acid pretreatment of titanium implants. Biomaterials 2003;24:1821–7. https://doi.org/10.1016/S0142-9612(02)00576-8.

[202] Steigerwald JM, Murarka SP, Gutmann RJ. Chemical mechanical planarization of microelectronic materials 1997:324.

[203] Variola F, Yi JH, Richert L, Wuest JD, Rosei F, Nanci A. Tailoring the surface properties of Ti6Al4V by controlled chemical oxidation. Biomaterials 2008;29:1285–98. https://doi.org/10.1016/j.biomaterials.2007.11.040.

[204] Liu L, Zhang Z, Wu B, Hu W, Meng F, Li Y. A review : green chemical mechanical n.d.

[205] Wang W, Ji S, Zhao J. Review of magnetorheological finishing on components with complex surfaces. Int J Adv Manuf Technol 2023. https://doi.org/10.1007/s00170-023-11611-x.

[206] Barman A, Das M. Nano-finishing of bio-titanium alloy to generate different surface morphologies by changing magnetorheological polishing fluid compositions. Precis Eng 2018;51:145–52. https://doi.org/10.1016/j.precisioneng.2017.08.003.

[207] Gouné M, Bouaziz O, Allain S, Zhu K, Takahashi M. Kinetics of bainite transformation in heterogeneous microstructures. Mater Lett 2012;67:187–9. https://doi.org/10.1016/J.MATLET.2011.09.053.

[208] Lee J, Na J, Lim S. Control of adhesion and desorption behavior of silica particles on InGaAs surfaces by addition of hexadecyltrimethylammonium bromide in ammonium hydroxide–hydrogen peroxide mixture solution. Appl Surf Sci 2022;590:152949. https://doi.org/10.1016/J.APSUSC.2022.152949.

[209] Han Z, Liu Q, Zhao H, Shi Y, Liu Y, Chen J. Preparation and properties of

polyaniline-silver composite by glucose reduction. Polym Compos 2022;43:1121–7. https://doi.org/10.1002/PC.26440.

[210] Kim JS, Park YM, Bae MK, Kim CW, Kim DW, Shin DC, et al. Cutting performance of tungsten carbide tools coated with diamond thin films after etching for various times. Https://DoiOrg/101142/S0217984918502366 2018;32. https://doi.org/10.1142/S0217984918502366.

[211] Agbonlahor SO, Short NR, Dennis JK. The nature of defects in polyester powder films on zinc coated steel substrates. Trans IMF 1986;64:115–8. https://doi.org/10.1080/00202967.1986.11870747.

[212] Bae M, Lee J chun, Lee H, Kim S. Recovery of nitric acid and gold from gold-bearing aqua regia by tributyl-phosphate. Sep Purif Technol 2020;235:116154. https://doi.org/10.1016/J.SEPPUR.2019.116154.

[213] Jovičević-Klug P, Lipovšek N, Jovičević-Klug M, Podgornik B. Optimized preparation of deep cryogenic treated steel and Al-alloy samples for optimal microstructure imaging results. Mater Today Commun 2021;27. https://doi.org/10.1016/j.mtcomm.2021.102211.

[214] Peng Z, Song WL, Ye CL, Shi P, Choi SB. Model establishment of surface roughness and experimental investigation on magnetorheological finishing for polishing the internal surface of titanium alloy tubes. J Intell Mater Syst Struct 2021;32:1278–89. https://doi.org/10.1177/1045389X20930095.

[215] Rabinow J. The Magnetic Fluid Clutch. Trans Am Inst Electr Eng 1948;67:1308–15. https://doi.org/10.1109/T-AIEE.1948.5059821.

[216] Jacob R. Magnetic fluid torque and force transmitting device 1951.

[217] Lim ST, Choi H, Jhon M. Magnetorheological characterization of carbonyl iron-organoclay suspensions. INTERMAG Asia 2005 Dig IEEE Int Magn Conf 2005 2005.

[218] Rodríguez-López J, Elvira Segura L, Montero De Espinosa Freijo F. Ultrasonic

velocity and amplitude characterization of magnetorheological fluids under magnetic fields. J Magn Magn Mater 2012;324:222–30. https://doi.org/10.1016/J.JMMM.2011.08.019.

[219] Zhang X, Li W, Gong XL. Study on magnetorheological shear thickening fluid. Smart Mater Struct 2008;17:015051. https://doi.org/10.1088/0964-1726/17/1/015051.

[220] Zite JL, Ahmadkhanlou F, Neelakantan VA, Washington GN. A magnetorheological fluid based orthopedic active knee brace. SPIE Smart Struct Mater + Nondestruct Eval Heal Monit 2006;6171:61710H. https://doi.org/10.1117/12.658693.

[221] Patil AN, Rivankar S. MAGNETORHEOLOGICAL FLUID - A REVIEW ON CHARACTERISTICS , DEVICES 2019.

[222] Olabi AG, Grunwald A. Design and application of magneto-rheological fluid. Mater Des 2007;28:2658–64. https://doi.org/10.1016/J.MATDES.2006.10.009.

[223] Bedi TS, Singh AK. Magnetorheological methods for nanofinishing – a review. Part Sci Technol 2016;34:412–22. https://doi.org/10.1080/02726351.2015.1081657.

[224] Srivastava M, Pandey PM. Experimental investigation into polishing of monocrystalline silicon wafer using double-disc chemical assisted magnetorheological finishing process. Proc Inst Mech Eng Part C J Mech Eng Sci 2021;235:5467–86. https://doi.org/10.1177/0954406220983849.

[225] Kumar M, Singh Yadav HN, Kumar A, Das M. An overview of magnetorheological polishing fluid applied in nano-finishing of components. J Micromanufacturing 2022;5:82–100. https://doi.org/10.1177/25165984211008173.

[226] Jackson JA, Messner MC, Dudukovic NA, Smith WL, Bekker L, Moran B, et al. Field responsive mechanical metamaterials. Sci Adv 2018;4:1–10. https://doi.org/10.1126/sciadv.aau6419.

[227] Kumar M, Kumar A, Alok A, Das M. Magnetorheological method applied to optics polishing: A review. IOP Conf Ser Mater Sci Eng 2020;804.

https://doi.org/10.1088/1757-899X/804/1/012012.

[228] Nagdeve L, Sidpara A, Jain VK, Ramkumar J. On the effect of relative size of magnetic particles and abrasive particles in MR fluid-based finishing process. Mach Sci Technol 2018;22:493–506. https://doi.org/10.1080/10910344.2017.1365899.

[229] Nagdeve L, Jain VK, Ramkumar J. Optimization of process parameters in nano-finishing of Co-Cr-Mo alloy knee joint. Mater Manuf Process 2020;35:985–92. https://doi.org/10.1080/10426914.2020.1750633.

[230] Srivastava M, Pandey PM. The influence of ultrasonic vibrations on material removal in the silicon wafer polishing using DDCAMRF: Experimental investigations and process optimization. Proc Inst Mech Eng Part C J Mech Eng Sci 2021. https://doi.org/10.1177/09544062211038979.

[231] Kumar Y, Singh H. Experimental investigations on chemo-mechanical magneto-rheological finishing of Al-6061 alloy using composite magnetic abrasive (CIP-Al2O3) developed via microwave-sintering route. J Manuf Process 2023;99:765–80. https://doi.org/10.1016/j.jmapro.2023.05.064.

[232] Ghosh G, Sidpara A, Bandyopadhyay PP. Magnetorheological finishing of WC-Co coating using iron-B4C-CNT composite abrasives. Tribol Int 2021;155:106807. https://doi.org/10.1016/j.triboint.2020.106807.

[233] Lin CT, Yang LD, Chow HM. Study of magnetic abrasive finishing in free-form surface operations using the Taguchi method. Int J Adv Manuf Technol 2007;34:122–30. https://doi.org/10.1007/s00170-006-0573-8.

[234] Qian C, Tian Y, Fan Z, Sun Z, Ma Z. Investigation on rheological characteristics of magnetorheological shear thickening fluids mixed with micro CBN abrasive particles. Smart Mater Struct 2022;31:095004. https://doi.org/10.1088/1361-665X/AC7BBD.

[235] Ma Z, Tian Y, Qian C, Ahmad S, Fan Z, Sun Z. Modeling and simulation of material removal characteristics in magnetorheological shear thickening polishing. Int J Adv

Manuf Technol 2023;128:2319–31. https://doi.org/10.1007/s00170-023-12093-7.

[236] Kumar Y, Singh H. Chemomechanical magnetorheological finishing: Process mechanism, research trends, challenges and opportunities in surface finishing. J Micromanufacturing 2022;5:193–206. https://doi.org/10.1177/25165984211038878.

[237] Liang HZ, Yan QS, Lu J Bin, Gao WQ. Experiment on chemical magnetorheological finishing of SiC single crystal wafer. Mater Sci Forum 2016;874:407–14. https://doi.org/10.4028/www.scientific.net/MSF.874.407.

[238] Ghai V, Ranjan P, Batish A, Singh H. Atomic-level finishing of aluminum alloy by chemo-mechanical magneto-rheological finishing (CMMRF) for optical applications. J Manuf Process 2018;32:635–43. https://doi.org/10.1016/j.jmapro.2018.03.032.

[239] Kumar Y, Singh H. Effect of sintering routes on CIP/EIP – Al2O3 composite magnetic abrasive for chemo-mechanical magneto-rheological finishing of aluminium 6061. vol. 237. 2023. https://doi.org/10.1177/09544062221122072.

[240] Taniguchi N. Current Status in, and Future Trends of, Ultraprecision Machining and Ultrafine Materials Processing. CIRP Ann 1983;32:573–82. https://doi.org/10.1016/S0007-8506(07)60185-1.

[241] Zuegel JD, Dorrer C. Optical testing using the transport-of-intensity equation. Opt Express, Vol 15, Issue 12, Pp 7165-7175 2007;15:7165–75. https://doi.org/10.1364/OE.15.007165.

[242] Kordonski W, Golini D. Multiple Application of Magnetorheological Effect in High Precision Finishing. Http://DxDoiOrg/101106/104538902026104 2002;13:401–4. https://doi.org/10.1106/104538902026104.

[243] Cho W, Ahn Y, Baek CW, Kim YK. Effect of mechanical process parameters on chemical mechanical polishing of Al thin films. Microelectron Eng 2003;65:13–23. https://doi.org/10.1016/S0167-9317(02)00726-8.

[244] Saraswathamma K, Jha S, Rao P V. Experimental investigation into Ball end Magnetorheological Finishing of silicon. Precis Eng 2015;42:218–23. https://doi.org/10.1016/j.precisioneng.2015.05.003.

[245] Khan DA, Jha S. Selection of optimum polishing fluid composition for ball end magnetorheological finishing (BEMRF) of copper. Int J Adv Manuf Technol 2019;100:1093–103. https://doi.org/10.1007/s00170-017-1056-9.

[246] Tian J, Liu H, Cheng J, Chen M, Qin B. Improving the small ball-end magnetorheological polishing efficiency of fused silica workpiece by the promoting effect of water-bath heating and sodium hydroxide addition on polishing velocity and chemical reaction. Int J Adv Manuf Technol 2022;123:645–56. https://doi.org/10.1007/s00170-022-10180-9.

[247] Iqbal F, Jha S. Experimental investigations into transient roughness reduction in ball-end magneto-rheological finishing process. Mater Manuf Process 2019;34:224–31. https://doi.org/10.1080/10426914.2018.1512131.

[248] Kavithaa TS, Balashanmugam N. Nanometric surface finishing of typical industrial components by abrasive flow finishing. Int J Adv Manuf Technol 2016;85:2189–96. https://doi.org/10.1007/S00170-016-8486-7/METRICS.

[249] Yang SY, Zhang K, Bai L, Song Z, Yu H, McQueen DA, et al. Polymethylmethacrylate and titanium alloy particles activate peripheral monocytes during periprosthetic inflammation and osteolysis. J Orthop Res 2011;29:781–6. https://doi.org/10.1002/JOR.21287.

[250] Ingham E, Fisher J. Biological reactions to wear debris in total joint replacement. Http://DxDoiOrg/101243/0954411001535219 2000;214:21–37. https://doi.org/10.1243/0954411001535219.

[251] Harris WHM. Wear and Periprosthetic Osteolysis: The Problem. : Clinical Orthopaedics and Related Research (1976-2007). Clin Orthop Relat Res 2001. https://journals.lww.com/corr/Abstract/2001/12000/Wear_and_Periprosthetic_Osteolysis__The_Problem_.7.aspx (accessed July 11, 2023).

[252] Archibeck MJ, Jacobs JJ, Roebuck KA, Glant TT. The basic science of periprosthetic osteolysis. Instr Course Lect 2001;50:185–95.

[253] Jawahir IS, Brinksmeier E, M'Saoubi R, Aspinwall DK, Outeiro JC, Meyer D, et al. Surface integrity in material removal processes: Recent advances. CIRP Ann 2011;60:603–26. https://doi.org/10.1016/J.CIRP.2011.05.002.

[254] Lee JK, Choi DS, Jang I, Choi WY. Improved osseointegration of dental titanium implants by TiO2 nanotube arrays with recombinant human bone morphogenetic protein-2: a pilot in vivo study. Int J Nanomedicine 2015;10:1145–54. https://doi.org/10.2147/IJN.S78138.

[255] Jardini AL, Larosa MA, Bernardes LF, Zavaglia CAC, Maciel Filho R. Application of Direct Metal Laser Sintering in Titanium. 6th Brazilian Conf Manuf Eng 2011.

[256] Longhitanoa GA, Larosaa MA, Munhoza ALJ, De Carvalho Zavagliaa CA, Ierardia MCF. Surface finishes for Ti-6Al-4V alloy produced by direct metal laser sintering. Mater Res 2015;18:838–42. https://doi.org/10.1590/1516-1439.014415.

[257] Vadiraj A, Kamaraj M. Fretting fatigue behavior of surface modified biomedical titanium alloys. Trans Indian Inst Met 2010;63:217–23. https://doi.org/10.1007/S12666-010-0030-0/METRICS.

[258] Cubillos PO, dos Santos VO, Pizzolatti ALA, Moré ADO, Roesler CRM. Surface finish of total hip arthroplasty implants: Are we evaluating and manufacturing them appropriately? J Test Eval 2022;50. https://doi.org/10.1520/JTE20200357.

[259] Cubillos PO, Santos VO, Pizzolatti ALA, da Rosa E, Roesler CRM. Evaluation of surface finish and dimensional control of tribological metal-UHMWPE pair of Commercially Available HIP implants. J Arthroplasty 2018;33:939–44. https://doi.org/10.1016/j.arth.2017.10.032.

[260] Carvalho SR, Horovistiz A, Davim JP. The role of roughness parameters in grading the machined surface quality in Ti-alloys. Proc Inst Mech Eng Part B J Eng Manuf 2023. https://doi.org/10.1177/09544054231179249.

[261] Liu Z, Gan L, Liu D, Rong H, Feng Y, Liu D-E. Advances in the study of adhesion behavior between bacteria and material interfaces. Authorea 2022:1–20.

[262] Chiu SY, Wang YL, Liu CP, Lan JK, Ay C, Feng MS, et al. The application of electrochemical metrologies for investigating chemical mechanical polishing of Al with a Ti barrier layer. Mater Chem Phys 2003;82:444–51. https://doi.org/10.1016/S0254-0584(03)00312-2.

[263] Ahmed F, Naji A, Murtaza Q. Colloids and Surfaces A : Physicochemical and Engineering Aspects A novel environmentally friendly thermochemical process for Ti64 alloy surface modification for biomedical implants. Colloids Surfaces A Physicochem Eng Asp 2025;706:135806. https://doi.org/10.1016/j.colsurfa.2024.135806.

[264] Ahmed F, Qasim AN, Narjes M, Khaled I, Nasr MM. Future perspectives and research trends in advanced chemo-mechanical magneto-rheological finishing for enhanced surface quality. Multiscale Multidiscip Model Exp Des 2025;123. https://doi.org/10.1007/s41939-024-00623-z.

[265] Singh DK, Jain VK, Raghuram V. Parametric study of magnetic abrasive finishing process. J Mater Process Technol 2004;149:22–9. https://doi.org/10.1016/J.JMATPROTEC.2003.10.030.

[266] Veza I, Spraggon M, Fattah IMR, Idris M. Response surface methodology (RSM) for optimizing engine performance and emissions fueled with biofuel: Review of RSM for sustainability energy transition. Results Eng 2023;18:101213. https://doi.org/10.1016/j.rineng.2023.101213.

[267] ASTM, International. Standard Practice for Calculation of Corrosion Rates and Related Information from Electrochemical Measurements. G 102-89 2004;89:1–7.

[268] Thangaraju P, Varthya SB. ISO 10993: Biological Evaluation of Medical Devices. Med Device Guidel Regul Handb 2022:163–87. https://doi.org/10.1007/978-3-030-91855-2_11.

[269] Liu H, Pan C, Zhou S, Li J, Huang N, Dong L. Improving hemocompatibility and accelerating endothelialization of vascular stents by a copper-titanium film. Mater Sci Eng C 2016;69:1175–82. https://doi.org/10.1016/j.msec.2016.08.028.

[270] Khaled NI, Santhiya D. Multifunctional poly(allylamine hydrochloride)/bioactive glass layer by layer surface coating on magnesium alloy for biomedical applications. Prog Org Coatings 2024;186:108059. https://doi.org/10.1016/j.porgcoat.2023.108059.

[271] Boyan BD, Dean DD, Lohmann CH, Cochran DL, Sylvia VL, Schwartz Z. The Titanium-Bone Cell Interface In Vitro: The Role of the Surface in Promoting Osteointegration 2001:561–85. https://doi.org/10.1007/978-3-642-56486-4_17.

[272] Schmuki P. From Bacon to barriers: A review on the passivity of metals and alloys. J Solid State Electrochem 2002;6:145–64. https://doi.org/10.1007/s100080100219.

[273] Wang S, Liao Z, Liu Y, Liu W. Influence of thermal oxidation duration on the microstructure and fretting wear behavior of Ti6Al4V alloy. Mater Chem Phys 2015;159:139–51. https://doi.org/10.1016/J.MATCHEMPHYS.2015.03.063.

[274] Kumar S, Sankara Narayanan TSN, Ganesh Sundara Raman S, Seshadri SK. Thermal oxidation of Ti6Al4V alloy: Microstructural and electrochemical characterization. Mater Chem Phys 2010;119:337–46. https://doi.org/10.1016/J.MATCHEMPHYS.2009.09.007.

[275] Corobea MS, Stoenescu M, Miculescu M, Raditoiu V, Fierascu RC, Sirbu I, et al. Titanium functionalizing and derivatizing for implantable materials osseointegration properties enhancing. Dig J Nanomater Biostructures 2014;9:1339–47.

[276] Zhou X, Fang C, Lei W, Su J, Li L, Li Y. Thermal and Crystalline Properties of Waterborne Polyurethane by in situ water reaction process and the potential application as biomaterial. Prog Org Coatings 2017;104:1–10. https://doi.org/10.1016/J.PORGCOAT.2016.12.001.

[277] Ferraris S, Spriano S, Pan G, Venturello A, Bianchi CL, Chiesa R, et al. Surface

modification of Ti-6Al-4V alloy for biomineralization and specific biological response: Part I, inorganic modification. J Mater Sci Mater Med 2011;22:533–45. https://doi.org/10.1007/S10856-011-4246-2/METRICS.

[278] J B, Puleo DA, Nanci A. Biomaterials and biomechanics of oral and maxillofacial implants: current status and future developments. Int J Oral Maxillofac Implants 2000;15:15–46.

[279] Ribeiro LMS, Costa da Rosa Simões LA, Espanhol-Soares M, Carvalho Teles V, Ribeiro TAN, Capellato P, et al. Surface Modification of Ti–30Ta Alloy by Deposition of P(VDF-TrFE)/BaTiO3 Coating for Biomedical Applications. Metals (Basel) 2022;12. https://doi.org/10.3390/met12091409.

[280] Taylor M, Urquhart AJ, Zelzer M, Davies MC, Alexander MR. Picoliter water contact angle measurement on polymers. Langmuir 2007;23:6875–8. https://doi.org/10.1021/LA070100J.

[281] Shen Y, Wu X, Tao J, Zhu C, Lai Y, Chen Z. Icephobic materials: Fundamentals, performance evaluation, and applications. Prog Mater Sci 2019;103:509–57. https://doi.org/10.1016/J.PMATSCI.2019.03.004.

[282] Nouri A, Wen C. Introduction to surface coating and modification for metallic biomaterials. Surf Coat Modif Met Biomater 2015:3–60. https://doi.org/10.1016/B978-1-78242-303-4.00001-6.

[283] D3359 Standard Test Methods for Rating Adhesion by Tape Test n.d. https://www.astm.org/standards/d3359 (accessed February 19, 2024).

[284] Chan CW, Lee S, Smith G, Sarri G, Ng CH, Sharba A, et al. Enhancement of wear and corrosion resistance of beta titanium alloy by laser gas alloying with nitrogen. Appl Surf Sci 2016;367:80–90. https://doi.org/10.1016/J.APSUSC.2016.01.091.

[285] Ju J, Zhao C, Kang M, Li J, He L, Wang C, et al. Effect of heat treatment on microstructure and tribological behavior of Ti–6Al–4V alloys fabricated by selective laser melting. Tribol Int 2021;159. https://doi.org/10.1016/j.triboint.2021.106996.

[286] Yang W, He X, Li H, Dong J, Chen W, Xin H, et al. A tribological investigation of SLM fabricated TC4 titanium alloy with carburization pre-treatment. Ceram Int 2020;46:3043–50. https://doi.org/10.1016/J.CERAMINT.2019.10.004.

[287] Materials. A-F-00. SP for A of HP of. ASTM International - ASTM F756-00. Annu B OfAstm Stand Am Soc Test Mater Philadelphia, PA, USA, 2000 Nov Biocompatible Zr-Based Alloy with Low Young's Modul Magn Susceptibility Biomed Implant Available from Https//WwwRes 2000.

[288] Hu W, Xu J, Lu X, Hu D, Tao H, Munroe P, et al. Corrosion and wear behaviours of a reactive-sputter-deposited Ta2O5 nanoceramic coating. Appl Surf Sci 2016;368:177–90. https://doi.org/10.1016/J.APSUSC.2016.02.014.

[289] Zhou, Yang et al. "Electrochemical corrosion behavior of powder metallurgy Ti6Al4V alloy. " J Mater Eng Perform 30 556-564 n.d.

[290] Bocchetta P, Chen LY, Tardelli JDC, Dos Reis AC, Almeraya-Calderón F, Leo P. Passive layers and corrosion resistance of biomedical ti-6al-4v and β-ti alloys. Coatings 2021;11. https://doi.org/10.3390/coatings11050487.

[291] Cordiolli LG, De Sousa LL, Ramos AS, Gargarella P, Mariano NA. Characterization alloys of the Sn-Zn system produced by melt spinning. Mater Res 2019;22:1–12. https://doi.org/10.1590/1980-5373-MR-2019-0144.

[292] Kuroda K, Okido M. Hydroxyapatite coating of titanium implants using hydroprocessing and evaluation of their osteoconductivity. Bioinorg Chem Appl 2012;2012. https://doi.org/10.1155/2012/730693.

[293] ISO 23317:2012 - Implants for surgery — In vitro evaluation for apatite-forming ability of implant materials n.d. https://www.iso.org/standard/54163.html (accessed April 27, 2024).

[294] Ergun C, Liu H, Webster TJ, Olcay E, Yilmaz Ş, Sahin FC. Increased osteoblast adhesion on nanoparticulate calcium phosphates with higher Ca/P ratios. J Biomed Mater Res - Part A 2008;85:236–41. https://doi.org/10.1002/jbm.a.31555.

[295] Lu J, Yu H, Chen C. Biological properties of calcium phosphate biomaterials for bone repair: A review. RSC Adv 2018;8:2015–33. https://doi.org/10.1039/c7ra11278e.

[296] Büyüksağiş A, Çiftçi N. HAP Coatings for Biomedical Applications: Biocompatibility and Surface Protection Against Corrosion of Ti, Ti6Al4V and AISI 316L SS. Prot Met Phys Chem Surfaces 2020;56:834–43. https://doi.org/10.1134/S2070205120040085.

[297] Bulina N V., Chaikina M V., Prosanov IY, Dudina D V., Solovyov LA. Fast synthesis of La-substituted apatite by the dry mechanochemical method and analysis of its structure. J Solid State Chem 2017;252:93–9. https://doi.org/10.1016/J.JSSC.2017.05.008.

[298] A. A. Al-esnawy, A. A. El-hadad, Islam S. EL-Sayed, Khairy M. T. Eraba. Thermochemical Modification of Ti–6Al–4V alloy for Biomedical Applications. Int J Sci Res Sci Eng Technol 2016;2:454–63. https://doi.org/10.32628/IJSRSET1625121.

[299] Jadhav U, Su C, Hocheng H. Leaching of metals from large pieces of printed circuit boards using citric acid and hydrogen peroxide. Environ Sci Pollut Res 2016;23:24384–92. https://doi.org/10.1007/s11356-016-7695-9.

[300] Deng C, Jiang L, Qian L. High-Efficiency Chemical Mechanical Polishing of Ti-6Al-4V Alloy via the Synergistic Action of H 2 O 2 and K + Under Alkaline Conditions . ECS J Solid State Sci Technol 2022;11:024005. https://doi.org/10.1149/2162-8777/ac495e.

[301] Chen, Wei, Qifeng Li a LZ. Oxidation mechanism of a near b-Ti alloy chen 2022.

[302] Tien DH, Trinh ND. Novel hybrid chemical magnetorheological fluid for polishing Ti–6Al–4V alloy. Mater Manuf Process 2024;39:1798–815. https://doi.org/10.1080/10426914.2024.2334674.

[303] Sato T, Kum CW, Venkatesh VC. Rapid magneto-rheological finishing of Ti-6Al-

4V for aerospace components. Int J Nanomanuf 2013;9:431–45. https://doi.org/10.1504/IJNM.2013.057590.

[304] Kumar Singh A, Jha S, Pandey PM. Nanofinishing of a typical 3D ferromagnetic workpiece using ball end magnetorheological finishing process. Int J Mach Tools Manuf 2012;63:21–31. https://doi.org/10.1016/j.ijmachtools.2012.07.002.

[305] Li Y, Ding D, Ning C, Bai S, Huang L, Li M, et al. Thermal stability and in vitro bioactivity of Ti–Al–V–O nanostructures fabricated onTi6Al4V alloy. Nanotechnology 2009;20:065708. https://doi.org/10.1088/0957-4484/20/6/065708.

[306] Hryniewicz T, Rokosz K, Rokicki R, Prima F. Nanoindentation and XPS Studies of Titanium TNZ Alloy after Electrochemical Polishing in a Magnetic Field. Mater 2015, Vol 8, Pages 205-215 2015;8:205–15. https://doi.org/10.3390/MA8010205.

[307] Saharudin KA, Sreekantan S, Aziz SNQAA, Hazan R, Lai CW, Mydin RBSMN, et al. Surface modification and bioactivity of anodic Ti6Al4V alloy. J Nanosci Nanotechnol 2013;13:1696–705. https://doi.org/10.1166/jnn.2013.7115.

[308] Balyakin A V., Shvetcov AN, Zhuchenko EI. Chemical polishing of samples obtained by selective laser melting from titanium alloy Ti6Al4V. MATEC Web Conf 2018;224. https://doi.org/10.1051/matecconf/201822401031.

[309] Chen JR, Tsai WT. In situ corrosion monitoring of Ti-6Al-4V alloy in H2SO 4/HCl mixed solution using electrochemical AFM. Electrochim Acta 2011;56:1746–51. https://doi.org/10.1016/j.electacta.2010.10.024.

RESEARCH PUBLICATIONS

List of Research Papers (Published)

I. Fadia Ahmed Abdullah Naji, Qasim Murtaza, MS Niranjan (2024). **Challenges and opportunities in nano finishing of titanium alloys for biomedical applications: A review,** Elsevier: Precision Engineering (SCIE indexed, Impact Factor:3.7).

II. Fadia Ahmed Abdullah Naji, Qasim Murtaza, Narjes Ibrahem Khaled, Mustafa M Nasr (2024). **Future perspectives and research trends in advanced chemo-mechanical magneto-rheological finishing for enhanced surface quality.** Springer. Multiscale and Multidisciplinary Modeling, Experiments and Design. (ESCI indexed, Impact Factor: 2.1).

III. Fadia Ahmed Abdullah Naji, Qasim Murtaza, (2025). **A novel environmentally friendly thermochemical process for Ti64 alloy surface modification for biomedical implants.** Elsevier: Colloids and Surfaces A: Physicochemical and Engineering Aspects (SCIE indexed, Impact Factor: 5.4).

IV. Fadia Ahmed Abdullah Naji, Qasim Murtaza, MS Niranjan (2025). **Sustainable and Optimized Chemical Magneto-Rheological Finishing of Ti64 Alloy for Enhancing Surface Finish through pH Regulation.** Wiley: Advanced Engineering Materials (SCIE indexed, Impact Factor: 3.4).

List of papers presented at International Conferences

I. Fadia Ahmed Naji, Qasim Murtaza, M.S. Niranjan. **Advanced Ball End Magneto-rheological (BEMR) Finishing for Surface Quality: A review.** Paper presented at International Conference on Advanced Materials, Manufacturing, and Sustainable Development (ICAMMSD-2024), Kurnool, Andhra Pradesh, India (November 22–23, 2024).

II. Fadia Ahmed Naji, Qasim Murtaza, M.S. Niranjan. **Optimization of Ball End Magneto-Rheological (BEMR) Process Parameters for Enhanced Finishing Quality of Ti64 Alloy.** Paper presented at the 2nd Global Students Research (GSR) Conference, KFUPM, Saudi Arabia (February 4–6, 2025).

CURRICULUM VITAE

Fadia Ahmed Naji has completed her Bachelor's degree in Industrial Manufacturing and Systems Engineering (IMSE) from Taiz University, Taiz, Yemen, and her Master's degree in Engineering and Management from Taiz University Center of Graduate Studies, Taiz, Yemen. She enrolled in a Ph.D. program in the Department of Mechanical Engineering at Delhi Technological University, Delhi, India, under an ICCR scholarship, under the supervision of Prof. Qasim Murtaza and Prof. M.S. Niranjan. Her work focuses on post-processing machining, MR finishing, Eco-friendly surface modification, thermochemical processing, corrosion, and advanced manufacturing processes. She has expertise in advanced material tribology and surface characterization, including SEM, FESEM, XRD, XPS, and FTIR. She has published 5 SCI/SCIE papers in reputable journals. Through her research, she delves into advanced surface engineering to develop next-generation biomedical implants that combine high performance with environmental sustainability. In addition to her academic background, she has industrial experience as a Head of Planning Engineer in the planning department at Alahlia Mineral Water Company (AMWC) in Yemen.